

AD-A125 027

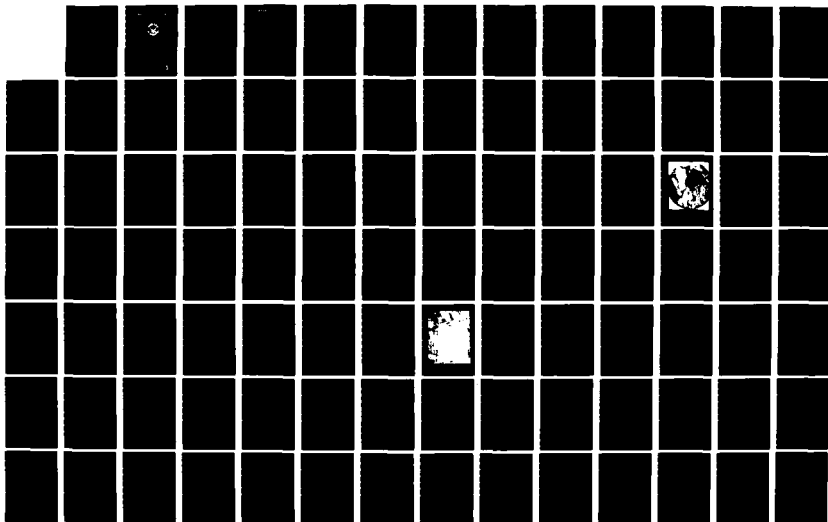
SATELLITE APPLICATIONS TO ACOUSTIC PREDICTION SYSTEMS
(U) NAVAL POSTGRADUATE SCHOOL MONTEREY CA 5 A COX
OCT 82 NP568-82-005

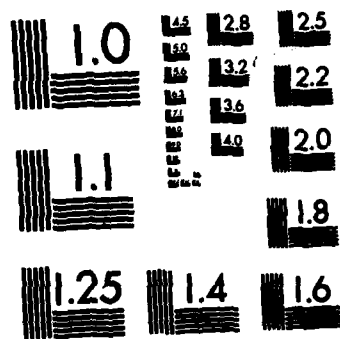
1/2

UNCLASSIFIED

F/G 8/10

NL





MICROCOPY RESOLUTION TEST CHART
NATIONAL BUREAU OF STANDARDS-1963-A

NPS68-82-005

AD A125027

NAVAL POSTGRADUATE SCHOOL

Monterey, California



THESIS

SATELLITE APPLICATIONS TO ACOUSTIC
PREDICTION SYSTEMS

by

Stephen A. Cox

October 1982

Thesis Advisor:

G. H. Jung

Approved for public release; distribution unlimited

Prepared for: Naval Ocean Systems Center
Code 531
San Diego, California 92152

DTIC FILE COPY

DTIC
ELECTE

FEB 28 1983

83 02 028

102

A

NAVAL POSTGRADUATE SCHOOL
Monterey, California

Rear Admiral John J. Ekelund, USN
Superintendent

David A. Schradly
Provost

This thesis was prepared in conjunction with research supported in part by Naval Ocean Systems Center under work order N6600182WR00214.

Reproduction of all or part of this report is not authorized without permission of the Naval Postgraduate School.

Released as a
Technical Report by


Dean of Research

UNCLASSIFIED

SECURITY CLASSIFICATION OF THIS PAGE (When Data Entered)

REPORT DOCUMENTATION PAGE		READ INSTRUCTIONS BEFORE COMPLETING FORM												
1. REPORT NUMBER NPS68-82-005	2. GOVT ACCESSION NO. AD-A125027	3. RECIPIENT'S CATALOG NUMBER												
4. TITLE (and Subtitle) Satellite Applications to Acoustic Prediction Systems		5. TYPE OF REPORT & PERIOD COVERED Master's Thesis October 1982												
7. AUTHOR(s) Stephen A. Cox in conjunction with Glen H. Jung and Calvin R. Dunlap		6. PERFORMING ORG. REPORT NUMBER												
8. PERFORMING ORGANIZATION NAME AND ADDRESS Naval Postgraduate School Monterey, California 93940		9. CONTRACT OR GRANT NUMBER(s)												
11. CONTROLLING OFFICE NAME AND ADDRESS Naval Ocean Systems Center Code 531 San Diego, California 92152		10. PROGRAM ELEMENT, PROJECT, TASK AREA & WORK UNIT NUMBERS N6600182WR00214												
12. MONITORING AGENCY NAME & ADDRESS (if different from Controlling Office) CNO Attn: OP095 Navy Department Washington, D.C. 20350		13. REPORT DATE October 1982												
		14. NUMBER OF PAGES 149												
		15. SECURITY CLASS. (of this report) Unclassified												
		16a. DECLASSIFICATION/DOWNGRADING SCHEDULE												
17. DISTRIBUTION STATEMENT (of this Report) Approved for public release; distribution unlimited														
18. DISTRIBUTION STATEMENT (of the abstract entered in Block 20, if different from Report)														
19. SUPPLEMENTARY NOTES														
20. KEY WORDS (Continue on reverse side if necessary and identify by block number) <table border="0"> <tr> <td>Satellite</td> <td>Sea Surface Temperature</td> <td>Satellite Oceanography</td> </tr> <tr> <td>Remote Sensing</td> <td>Fronts</td> <td>Infrared Sensing</td> </tr> <tr> <td>Northeast Pacific Ocean</td> <td>Eddy</td> <td></td> </tr> <tr> <td>Thermal Structure</td> <td>Subsurface Thermal Structure</td> <td></td> </tr> </table>			Satellite	Sea Surface Temperature	Satellite Oceanography	Remote Sensing	Fronts	Infrared Sensing	Northeast Pacific Ocean	Eddy		Thermal Structure	Subsurface Thermal Structure	
Satellite	Sea Surface Temperature	Satellite Oceanography												
Remote Sensing	Fronts	Infrared Sensing												
Northeast Pacific Ocean	Eddy													
Thermal Structure	Subsurface Thermal Structure													
21. ABSTRACT (Continue on reverse side if necessary and identify by block number) <p>Predicting the thermal structure of the oceans is of importance to the naval tactician, logistician, or search and rescue coordinator. Understanding the structure of the oceans provides valuable insights to those who must utilize the oceanic environment effectively in their day to day operations.</p> <p>Today, recent information about an area is limited to point observations of single bathythermographs. Few models produce an accurate picture of the ocean environment that can be used for updating tactics to conform to a changing situation. Producing a reliable prediction of conditions for a large area</p>														

DD FORM 1 JAN 72 1473

EDITION OF 1 NOV 66 IS OBSOLETE
S/N 0102-014-0001

UNCLASSIFIED

SECURITY CLASSIFICATION OF THIS PAGE (When Data Entered)

UNCLASSIFIED

SECURITY CLASSIFICATION OF THIS PAGE/When Data Entered

#20 ABSTRACT (Continued)

while using limited resources, is the basic objective of this paper.

Satellite infrared imaging of the ocean surface has been used effectively to map sea surface temperature patterns. Such sea surface temperature patterns can be used, along with climatology, to identify subsurface thermal structure in an ocean area according to results of this study. More accurate inputs can be made to range dependent acoustic prediction models, thus improving the ASW environmental predictions available to fleet users.



1. TITLE	
2. AUTHOR	
3. PERIODICAL	
4. DATE	
5. AVAILABILITY STATEMENT	
6. DISTRIBUTION STATEMENT	
7. SECURITY CLASSIFICATION	
8. SPECIAL	

Approved for public release: distribution unlimited

Satellite Applications to Acoustic Prediction Systems

by

Stephen A. Cox

Lieutenant Commander, United States Navy
B.S., United States Naval Academy, 1974

Submitted in partial fulfillment of the
requirements for the degree of

MASTER OF SCIENCE IN SYSTEMS TECHNOLOGY

from the

NAVAL POSTGRADUATE SCHOOL

October 1982

Author

Stephen A. Cox

Approved by:

Glen H. Jones

Thesis Advisor

Calvin R. Dunlap

Second Reader

W. H. Hunt

Chairman, ASW Academic Group

R. Shady

Academic Dean

✓

ABSTRACT

Predicting the thermal structure of the oceans is of importance to the Naval tactician, logistician, or search and rescue coordinator. Understanding the structure of the oceans provides valuable insights to those who must utilize the oceanic environment effectively in their day to day operations.

Today, recent information about an area is limited to point observations of single bathythermographs. Few models produce an accurate picture of the ocean environment that can be used for updating tactics to conform to a changing situation. Producing a reliable prediction of conditions for a large area, while using limited resources, is the basic objective of this paper.

Satellite infrared imaging of the ocean surface has been used effectively to map sea surface temperature patterns. Such sea surface temperature patterns can be used, along with climatology, to identify subsurface thermal structure in an ocean area according to results of this study. More accurate inputs can be made to range dependent acoustic prediction models, thus improving the ASW environmental predictions available to fleet users.

↑
Antisubmarine warfare

TABLE OF CONTENTS

I.	INTRODUCTION	13
	A. PREDICTION OF OCEAN THERMAL STRUCTURE	13
	B. PROBLEM OF ACOUSTIC PREDICTIONS	13
	C. EXPERIMENTAL BASIS FOR THIS THESIS	14
II.	CLIMATOLOGY OF THE EASTERN NORTH PACIFIC OCEAN . .	17
	A. OVERVIEW OF THE EASTERN NORTH PACIFIC OCEAN . .	17
	B. WATER MASS CHARACTERISTICS	19
	1. Watermass Analysis	20
	2. Domain Analysis	23
	3. Temperature Structure	29
	C. METEOROLOGY OF THE EASTERN NORTH PACIFIC OCEAN	31
III.	SATELLITES IN OCEANOGRAPHY	34
	A. INSTRUMENTS FOR OBSERVING THE OCEANS	34
	1. Visual and Infrared Imaging	34
	2. Passive Microwave Radiometry	40
	3. Satellite Radar Altimeter	41
	B. OTHER INSTRUMENTS FOR OBSERVING THE OCEANS . .	42
IV.	EXPERIMENTAL DESIGN	44
	A. OBJECTIVE	44
	B. DATA ACQUISITION	45
	C. DATA ANALYSIS	49
	1. Data Plots	49
	2. Statistical Procedure	49
	D. OBSERVATIONS BY FLIGHT	51
	1. Flight Track One	51
	2. Flight Track Two	56
	3. Flight Track Three	63
	4. Flight Track Four	67
	5. Flight Track Five (Center and South) . . .	72
	6. Flight Track Six (Center and North) . . .	80
	E. DYNAMIC HEIGHT COMPARISONS, 17 NOVEMBER . . .	87
	F. OVERALL OBSERVATIONS	90

1.	An Eddy on the Southeastern Part of the Track	90
2.	Gradients in the Thermocline	92
3.	Sea Surface Temperature	94
4.	Mixed Layer Depth	95
5.	Mixed Layer Depth and Sea Surface Temperature Correlations	97
V.	CONCLUSIONS AND RECOMMENDATIONS	98
A.	CONCLUSIONS	98
B.	RECOMMENDATIONS	99
APPENDIX A: VARIATION OF THERMOCLINE GRADIENTS WITH POSITION FOR NOVEMBER 101		
APPENDIX B: VARIATION OF THERMOCLINE GRADIENTS WITH POSITION FOR DECEMBER 113		
APPENDIX C: TABLES OF NORMALIZED GRADIENTS IN THE THERMOCLINE 133		
APPENDIX D: MODEL EQUATIONS FOR EACH FLIGHT 138		
LIST OF REFERENCES 143		
INITIAL DISTRIBUTION LIST 148		

LIST OF TABLES

I.	Visible and Infrared Spin Scan Radiometer (VISSR) Channelization.	35
II.	Coastal Zone Color Scanner (CZCS) Channelization.	38
III.	Advanced Very High Resolution Radiometer (AVHRR) Channelization	38
IV.	MLD, SST and Gradients at the Thermocline, 15 November 1980.	55
V.	Models of MLD for 15 November.	55
VI.	MLD, SST and Gradients at the Thermocline, 17 November 1980.	62
VII.	Models of MLD for 17 November.	63
VIII.	MLD, SST and Gradients at the Thermocline, 19 November 1980.	67
IX.	Models of MLD for 19 November.	68
X.	MLD, SST and Gradients at the Thermocline, 1 December 1980.	69
XI.	Models of MLD for 1 December.	72
XII.	MLD, SST and Gradients at the Thermocline, 3 December 1980.	79
XIII.	MLD, SST and Gradients at the Thermocline, 3 December 1980 (South)	79
XIV.	Models of MLD for 3 December, Center Track. . . .	80
XV.	Models of MLD for 3 December, South Track. . . .	80
XVI.	MLD, SST and Gradients at the Thermocline, 5 December 1980.	87
XVII.	MLD, SST and Gradients at the Thermocline, 5 December 1980 (North)	87
XVIII.	Models of MLD for 5 December, Center Track. . . .	88
XIX.	Models of MLD for 5 December, North Track. . . .	88

XX.	Dynamic Heights Relative to 350 meters (17 Nov).	89
XXI.	Correlation Coefficient (r) for Gradient from 5 meters vs. Position	93
XXII.	Gradients Most Correlated with Position (by Flight).	93
XXIII.	Correlation Coefficient (r) for SST vs. Track Position.	94
XXIV.	Correlation Coefficient (r) - MLD vs. Track Position.	95
XXV.	Correlation Coefficients (r) for MLD vs. SST. .	96
XXVI.	Normalized Gradients for Flight Track One. . . .	133
XXVII.	Normalized Gradients for Flight Track Two. . . .	134
XXVIII.	Normalized Gradients for Flight Track Three. . .	134
XXIX.	Normalized Gradients for Flight Track Four. . .	135
XXX.	Normalized Gradients for Flight Track Five (Center).	135
XXXI.	Normalized Gradients for Flight Track Five (South).	136
XXXII.	Normalized Gradients for Flight Track Six (Center).	136
XXXIII.	Normalized Gradients for Flight Track Six (North).	137
XXXIV.	Model Equations for MLD (15 November).	138
XXXV.	Model Equations for MLD (17 November).	139
XXXVI.	Model Equations for MLD (19 November).	139
XXXVII.	Model Equations for MLD (1 December).	140
XXXVIII.	Model Equations for MLD (3 December, Center). .	140
XXXIX.	Model Equations for MLD (3 December, South). . .	141
XL.	Model Equations for MLD (5 December, Center). .	141
XLI.	Model Equations for MLD (5 December, North). . .	142

LIST OF FIGURES

1.1	Eastern North Pacific with ASTREX Region Defined.	15
2.1	Watermasses of the Eastern North Pacific Ocean [Ref. 6].	18
2.2	Three Zone Structure in the Eastern North Pacific Ocean [Ref. 15].	21
2.3	Domains in the ASTREX Region.	24
2.4	Upper Zone Domains [Ref. 20]	25
2.5	Growth/decline of the Thermocline at OWS-P [Ref. 26].	27
2.6	Lower Zone Domains [Ref. 27].	28
3.1	GOES Visible Image (Full Disk) [Ref. 38]	36
3.2	Atmospheric Transmittance (Visible and Infrared Spectra) [Ref. 39]	37
4.1	Digitized Temperatures at Five Meter Increments [Ref. 54].	46
4.2	Digitized Depths of Isotherms [Ref. 55].	47
4.3	FNOC Salinity Profile Along the Flight Track for 13 November.	48
4.4	Vertical Temperature Cross-section (15 November).	52
4.5	Mixed Layer Depth and Sea Surface Temperature (15 November).	53
4.6	Vertical Temperature Cross-section (17 November).	57
4.7	Mixed Layer Depth and Sea Surface Temperature (17 November).	59
4.8	NOAA-6 Image (17 November) [Ref. 60]	60
4.9	Flight Track, Buoy Numbers and Meander Location in Figure 4.8.	61

4.10	Vertical Temperature Cross-section (19 November)	65
4.11	Mixed Layer Depth and Sea Surface Temperature (19 November)	66
4.12	Vertical Temperature Cross-section (1 December)	70
4.13	Mixed Layer Depth and Sea Surface Temperature (1 December)	71
4.14	Vertical Temperature Cross-section (3 Dec, Center)	74
4.15	Vertical Temperature Cross-section (3 Dec, South)	75
4.16	Mixed Layer Depth and Sea Surface Temperature (3 Dec, Center)	76
4.17	Mixed Layer Depth and Sea Surface Temperature (3 Dec, South)	77
4.18	Vertical Temperature Cross-section (5 Dec, Center)	82
4.19	Vertical Temperature Cross-section (5 Dec, North)	83
4.20	Mixed Layer Depth and Sea Surface Temperature (5 Dec, Center)	84
4.21	Mixed Layer Depth and Sea Surface Temperature (5 Dec, North)	85
4.22	Dynamic Heights Along the Center Track (17 Nov) 0/350.	91
A.1	Gradient from 5 meters vs. Position (15 Nov)	101
A.2	Gradient from 15 meters vs. Position (15 Nov)	102
A.3	Gradient from 50 meters vs. Position (15 Nov)	103

A.4	Gradient from 100 meters vs. Position (15 Nov).	104
A.5	Gradient from 5 meters vs. Position (17 Nov).	105
A.6	Gradient from 15 meters vs. Position (17 Nov).	106
A.7	Gradient from 50 meters vs. Position (17 Nov).	107
A.8	Gradient from 100 meters vs. Position (17 Nov).	108
A.9	Gradient from 5 meters vs. Position (19 Nov).	109
A.10	Gradient from 15 meters vs. Position (19 Nov).	110
A.11	Gradient from 50 meters vs. Position (19 Nov).	111
A.12	Gradient from 100 meters vs. Position (19 Nov).	112
B.13	Gradient from 5 meters vs. Position (1 Dec).	113
B.14	Gradient from 15 meters vs. Position (1 Dec).	114
B.15	Gradient from 50 meters vs. Position (1 Dec).	115
B.16	Gradient from 100 meters vs. Position (1 Dec).	116
B.17	Gradient from 5 meters vs. Position (3 Dec).	117
B.18	Gradient from 15 meters vs. Position (3 Dec).	118
B.19	Gradient from 50 meters vs. Position (3 Dec).	119

B.20	Gradient from 100 meters vs. Position (3 Dec)	120
B.21	Gradient from 5 meters vs. Position (3 Dec - South)	121
B.22	Gradient from 15 meters vs. Position (3 Dec - South)	122
B.23	Gradient from 50 meters vs. Position (3 Dec - South)	123
B.24	Gradient from 100 meters vs. Position (3 Dec - South)	124
B.25	Gradient from 5 meters vs. Position (5 Dec)	125
B.26	Gradient from 15 meters vs. Position (5 Dec)	126
B.27	Gradient from 50 meters vs. Position (5 Dec)	127
B.28	Gradient from 100 meters vs. Position (5 Dec)	128
B.29	Gradient from 5 meters vs. Position (5 Dec - North.)	129
B.30	Gradient from 15 meters vs. Position (5 Dec - North.)	130
B.31	Gradient from 50 meters vs. Position (5 Dec - North.)	131
B.32	Gradient from 100 meters vs. Position (5 Dec - North.)	132

I. INTRODUCTION

A. PREDICTION OF OCEAN THERMAL STRUCTURE

Attempts to predict the vertical temperature profile in a large body of water can be quite varied. A climatological atlas may be used and a profile chosen which corresponds to the location and time of interest. The climatology may be updated using an interpolation from one climatological period to another. A recent measurement in an area can be used to modify the climatological prediction, thus producing a more time-sensitive prediction. Measurements which may be used to to modify climatological predictions are temperature structure in the upper ocean and sea surface temperature (SST).

The bathythermograph (BT) provides a temperature profile at a point, while satellite measurements can provide recent sea surface temperature patterns over an area of interest. A combination of climatology, recently-measured temperature structure (BT), and satellite-derived SST could provide a very reasonable prediction of the vertical temperature profile for a body of water.

B. PROBLEM OF ACOUSTIC PREDICTIONS

Accurate predictions of transmission loss depend on accurate specifications of water masses along an acoustic path. The primary physically-measurable quantity which affects sound speed (and thus transmission loss) is temperature. Temperature structure of the water is an important factor in acoustic losses along a transmission path. There is no way to gather temperature profiles rapidly along a

desired track. To measure temperatures along the tracks analyzed for the experiment discussed in this thesis required a nine-hour mission by a dedicated patrol aircraft. The operational fleet user does not have the luxury of dedicated air assets to provide a detailed thermal description of an area of acoustic interest.

Obviously, the employment of a dedicated patrol aircraft loaded with a store of expendable bathythermographs is not a realistic solution to the problem of predicting acoustic properties in various locations of the world. The use of numerical models, relying on climatological files, and modified by recent observations, provides a first guess in predicting thermal structure. However, these models require time to produce results, and may therefore not accurately present the actual thermal structure.

If a coupling exists between conditions at the air-sea boundary and the depth of the mixed layer, satellites can provide a means of rapidly surveying the sea surface in an oceanic operating area. The satellite sea surface observations could then be used to estimate the vertical temperature structure throughout the operating area. If a good linkage exists between sea surface conditions and the mixed layer depth, the accuracy and timeliness of acoustic predictions could be improved. Such ocean surface conditions observable remotely by satellite include sea surface temperature, ocean color, and topography.

C. EXPERIMENTAL BASIS FOR THIS THESIS

In November and December of 1980, the Naval Postgraduate School conducted the Acoustic Storm Transfer and Response Experiment (ASTREX). This experiment was conducted as part of the first Storm Transfer and Response Experiment (STREX), a joint investigation by United States and Canada to

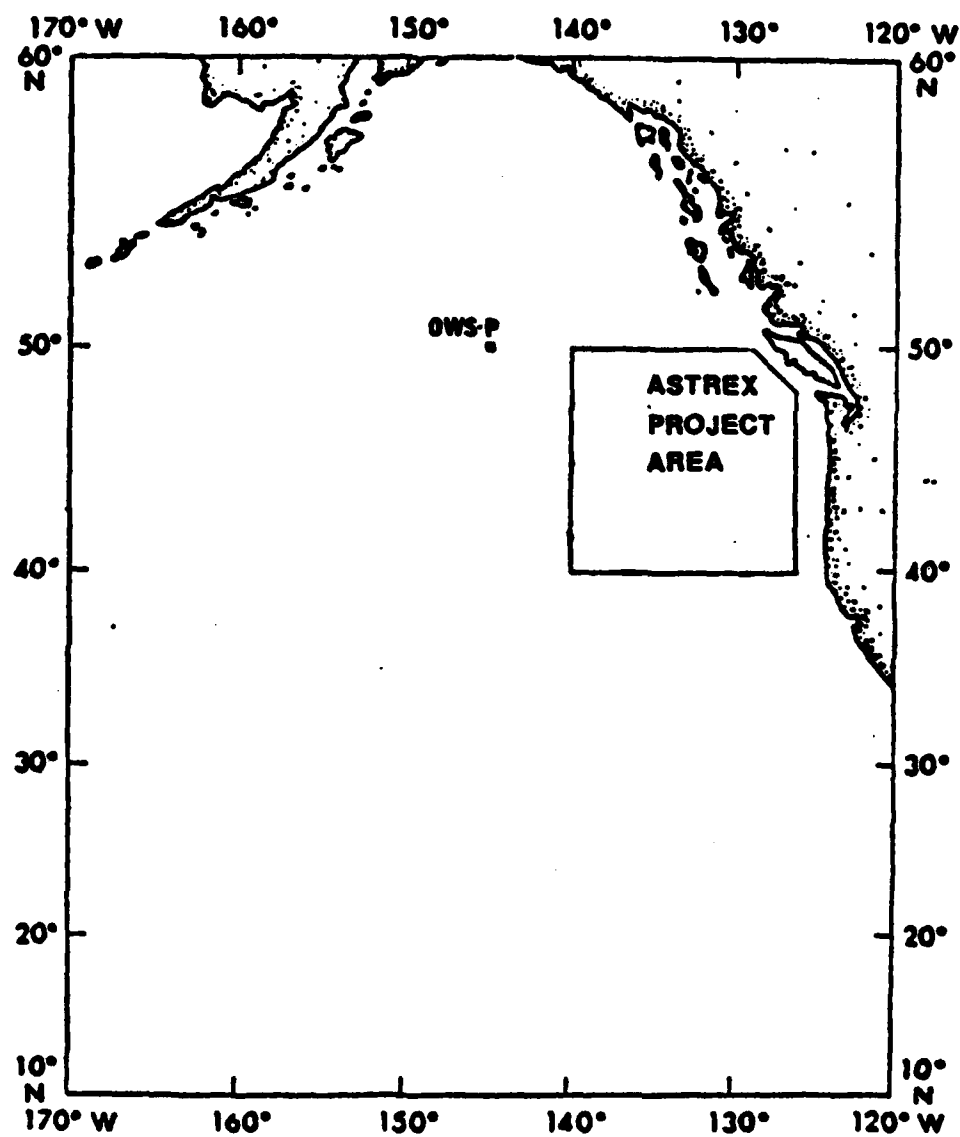


Figure 1.1 Eastern North Pacific with ASTREX Region Defined.

determine the effects on the air-sea boundary of North Pacific storms, and the converse [Ref. 1]. Figure 1.1 shows the location of the ASIREX area in the context of the eastern North Pacific Ocean. Three flight tracks were examined within this area. Each track covered a diagonal through the central area of the square from the southeast to the northwest.

II. CLIMATOLOGY OF THE EASTERN NORTH PACIFIC OCEAN

A. OVERVIEW OF THE EASTERN NORTH PACIFIC OCEAN

Much of the research conducted in the Eastern North Pacific Ocean relies on data collected at Ocean Weather Station "P" (OWS-P), located at 50N, 145W, in the center of the Gulf of Alaska. The research project reported here operated in an area of the North Pacific to the east and south of OWS-P. Tabata [Ref. 2] concluded that the characteristics of OWS-P were representative of the waters in the northeast Pacific region.

Ocean Station "P" is situated north of the Subarctic Current, well to the northwest of the divergence which is formed when the West Wind Drift approaches the North American continent [Ref. 3]. The California Current is the southerly component of the West Wind Drift after it divides, while the northerly component forms the Alaska Current and continues its flow into the Alaska Gyre [Ref. 4].

The climatological description of the project area depends on a combination of multiple-year observations from OWS-P and observations within the area itself. The region from which the data were taken includes the subarctic front and the source of the California Current. The California Current is a permanent feature in the observation area.

The observation area may be described by three regions: the Coastal, or Transition Region, extends from the coast out to 130W; the Subarctic Watermass extends seaward beyond the coastal zone to the north of 42N; and the Central Pacific Watermass is south of 42N. [Ref. 5]. Boundaries separating these zones are dynamic, and demarcation lines serve only as initial positions for observing variability.

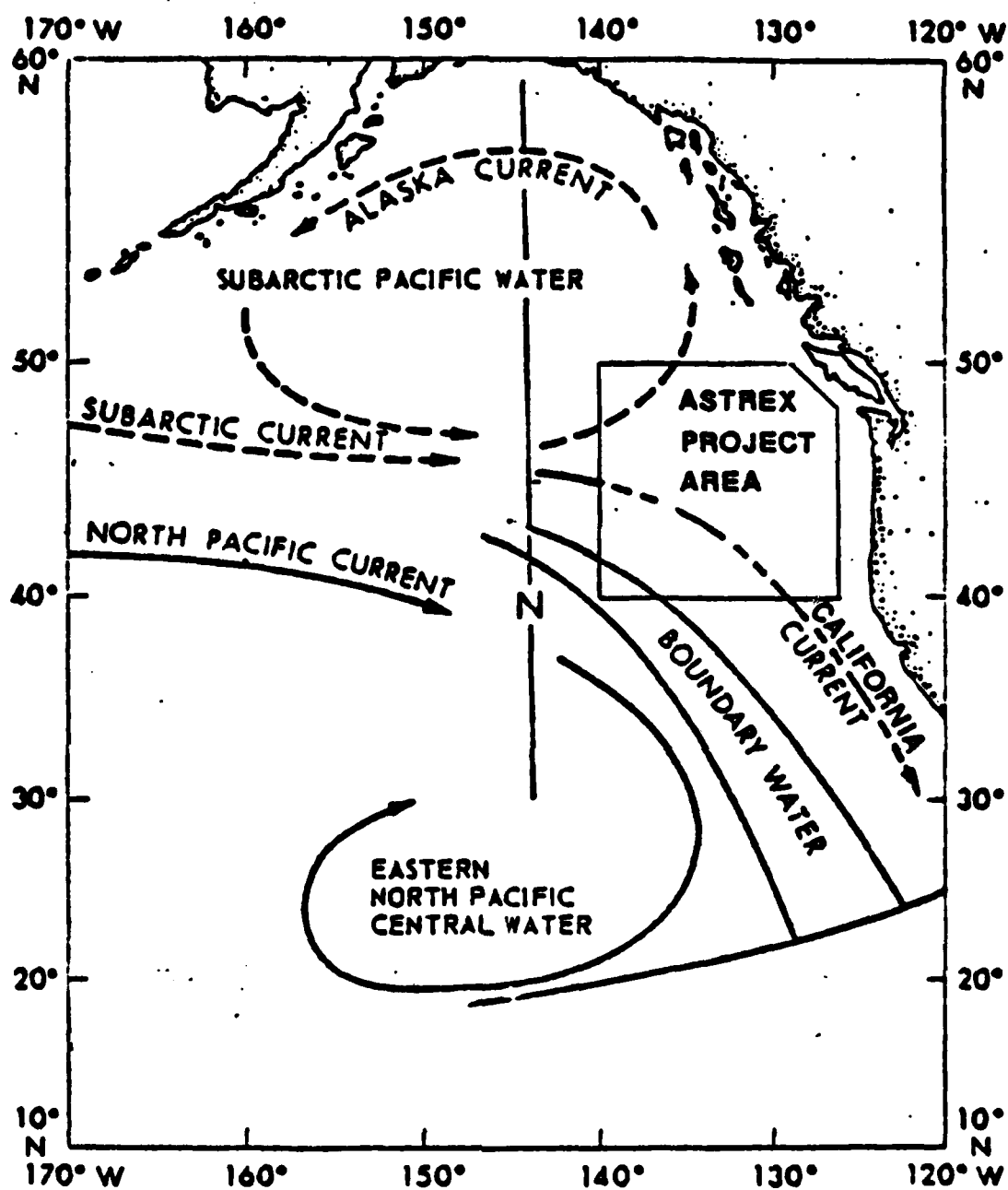


Figure 2.1 Watermasses of the Eastern North Pacific Ocean [Ref. 6].

A seasonal change in the location of these boundaries can be noted from observations of climatological data. These seasonal changes can be related, in part, to weather conditions in the Northeast Pacific. In the winter, the Aleutian Low dominates the atmospheric sea level pressure patterns, and in the summer the region is under the influence of the North Pacific High. These systems both drive the prevailing westerly winds, which give rise to the West Wind Drift in the upper ocean [Ref. 7].

Although the boundaries do vary, the variation of the boundary between the Subarctic and the Subtropic watermasses is low. The position of the front was "relatively constant", between 40N and 42N, as observed by Dodimead et al. [Ref. 8]. Roden [Ref. 9] found the position of the front to vary from 40N to 45N, and stated that this frontal position was highly dependent on the prevailing wind fields. This seems reasonable for a latitudinal boundary as the wind direction remains predominately westerly from month to month, while wind speed in winter is generally twice that of summer [Ref. 10].

Dodimead et al. found that the coastal zone was much smaller in winter than in summer [Ref. 11]. This could be due in part to an increase in wind speed in winter (compared to summer) along a longitudinal boundary that is terminated by the coastal zone and North America.

B. WATER MASS CHARACTERISTICS

The region used for ASTREX contains three water masses. These are: 1) Coastal Water extending from the coast to the California Current (130W); 2) Eastern Subarctic Pacific Water extending southward to about 42N; and 3) Subtropic Pacific Water to the south of 42N [Ref. 12].

Dodimead et al. reviewed the area in terms of various domains. This description shows three zones in the vertical salinity structure: the upper zone, located above a permanent halocline, displays a seasonal variation; the permanent halocline (100-200m) represents the second zone whose vertical extent varies with latitude; below the halocline is the lower zone, which begins at the salinity surface ($S = 33.8$ g/kg), and has gradually-increasing salinity and decreasing temperature with depth. It displays less seasonal variation in temperature and salinity than the upper zone. [Ref. 13].

In the upper zone, the region is influenced by both Coastal and Transitional Domains. The lower zone can be partitioned into the Central Subarctic, Transitional and California Undercurrent Domains [Ref. 14].

The Tabata and Dodimead et al. descriptions vary in approach, but results are similar for the watermass structure of the ASTREX region.

1. Watermass Analysis

The Coastal Watermass, referred to as the Transition Region by Sverdrup, Johnson and Fleming (1942), extends from the coast of California to about 130°W Longitude, where it is bounded by the Eastern North Pacific Central Water (or Subtropic Pacific Water according to Tully, 1964).

Both the southward California Current and the inshore countercurrent (Davidson Current) make the Transition Zone highly variable. By contrast, both the Subarctic Pacific Water and the Subtropic Pacific Water have much less variability over time.

Predominately during spring and summer, upwelling occurs off the California coast. In regions of upwelling, the sea surface temperatures in summer may be lower than in

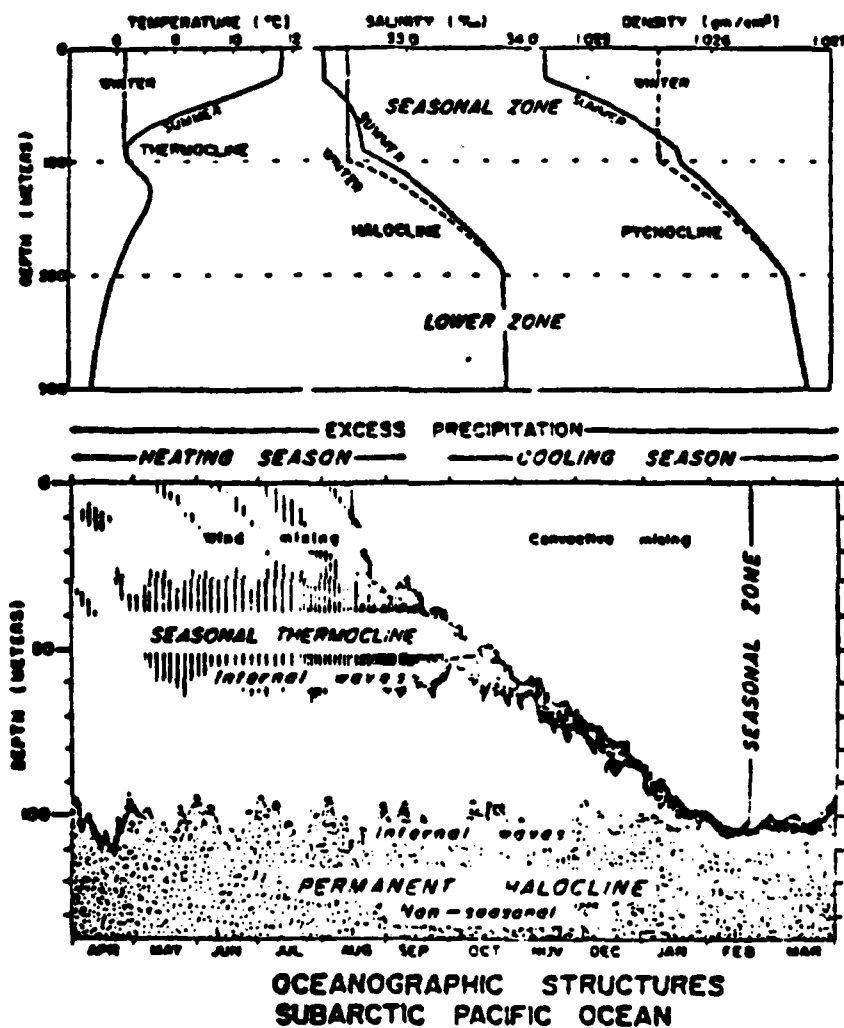


Figure 2.2 Three Zone Structure in the Eastern North Pacific Ocean [Ref. 15].

winter. The Davidson countercurrent continues to flow northward during the upwelling season, but at depths greater than 200 meters. During the winter, the Davidson Current may extend to the surface and flow northward to about 48N.

An examination of monthly mean depths to the top of the thermocline shows a depth variation of 15 to 60 meters at the end of the upwelling season (July-September). A variation of 45 to 90 meters in the depth of the thermocline can be noted at the end of the winter season (January-February). Additionally, in all seasons, the mixed layer deepens with increasing distance from the coast. [Ref. 16].

Close to the coast, in the Transition Zone, salinity and temperature structures will be affected by both upwelling and coastal run-off. With increasing distance from the coast, a more stable structure develops. West of 130W, salinities at the surface are 32.5 to 33.0 g/kg, increasing to about 33.0 to 33.5 g/kg at 120 meters depth.

The Eastern Subarctic Pacific Watermass is characterized by three layers. The upper layer (surface to approximately 100 meters) is seasonal in structure. In winter this layer is well-mixed, but in summer a sharp thermocline and a halocline form in this layer. The second layer is the "principal" halocline (from 100 to 200 meters) which marks the transition from the seasonal layer to the "stable" deep layer. In the deep or lower layer (depths greater than 200 meters), the salinity increases with depth and the temperature decreases. At 1000 meters depth, the temperature is 2.8C and salinity is 34.4 g/kg.

By contrast, the Subtropic Pacific Water has no permanent halocline. Rather, it shows a salinity decreasing with depth to a minimum between 200 and 800 meters. Temperature is the dominating factor in the formation of the seasonal layer. The upper zone, which displays seasonal

temperature variations, extends to a depth of about 150 meters, beyond which a permanent thermocline exists. This seasonal zone is isothermal to a depth of 150 meters in early spring, shallowing to a depth of 40 to 60 meters during the summer and into fall.

2. Domain Analysis

By partitioning the area into well-defined domains, a more detailed description of the water masses can be made. However, there are few clear-cut boundaries in either the upper or lower zones, and the halocline vanishes in certain situations [Ref. 17].

The upper zone of the test region is a combination of Transitional and Coastal Domains. The Coastal Domain has a thermal structure which is very dependent on location. Such location-dependent processes as river run-off, heating and cooling, and wind cause the Coastal Domain to be highly variable from place to place [Ref. 18].

The Transitional Domain can be identified by relatively warm waters ($T > 15^{\circ}\text{C}$ in summer and $T > 7^{\circ}\text{C}$ in winter), and relatively high salinities ($S > 32.2$ g/kg at the surface and $S > 33.4$ g/kg at the top of the halocline). In the test region however, the salinities may be somewhat lower [Ref. 19] (as discussed earlier, mean salinities at the surface in the test region were 32.5 to 33.0 g/kg; at the top of the halocline the salinities were 33.0 to 33.5 g/kg).

Based on the domain description, the upper zone of the test region can be characterized by a layer of water approximately one hundred meters deep, which varies seasonally. This upper zone shows an increase of salinity with depth to the halocline when it exists. An even stronger increase of salinity occurs through the halocline ($.003 \text{ g/kg/m} < \text{GRAD } (S) < .008 \text{ g/kg/m}$). At the bottom of

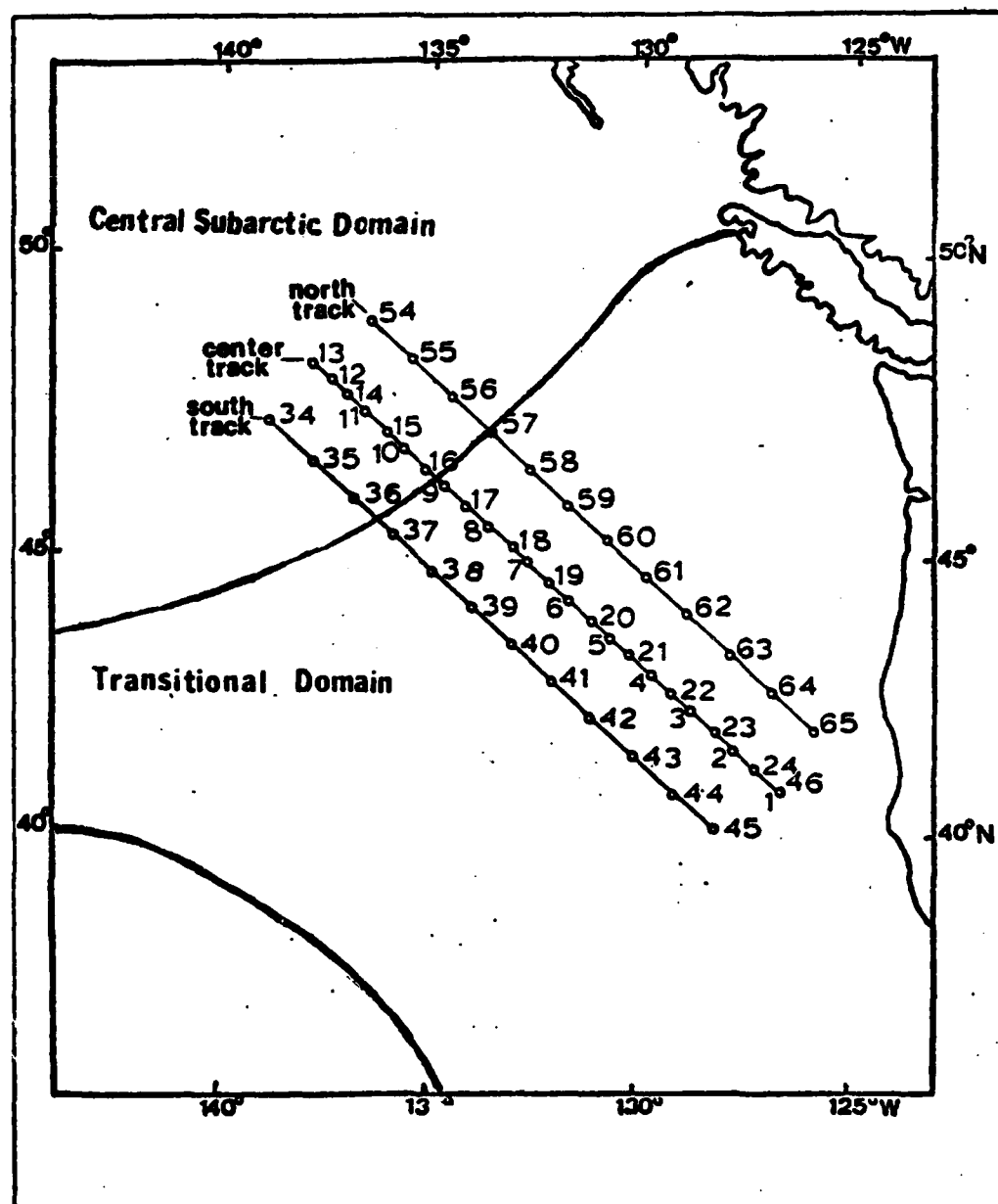


Figure 2.3 Domains in the ASTREX Region.

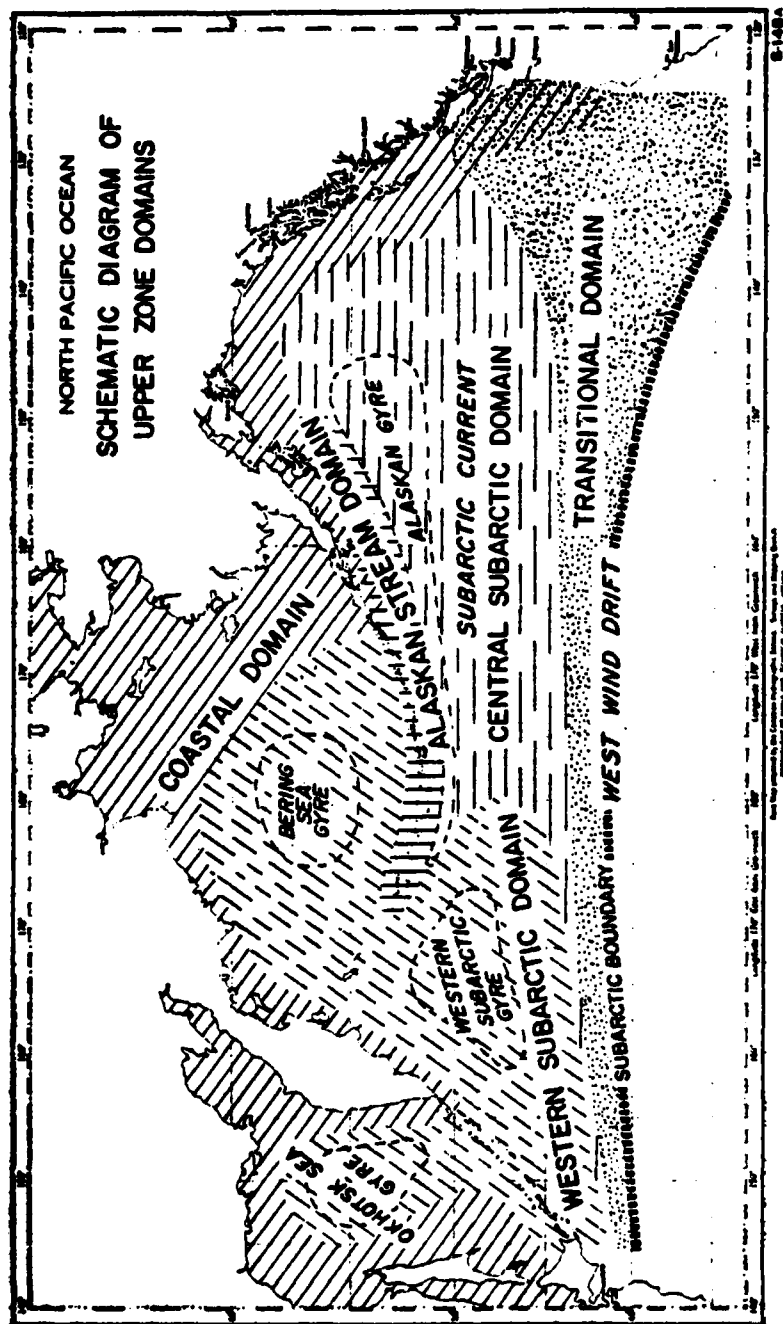


Figure 2.4 Upper Zone Domains [Ref. 20].

the halocline the salinity approaches 33.8 g/kg. Also, a temperature minimum may occur at the bottom of the upper layer [Ref. 21].

The upper zone responds to atmospheric affects and shows much more variability than does the lower zone. The halocline acts as a "permanent boundary" between the upper zone and the lower zone. Compared to the upper zone, the lower zone has a stable salinity structure. [Ref. 22].

A second halocline forms in the upper zone during the summer. This halocline begins at 10 to 30 meters depth and is due to the mixing effects of the light summer winds. Below this secondary halocline (which can extend to 75 meters), the water is nearly isohaline down to the principal halocline (100 to 200 meters depth in the Subarctic Water) [Ref. 23].

The lower zone of the test region can be partitioned into (at most) three domains, depending on the season. These lower domains are the Central Subarctic, Transitional, and the California Undercurrent [Ref. 24].

The Central Subarctic Domain is typical of the lower layer water in the northwest corner of the test region. This is also the water type associated with OWS-P. Dodimead et al. identify this domain as water underlying a well-defined halocline. At OWS-P, the halocline is defined by a salinity gradient of 0.01 g/kg per meter. The salinity increases with depth very slowly in the lower layer [Ref. 25].

The Transitional Domain underlies its surface counterpart throughout the southern half of the test region and also extends through the northeast quarter of the region. Near the coast, both this domain and the California Undercurrent can exist. The Transitional Domain is strongly influenced by the major geostrophic currents in the area.

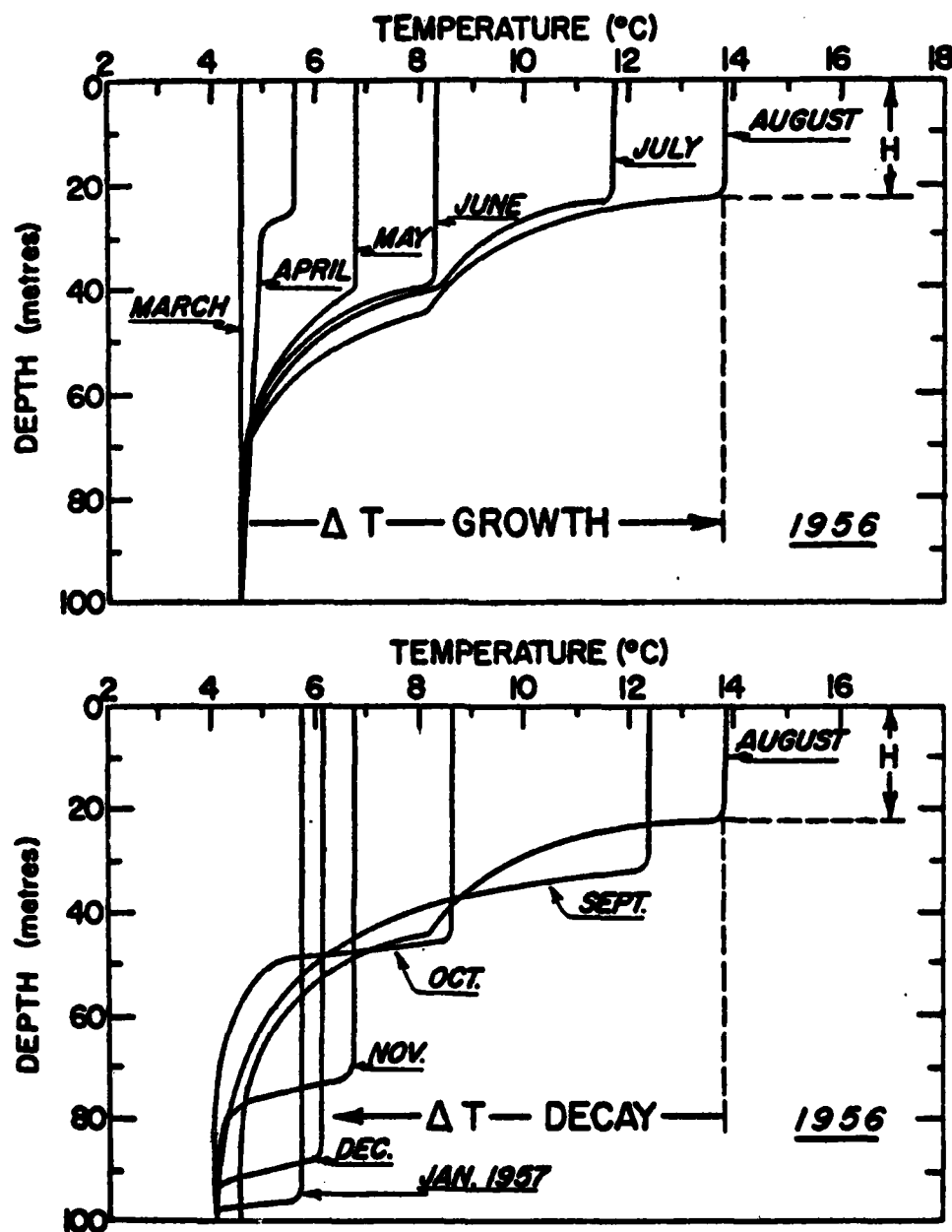


Figure 2.5 Growth/decline of the Thermocline at OWS-P [Ref. 26].

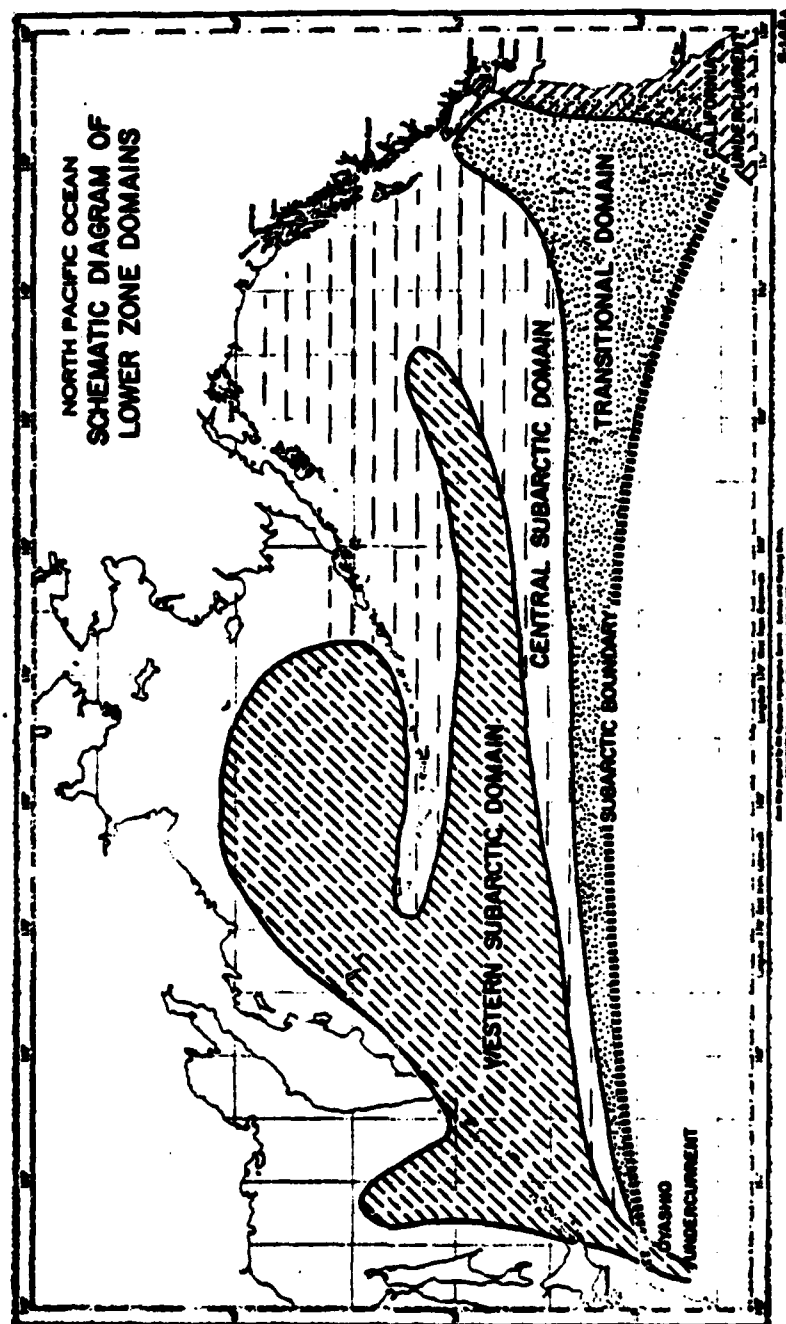


Figure 2.6 Lower Zone Domains [Ref. 27].

It is a narrow band underlying the West Wind Drift and broadens as this current separates to form the Alaskan and California currents. In the Transitional Domain the halocline is less pronounced than in the Central Subarctic Domain. The Transitional Domain bridges the gap between the strongly-layered Subarctic Water and the Subtropical Water which has no distinct halocline [Ref. 28].

The third lower domain present in the test area is the California Undercurrent Domain. As the name implies, this domain is influenced principally by the subsurface countercurrent which runs northward near the coast. The countercurrent originates in the warm water of the Eastern Central Pacific Water. Dodimead et al. characterizes California Undercurrent water by temperatures greater than 6C on the 34 g/kg surface of salinity, as opposed to the Transitional Domain defined at a salinity of 33.8 g/kg with temperatures less than 6.5C [Ref. 29].

3. Temperature Structure

The salinity structure of the eastern North Pacific provides a relatively stable basis for defining water masses in the area. However, characterization of water masses requires a salinity-temperature relationship as well. The true variability of acoustic conditions in the eastern North Pacific must come from periodic and/or random variations in temperature which are superimposed on the basic density structure determined by salinity. Of course, salinity variations may be of importance in the coastal regions too, where significant intrusions of fresh water or more saline upwelled water may occur.

At OWS-P, the temperature of the upper zone has an annual periodic variation, reaching a maximum in the late summer, and a minimum in late winter. The maximum annual

temperature variation noted between 1956 and 1962 was about 9C. Variations of temperature in the entire upper zone followed the same cycle as sea surface temperature, appearing to be in phase with the periodic sea surface temperature variation [Ref. 30].

As with salinity, the temperature variations are greatest in the upper zone. The temperature range decreases from a maximum of 9C in the upper 50 meters to less than 3C variation at 125 meters depth. Below the halocline, the small temperature variation with depth (gradient) should be reasonably well predicted from monthly climatological data.

In the upper zone, a seasonal thermocline begins to develop in spring with the advent of the heating season. The isothermal March layer becomes a two-layer medium through April when a seasonal thermocline begins to develop at about 30 meters. This seasonal thermocline reaches a maximum depth of about 50 meters, depending on the strength of the prevailing winds, but can be expected to occur between 30 and 50 meters during the spring and summer. The thermocline shows the strongest gradient in late summer (August-September), when it is at its shallowest depth (30 meters) [Ref. 31].

With the advent of autumn, the cooling season begins. The seasonal thermocline deepens throughout the cooling season due to the effects of colder surface water and increased mixing caused by the strong winter winds.

The seasonal thermocline forms, coincident with the formation of the secondary or seasonal halocline. This thermocline is very stable, and hence, the structure of the upper zone is quite predictable [Ref. 32]. The seasonal thermocline and permanent halocline locations can be used as inputs to predict the vertical structure of the upper 100 meter layer during the heating and cooling seasons. Sea

surface temperatures may provide input regarding the strength of the seasonal thermocline (gradient) since both the layer thickness and the temperature at the bottom of the thermocline remain relatively constant.

Characteristics of the Subarctic Water are found in the waters which comprise the Transitional Domain. Waters in the Coastal Domain, on the other hand, will vary from the Subarctic Water structure. Coastal Waters remain very near the coast in winter, but extend further seaward in the summer. The primary effect of mingling Coastal Waters with Transition Water will be on salinity structure. The Coastal Water tends to be less saline than Transition Water. A winter section of temperature and salinity taken through the test region in 1959 indicated a narrow zone of coastal influence (to about 130W), which showed as an increase in temperature and decrease in salinity from the Transitional Domain. A summer section at the same latitude showed a strong coastal influence out to 130W; the temperatures were much warmer and salinities much lower in the Coastal Domain than in the Transitional Domain.

C. METEOROLOGY OF THE EASTERN NORTH PACIFIC OCEAN

The discussion of the meteorology of the ASTREX region and the northeast Pacific Ocean will be limited to factors which affect spaceborne instruments, rather than those factors which influence the circulation and heat transfer in the area.

The most obvious path interference encountered by a spaceborne instrument is atmospheric moisture in the form of clouds. During ASTREX, clouds obscured most of the satellite field of view on every measurement day. Since the purpose of the experiment involved studying the effects of North Pacific storms, cloudiness was an unavoidable obstacle

for the secondary mission of comparing satellite data to In Situ observations. Winter cloudiness in the North Pacific is a major problem for visual and infrared imaging of the ocean surface.

The meteorological phenomena which directly affect space-based ocean viewing instruments are aerosols in the form of moisture and salts. Moisture, in its obvious forms of clouds and rain, severely degrades passive observation instruments which rely on visual or infrared energy. Passive microwave radiometers suffer degradation when the viewing area includes severe rains.

The Navy Marine Climatic Atlas of the World [Ref. 33] was consulted to determine climatic conditions in the Eastern North Pacific in November and December. For both months, cloudiness greater than 4/8 can be expected about four days in five. This represents a severe degradation for visual and infrared imaging of the North Pacific waters in November and December.

Precipitation reported in the Atlas increases from 19 percent in November to about 24 percent in December. In other words, rain occurs about one day in five in November and one day in four in December. Rain constitutes an interference effect for passive microwave systems and total degradation for visual and infrared systems.

Relative humidity was reported as greater than 90 percent one day in five in November and one day in four in December. This follows the precipitation variation. Maul and Sidran [Ref. 34] reported on effects of water vapor at 45N and 60N. From their report, water vapor content in the atmosphere over the Eastern North Pacific (between 40-50N) can cause a temperature error of the order of 2 degrees Kelvin in winter and 6 degrees Kelvin in summer. These errors represent the difference between uncorrected

satellite sea surface temperature observations and actual
sea surface temperatures.

III. SATELLITES IN OCEANOGRAPHY

A. INSTRUMENTS FOR OBSERVING THE OCEANS

1. Visual and Infrared Imaging

Several series of satellites have both visual and infrared capabilities. Among these satellites are the GOES series, Nimbus series, and NOAA series. Stewart (1981) presents an excellent summary of satellite instruments used for oceanography. He also lists the satellites which carry oceanographic instruments and the specific instruments each satellite carries [Ref. 35].

The Geostationary Observational Environmental Satellite (GOES) system is composed of two satellites in geosynchronous earth orbits over the equator. The satellites, designated GOES-East (subpoint at 75 degrees west Longitude) and GOES-West (subpoint at 135 degrees west Longitude), scan the earth, with overlapping coverage over the Americas, from Africa to the western Pacific Ocean [Ref. 36].

The GOES satellites, using the visible and infrared spin scan radiometer (VISSR), can scan the full disk of the earth in 18.2 minutes and generate an image every thirty minutes [Ref. 37]. Figure 3.1 is a visual image produced by the GOES VISSR. Table I lists the spectral channels and resolutions for the VISSR. Figure 3.2 presents the atmospheric transmission windows for the visible and infrared portions of the electromagnetic spectrum.

GOES can provide near-real-time coverage of oceanic areas in the Atlantic and Pacific Oceans. GOES imagery was utilized during the STREX experiment as a meteorological

TABLE I

Visible and Infrared Spin Scan Radiometer (VISSR)
Channelization.

Channel	Spatial Resolution (at subpoint)	Wavelength (micrometers)
Visible	1 km	0.55 - 0.75
Infrared	8 km	10.5 - 12.6

Note:

1. Pett et al. list spatial resolution for the visible channel as 0.5 nautical miles, and 5 nautical miles for the infrared channel.

aid. GOES images of sea surface temperature are useful for studying oceanic circulation, but the spatial resolution is not as good (8 km) as the resolution from satellites in low earth orbits, such as NOAA-6 (1.1 km resolution at infrared wavelengths).

The Nimbus-7 spacecraft carries the Coastal Zone Color Scanner (CZCS), which is a visual radiation instrument centered in specific wavelength bands to measure concentrations of phytoplankton in the ocean. Table II shows the wavelengths for indicated CZCS channels.

The Advanced Very High Resolution Radiometer (AVHRR) is a five-channel instrument used on the NOAA-6 and NOAA-7 spacecraft. The AVHRR on the NOAA-6 has one visual channel and three infrared channels (the fifth channel is a repeat of channel four). NOAA-7 utilizes all five channels. The AVHRR has a ground resolution of 1.1 km in all channels. In the daytime, the first two channels (visible and far red to near IR) can be used to filter cloud-contaminated infrared measurements. Channel three (3.5-3.93 μm) can only be used at night because of severe contamination by reflected solar energy. Channel four (10.5-11.5 μm) can be used day or night for measuring sea surface temperature.



Figure 3.1 GOES Visible Image (Full Disk) [Ref. 38].

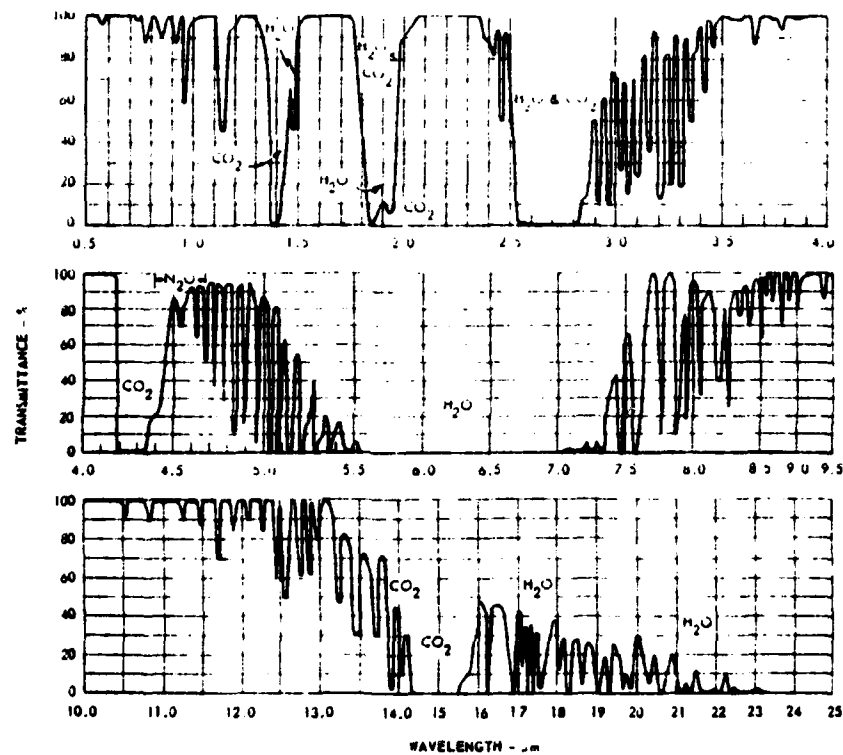


Figure 3.2 Atmospheric Transmittance (Visible and Infrared Spectra) [Ref. 39].

TABLE II

Coastal Zone Color Scanner (CZCS) Channelization.

Channel	Wavelength (micrometers)		
1	0.433 - 0.453	(blue)	
2	0.510 - 0.530	(green)	
3	0.540 - 0.560	(green)	
4	0.660 - 0.680	(red)	
5	0.700 - 0.800	(far red/near IR)	
6	10.5 - 12.5	(far IR)	

Note:

1. Channel 6 failed in 1979.
2. Resolution is approximately 1 km for all channels.

Table III is adapted from both Reference 36 and 37. It lists the AVHRR spectral channels for the AVHRR/1 and AVHRR/2.

TABLE III

Advanced Very High Resolution Radiometer (AVHRR)
Channelization

Channel	Wavelength (micrometers)		
1	0.58 - 0.68	(visible)	
2	0.725 - 1.10	(far red-near IR)	
3	3.55 - 3.93	(middle IR)	
4	10.5 - 11.5	(far IR)	
5	11.5 - 12.5	(far IR)	

Note:

1. Spatial resolution at satellite subpoint is 0.5 nautical miles (1.1 km).
2. Channel 4 wavelength is 10.3 - 11.3 um for all AVHRR/2 instruments.
3. Channel 5 added to further enhance sea surface measurements in the tropics.

The noise equivalent temperature (NETD) of the AVHRR is less than 0.12 degrees Kelvin for a 300 degree Kelvin scene [Ref. 40]. The temperature sensitivity for the channels is approximately 0.5-degrees-Kelvin when viewing a 300-degree-Kelvin scene. Since the noise equivalent temperature of the system is less than the temperature sensitivity of the channels, identification of thermal gradients on the order of 0.5-degrees-Kelvin per kilometer is feasible.

In Chapter two, the meteorological phenomena which interfere with visible and infrared imagery of the ocean surface were discussed. The following discussion deals with the AVHRR and techniques used to compensate for atmospheric effects. The AVHRR measures a "brightness temperature" of the sea surface, and the actual temperature can be computed using physical radiation laws. The sea surface temperature is calculated from the brightness temperature by correcting for attenuation and emission of the atmosphere. The radiometer is calibrated on board the spacecraft by having the instrument view deep space (approximately 2-degree-Kelvin black body), and the radiometer housing (monitored by thermistors). The multi-channel simultaneous imaging of the sea surface forms the basis for the atmospheric corrections used for the AVHRR measurements.

Deschamps and Phulpin [Ref. 41] proposed a multispectral correction method which is the basis for the AVHRR measurement accuracy of sea surface temperature. The simultaneous solution of three different "window" measurements removes many non-linearities caused by atmospheric effects and approximations used to calculate radiances. The cost of improving atmospheric corrections is an increase in the noise equivalent temperature of the system.

The AVHRR/1 (NOAA-6) uses two bands for analysis and atmospheric corrections. The analysis bands are channels three and four. Each channel has a different response to water vapor in the atmosphere. The variation of response of the two channels makes the corrections more reliable. However, channel three operates very near the five micrometer wavelength where solar energy is about equal to the emitted energy of a 300-degree-Kelvin black body (sea surface). Therefore, channel three is a night channel. Channel four can be used day or night.

Leitao et al. [Ref. 42] discuss the use of satellite infrared imagery to locate the northern surface boundary of the Gulf Stream. They conclude that the maximum sea surface temperature gradient is a good approximation to the location of the northern boundary.

A problem with determining sea surface temperature gradients from space is the variability of the atmosphere. Maul [Ref. 43] discusses the effects of the atmosphere on ocean surface thermal gradients. In a moist atmosphere, a thermal gradient can be reduced to less than half of its actual value by the atmosphere.

2. Passive Microwave Radiometry

The latest instrument used for passive microwave observations of the earth is the Scanning Multi-frequency (channel) Microwave Radiometer (SMR). This instrument is operational on NIMBUS-7. Sea surface temperatures are calculated from brightness temperatures measured at 6.6 gigahertz (4.54 cm wavelength). At this frequency, spatial resolution is generally considered to be 150 km. Test results of the NIMBUS-7 system indicated that resolution cells for the 6.6 GHz channel were 157x156 km [Ref. 44].

Lipes [Ref. 45] referred to the detrimental effects of rain and sunglint (reflection of the sun off of the water surface) on the SEASAT SMNR (a similar instrument is on NIMBUS-7). Rain and sunglint caused the SMNR derived sea surface temperature to be much higher than the actual sea surface temperature. Areas without sunglint or rain were more accurately measured by the SEASAT SMNR.

In addition to problems with rain and sunglint, the SMNR is also susceptible to radio frequency interference (RFI), and severe sidelobe contamination within 600 km of land [Ref. 46]. Improvements in the instrument design and in the ground-based processing design would reduce the sidelobe contamination problem for the SMNR [Ref. 47].

3. Satellite Radar Altimeter

Satellite altimetry presents an active approach to locating water mass boundaries and other density related anomalies in the oceans. The satellite measures height above the surface of the earth. These data, combined with the orbital parameters of the spacecraft, form the basis for measuring the height of the sea surface along the sub-satellite track. The radar altimeter maps the topography of the ocean along the satellite ground track, since the instrument is fixed at nadir and does not scan across track. The ocean topography is the difference between the sea surface and the geoid. Surface geostrophic currents can be derived from the ocean topography generated by a radar altimeter.

Altimeter height measurement uncertainties exist due to atmospheric propagation and ionospheric effects, local deviations of the ocean surface topography from the geoid, and inaccuracies in the satellite orbit. Density gradients associated with geostrophic currents account for a small part of the topographic variations [Ref. 48].

The SEASAT altimeter, accurate to 10 centimeters in absolute altitude measurement, was an excellent instrument for measuring the location of surface geostrophic currents. The GEOS-3 altimeter, accurate to 50 centimeters in absolute altitude, was capable of locating the slope associated with the Gulf Stream by using an averaging process [Ref. 49].

The altimeter is a promising instrument for the future. It is capable of detecting western boundary currents such as the Kuroshio, but the error of the height measurement is still larger than the signal generated by a weak current. A western boundary current will cause the sea surface to rise one meter over 100 kilometers. A 10 centimeter accuracy of height measurement is required to measure such a slope of the sea surface accurately. When the slope of the sea surface is an order of magnitude less than $1\text{m}/100\text{km}$, more accurate height measurements are required.

B. OTHER INSTRUMENTS FOR OBSERVING THE OCEANS

This chapter has been directed toward those instruments which may be of importance to the problem of predicting the mixed layer depth from sea surface temperature. The problem is much more complex than cause and effect between sea surface temperature and mixed layer depth. This report is limiting the scope of the investigation to ascertaining a relationship between sea surface temperature, thermocline gradient, and mixed layer depth, if indeed one exists.

The problem can be expanded to include the effects of wind mixing and heat budget. The space technology needed to provide observations of wind speed, wave height, and temperature has been demonstrated on SEASAT. The SMMR can provide information on the wind speed, in addition to sea surface temperatures. Besides surface topography, the altimeter on SEASAT could provide information on significant wave height.

Additional instruments on SEASAT provided wind velocity (Scatterometer), and surface wave direction and wavelength (SAR). The Scatterometer (SCAT) and the Synthetic Aperture Radar (SAR) are active microwave imagers and not subject to many of the problems encountered by passive systems.

IV. EXPERIMENTAL DESIGN

A. OBJECTIVE

The objective of this investigation was to determine if a relationship between sea surface temperature, mixed layer depth, and thermocline gradient could be established. By reviewing the climatology of the area, and including the sea surface temperature patterns and sub-surface structure, an empirical approach to forecasting the extent of the mixed layer from surface observations and limited bathythermographs was to be developed.

Legeckis and Gordon [Ref. 50] found that satellite-derived sea surface temperature fronts corresponded to deep-reaching subsurface temperature structure. They also concluded that the observed mixed layer depth correlated with the surface temperature patterns observed for the Brazil Current and two warm core eddies.

Blackstone and Whritner [Ref. 51] studied the persistence of observed sea surface temperature patterns to a depth of 1000 feet off the coast of southern California. Air-dropped Expendable Bathythermographs (AXBT) were employed to examine regions which displayed a strong sea surface temperature gradient in Defense Meteorological Satellite imagery. The AXBT's provided observations of the vertical temperature structure associated with the observable sea surface temperature patterns. From analysis of temperature patterns at various depths, Whritner and Blackstone observed that the temperature gradient associated with sea surface temperature patterns was still recognizable at 1000 feet.

Leitao et al. [Ref. 52] found that the maximum sea surface temperature gradient (as observed from space) was useful for approximating the northern surface boundary of the Gulf Stream.

B. DATA ACQUISITION

In November and December of 1980, the Naval Postgraduate School conducted the Acoustic Storm Transfer and Response Experiment (discussed in chapter 1). As part of this experiment, Air-Dropped Expendable Bathythermographs (AXBT) were placed along the same track on six days. There were three flights in November, covering the center track. In December, another three flights were conducted. The center track was again covered three times, but on the last two flights, tracks offset from the center also were flown. The offset tracks necessitated a reduction in the number of stations which could be taken along either the center track or the offset track [Ref. 53].

Satellite observations of sea surface temperature were collected from infrared imaging by the Advanced Very High Resolution Radiometer (AVHRR) on board the NOAA-6 spacecraft. AXBT's were placed along a 1000-km track (at 55-km intervals). The data from the AXBT's were digitized in five-meter increments of depth (see Figures 4.1 and 4.2), and the printed output was used to construct the vertical cross-sections of temperature used in this thesis.

In addition to temperature soundings collected from the AXBT's, soundings were made from a research vessel in the operating area using a Neil Brown conductivity temperature depth (CTD) microprofiler [Ref. 56].

13191180	3	211216	414800	1275300	60	23	301526	351525	401524	451524	77
01538	51535	101529	151526	201529	251529	251529	301526	351525	401524	451524	77
501521	551502	601446	651338	701239	751174	751174	801128	851102	901069	951050	
1001039	1051023	110 994	115 970	120 961	125 956	125 956	130 935	135 926	140 905	145 894	
150 883	155 875	160 872	165 861	170 849	175 840	175 840	180 830	185 819	190 814	195 802	
200 797	205 791	210 784	215 781	220 776	225 773	225 773	230 773	235 767	240 763	245 756	
250 744	255 744	260 738	265 735	270 725	275 714	275 714	280 713	285 705	290 698	295 692	
300 684	305 676	310 674	315 667	320 665	325 659	325 659	330 652	335 649	340 641	345 639	
350 636	355 632	360 630	365 624	370 620	375 614	375 614	380 612				
14191180	3	222521	41 700	127 0	50 24	24	301298	351295	401294	451292	69
01351	51320	101308	151306	201300	251300	251300	301298	351295	401294	451292	69
501276	551251	601190	651147	701117	751049	751049	801007	85 970	90 943	95 924	
100 913	105 910	110 905	115 889	120 881	125 871	125 871	130 857	135 851	140 846	145 838	
150 827	155 818	160 815	165 808	170 797	175 789	175 789	180 787	185 768	190 768	195 761	
200 756	205 753	210 746	215 738	220 727	225 719	225 719	230 709	235 705	240 702	245 691	
250 684	255 679	260 684	265 666	270 662	275 657	275 657	280 656	285 637	290 635	295 664	
300 641	305 631	310 631	315 627	320 623	325 620	325 620	330 615	335 617	340 614		
15191180	3	223245	404000	1263000	31 1	1	301217	351193	401135	451083	77
01317	51314	101298	151290	201263	251225	251225	301217	351193	401135	451083	77
501018	55 983	60 967	65 953	70 926	75 917	75 917	80 910	85 908	90 892	95 878	
100 875	105 870	110 848	115 833	120 823	125 821	125 821	130 816	135 805	140 803	145 792	
150 787	155 772	160 768	165 753	170 746	175 741	175 741	180 733	185 727	190 722	195 717	
200 711	205 709	210 703	215 698	220 692	225 692	225 692	230 687	235 684	240 682	245 681	
250 684	255 676	260 692	265 687	270 682	275 679	275 679	280 682	285 647	290 644	295 641	
300 631	305 631	310 628	315 631	320 627	325 622	325 622	330 629	335 617	340 606	345 604	
350 601	355 598	360 592	365 588	370 585	375 579	375 579	380 577				

Figure 4.1 Digitized Temperatures at Five Meter Increments [Ref. 54].

CRUISE # 3	LAT	LONG	YMDDAHHMM	DEPTHS OF ISOOTHERMS IN METERS															SST	MLD
				17	16	15	14	13	12	11	10	9	8	7	6	5	4	3		
	42.9	129.2	8011191926				56	61	64	69	91	131	188	276					14.81	58
	43.6	130.1	8011191938				55	59	61	67	93	123	181	283	346				14.43	59
	44.4	131.1	8011191950					52	55	60	66	102	141	235	314				13.95	54
	45.1	132.1	8011192002					54	57	59	66	89	117	202	324				13.14	58
	45.8	133.1	8011192015						60	63	65	80	113	136	315				13.00	62
	46.5	134.2	8011192028							64	66	68	99	129	300				11.98	66
	46.1	133.7	8011192041							61	65	69	88	116	237	324			12.79	64
	45.4	132.6	8011192053							60	63	66	88	115	229	314			12.95	61
	44.0	130.6	8011192121				60	64	66	68	80	110	150	246	331				14.32	64
	43.3	129.7	8011192131				51	53	55	59	78	114	147	252	330				14.35	54
	42.6	128.8	8011192143							75	116	145	201	299	365				15.80	43
	42.2	128.3	8011192159		41	67	73	80	91	104	126	155	216	283					16.04	67
	41.8	127.9	8011192112	2	67	84				71	84	107	140	195	287				15.40	59
	41.1	127.0	8011192225				60			19	50	80	111	167	240				13.51	54
	40.7	126.5	8011192232						7	32	42	52	87	141	212	351			13.17	30

EOF..

Figure 4.2 Digitized Depths of Isotherms [Ref. 55].

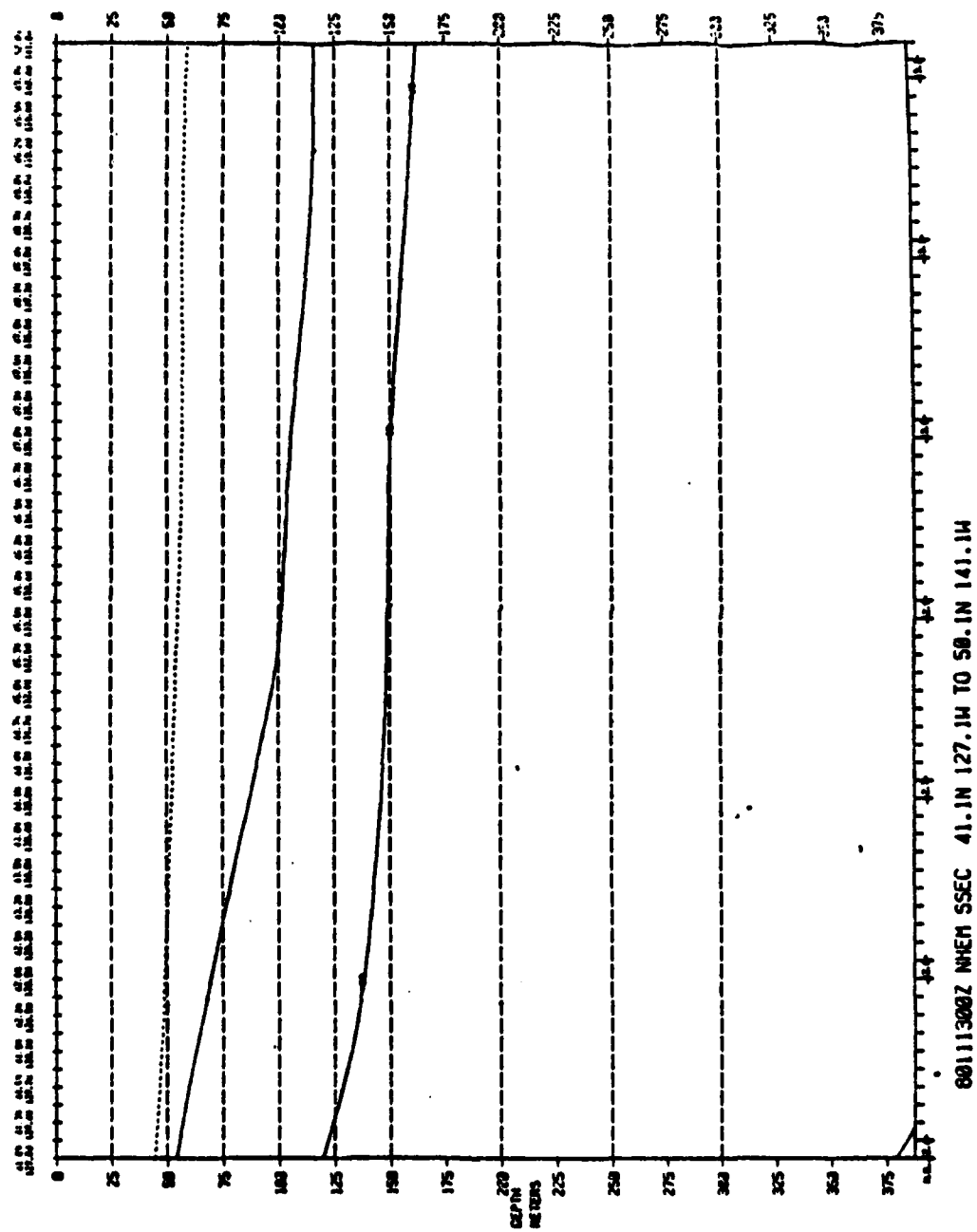


Figure 4.3 PNOC Salinity Profile Along the Flight Track for 13 November.

C. DATA ANALYSIS

1. Data Plots

As a means of beginning an analysis of the possible relationship between sea surface temperature patterns and corresponding patterns of mixed layer depth, vertical cross-sections of temperature for each flight track in ASTREX were constructed. In addition to these transects, sea surface temperature was plotted by position along the flight track as well as mixed layer depth. A correlation was noted visually between track position and both sea surface temperature and mixed layer depth.

The measurements taken with the CTD were in the northwest corner of the ASTREX region. A Fleet Numerical Oceanography Center salinity profile for the track (Figure 4.3) shows very little variation of salinity profiles between stations 2 and 13. Since the variability of salinity in the Northeast Pacific is low, the soundings which were taken with the CTD were assumed to be reasonably representative of the area.

2. Statistical Procedure

Sea surface temperatures and mixed layer depths were taken from Kilonski's [Ref. 57] digitized depths of the isotherms. The mixed layer depth at a location as reported by Kilonski sometimes showed a variation of one meter between the two data formats (digitized temperatures at five-meter increments vs. digitized depths of the isotherms).

To examine variations with position along the track, the outermost station on each flight was assigned as the origin. All other stations were listed by (nautical mile) distance from the origin. For example, station nine was the

outermost station on 19 November. It was assigned the origin position (0.0) for that flight track. The adjacent station (seventeen) is thirty nautical miles from station nine. Therefore, its position is listed as thirty (30).

In addition to position, sea surface temperature, and mixed layer depth, the gradient at the thermocline was considered a necessary factor to include in the list of variables. Four depth intervals were selected for computing gradients in the thermocline. The variations of gradients with track position are plotted in Appendix A (November tracks) and Appendix B (December tracks).

From the vertical cross-sections, an initially small interval was considered necessary for computing the gradient. The smallest interval available from Kilonski's data was five meters. Since the mixed layer depths did not fall on multiples of five meters, the first level above the reported mixed layer depth was used as a reference level for computing temperature changes at the top of the thermocline. For example, if the mixed layer depth was 67 meters, the temperature at 65 meters depth was used as the temperature at the top of the thermocline. To smooth gradient variations caused by this method of defining the temperature at the top of the thermocline, gradients were also computed over intervals of fifteen, fifty, and one-hundred meters.

The computed temperature changes are listed in various tables associated with each flight track. The normalized values of gradient computed from each interval are listed in Appendix C.

The data analysis was done using the interactive statistical computing system MINITAB [Ref. 58]. Basic statistics (means and standard deviations), correlation, and linear regression analysis were performed for each flight track. MINITAB correlation of data resulted in the

computation of the correlation coefficient (r) as discussed in Miller and Freund [Ref. 59].

Three models of mixed layer depth were developed for each flight track. These models were simply the least squares regression of mixed layer depth as a function of sea surface temperature, position, and gradient in the thermocline. If the correlation between sea surface temperature and mixed layer depth was weak, then the model of mixed layer depth as a function of sea surface temperature was ignored.

Regression analysis in MINITAB yields a curve and a coefficient of determination as a measure of the goodness of the curve-fit (the coefficient of determination is the square of the correlation coefficient). To avoid confusion, each of the measures of correlation between various combinations of parameters will be identified whenever used.

D. OBSERVATIONS BY FLIGHT

1. Flight Track One

The vertical temperature cross-section for flight track one is shown in Figure 4.4. Ten stations were used to construct this profile. Isotherms tended to be deeper nearer the coast than out at sea.

A warm water pocket exists between stations four and two. This warm pocket persisted through the vertical extent of the soundings between these stations.

Figure 4.5 shows both the sea surface temperature and mixed layer depth along the flight track. A possible correlation between sea surface temperature and mixed layer depth along the flight track is suggested by the variations of both with position along the track ($r = 0.33$).

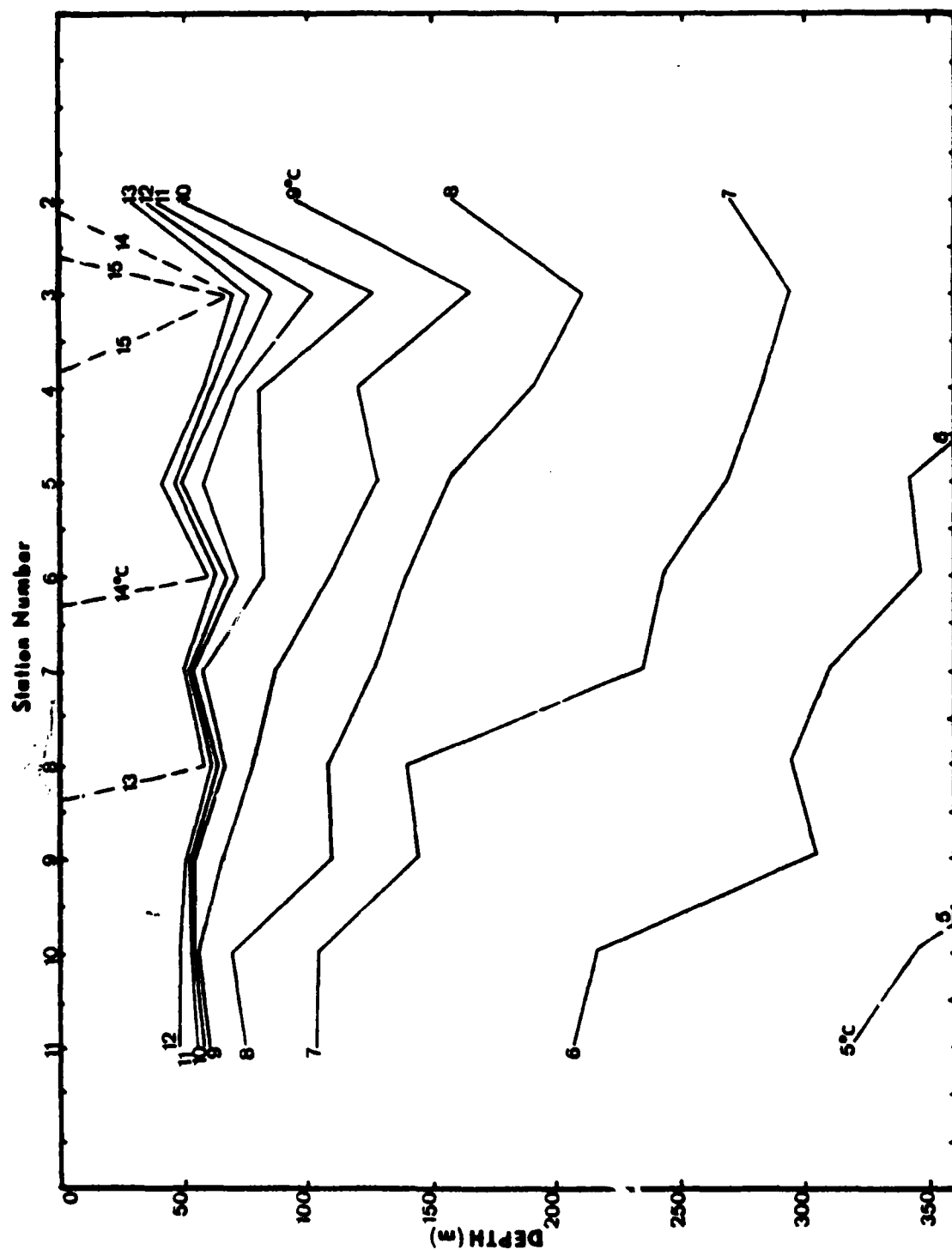


Figure 4.4 Vertical Temperature Cross-section
(15 November).

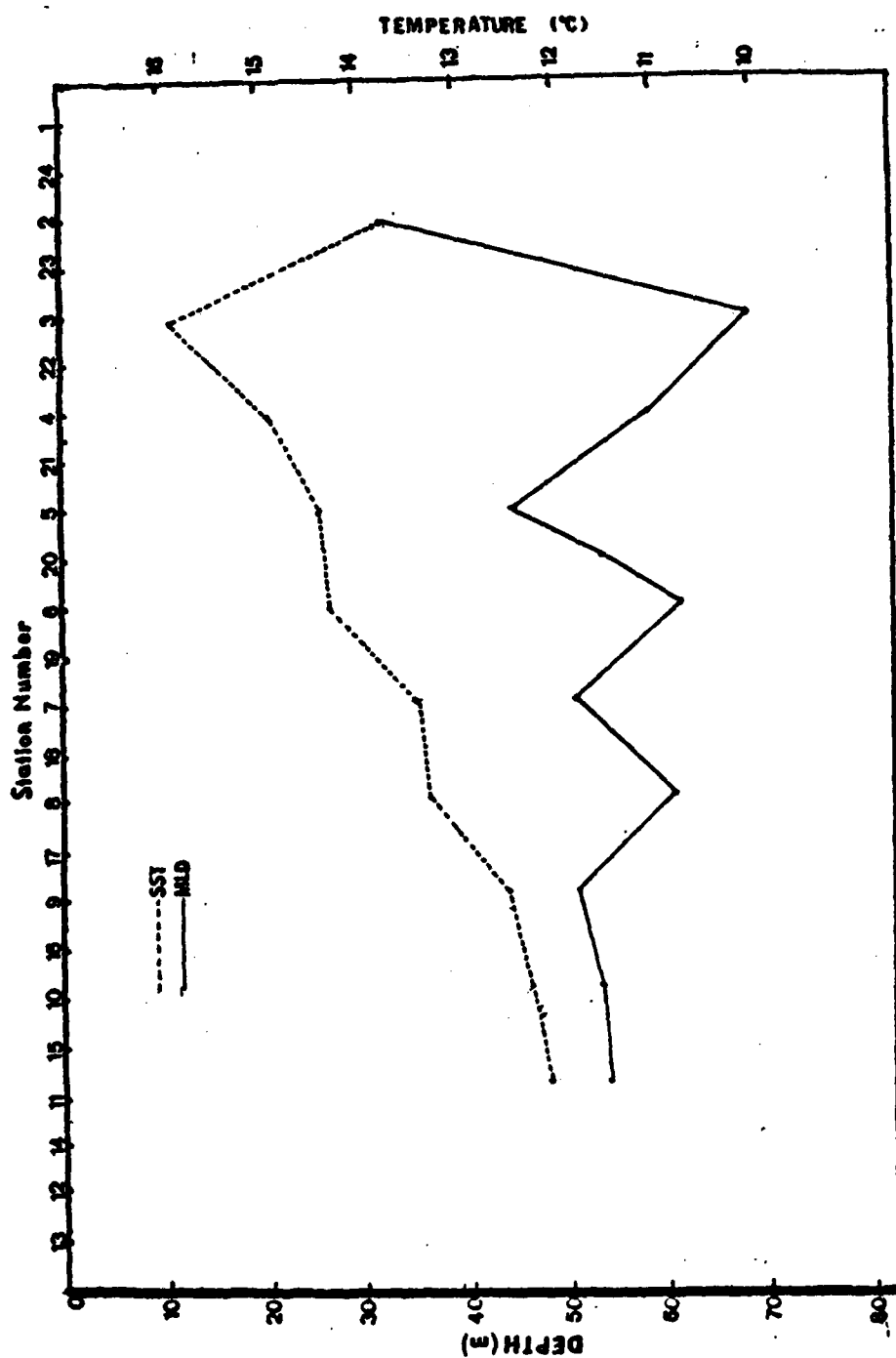


Figure 4.5 Mixed Layer Depth and Sea Surface Temperature (15 November).

For flight one, a strong negative correlation ($r = -0.818$) exists for the gradient computed from the upper five meters of the thermocline. This suggests that the initial gradient at the thermocline weakens in the transition region (coastal waters). The weakening of this initial gradient could also be due to the presence of a warm meander or eddy as suggested by the vertical temperature cross-section.

Table IV lists, by station:

1. position relative to the most-seaward buoy;
2. mixed layer depth;
3. sea surface temperature;
4. temperature change in the upper five meters of the thermocline ($dT/5$);
5. temperature change in the upper 15 meters of the thermocline ($dT/15$);
6. temperature change in the upper 50 meters of the thermocline ($dT/50$); and
7. temperature change in the upper 100 meters of the thermocline ($dT/100$).

Table IV is the matrix which was manipulated to examine correlations between various elements in the problem, and was a source of values in regression analysis for model equations.

Attempts to fit several equations for mixed layer depth were made using various measurable quantities. The results are listed in Appendix D. Table V lists the model variables used and provides the computed coefficient of determination for each model. The most striking relationship occurred for a fit of mixed layer depth as a function of track position, sea surface temperature, and gradient from 100 meters. The coefficient of determination for the fit was 0.88. The correlation (r) between MLD and the function of the three variables was 0.94. Position and

TABLE IV

MLD, SST and Gradients at the Thermocline, 15 November 1980.

Buoy Position	MLD	SST	dT/5m	dT/15m	dT/50m	dT/100m
2	540	32	13.81	1.15	2.86	3.90
3	480	69	15.88	1.41	2.69	4.62
4	420	59	14.86	1.13	3.14	5.35
5	360	45	14.43	1.56	2.58	4.01
6	300	62	14.32	1.70	3.64	5.27
7	240	51	13.41	2.52	3.36	4.22
8	180	61	13.27	1.94	3.33	4.49
9	120	51	12.52	2.48	3.04	4.01
10	60	53	12.33	2.67	3.66	4.74
11	0	54	12.09	1.99	2.88	4.09

Notes:

1. Buoy column indicates station number in vertical temperature cross-sections.
2. position column lists the range (in nautical miles) from the most seaward buoy.
3. dT/5m is the temperature change over the first five meter interval in the thermocline; dT/15 is the temperature change over the first fifteen meter interval in the thermocline; dT/50 and dT/100 follow in the same manner.

TABLE V

Models of MLD for 15 November.

Model Variables	Coefficient of Determination
SST	0.111
SST, Position	0.818
SST, Position, Gradient (100)	0.880

Notes:

1. SST is sea surface temperature.
2. Position refers to station position relative to the most seaward station.
3. Gradient (100) refers to the gradient computed from the upper 100 meters of the thermocline.
4. The coefficient of determination will equal one for a perfect fit of the curve to data.

temperature are easily measured by satellite. Gradient then becomes the primary factor of uncertainty.

2. Flight Track Two

The vertical temperature cross-section for 17 November is shown in Figure 4.6. Twenty-three stations were used to construct this transect. The profile is interesting for three reasons:

1. This flight has no observational "holes" along the track;
2. Satellite imagery from NOAA-6 is available for a portion of the track;
3. The vertical temperature structure of a satellite-observed sea-surface-temperature anomaly can be studied.

At the top of the thermocline, the gradient appears strong between stations 13 and 16 (isotherms are densely packed). Beginning at station nine, the isotherms begin to diverge. This indicates a weakening of the gradient in the upper five to fifteen meters of the thermocline. As with flight one, the initial gradient (from five meters) is inversely correlated with position along this track. The initial strength of the gradient at the top of the thermocline decreases towards the coast.

The location of the divergence of the isotherms at the top of the thermocline (station 9) corresponds to the location of the change from the Central Subarctic Domain to the Transitional Domain as presented by Dodimead et al.

Figure 4.7 is a plot of sea surface temperature and mixed-layer-depth variation with position. From station nine to station twenty-one, the sea surface temperature increases almost linearly with position, while mixed layer depth fluctuates around sixty meters. Satellite imagery

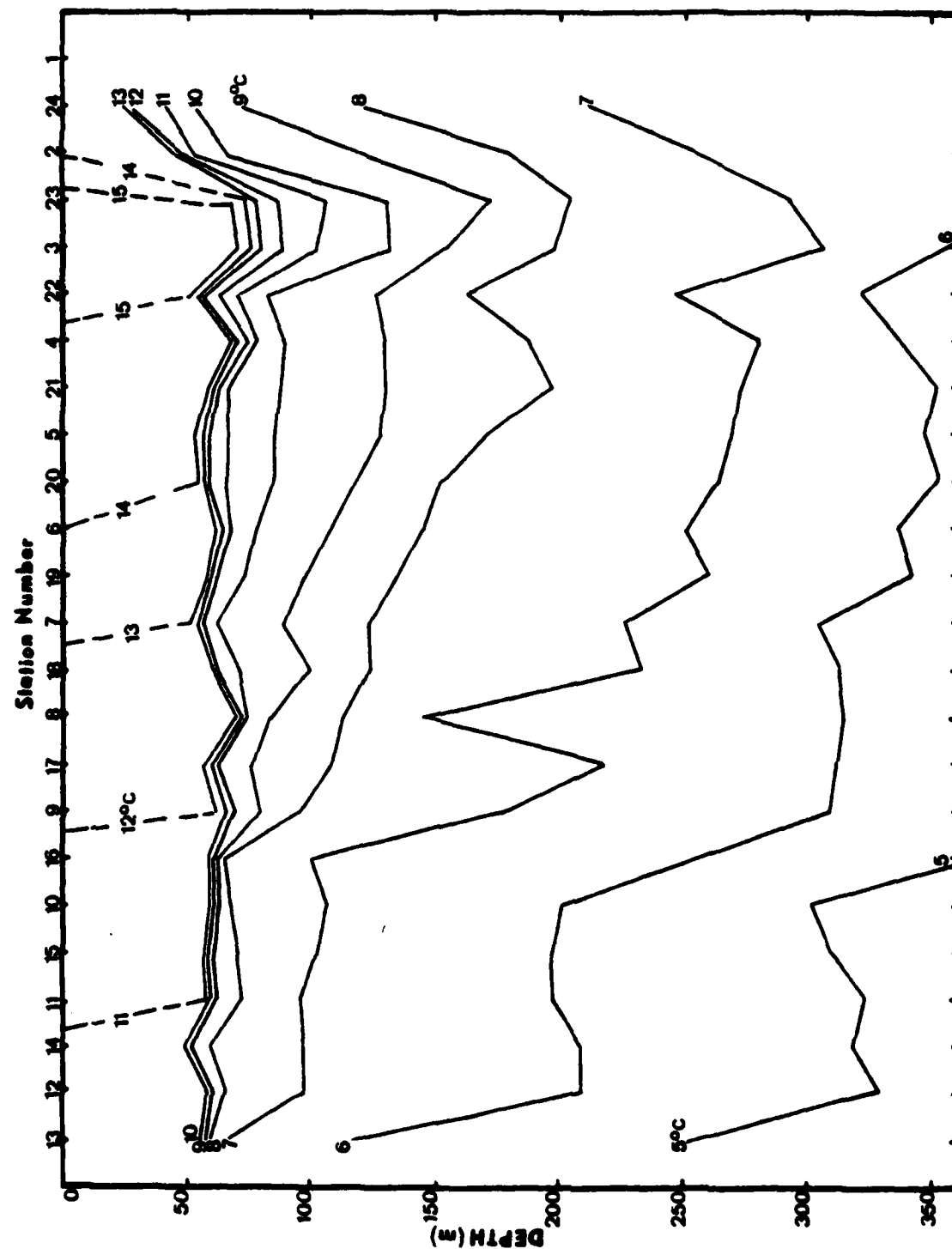


Figure 4.6 Vertical Temperature Cross-section (17 November).

identified a warm meander between station four and station twenty-two (Figures 4.8 and 4.9). This shows up as a rapid increase in sea surface temperature over a (longer) distance from station four to station three. The sea surface temperature reaches a maximum in the vicinity of station three, and then falls rapidly across the southeast wall of the meander. The mixed layer depth also reaches a maximum at station three, and then falls rapidly across the southeast wall. This correlation between sea surface temperature patterns and vertical structure in the vicinity of frontal positions was also noted by Legeckis and Gordon (Ref. 33), cited earlier.

Examinations of this track based on domains and satellite imagery requires that the track be split into three separate sections. The first section, in the Central Subarctic Domain, includes stations thirteen through sixteen. The Transitional Domain is then split using the satellite imagery. One section extends from station nine to station twenty-one. The warm meander then constitutes the final section and includes stations four to twenty-four.

Table VI provides position, mixed layer depth, sea surface temperature, and gradients in the thermocline for each station occupied for flight track two. As with flight one, this table constitutes the matrix used to examine relationships between various elements which may lead to a prediction of mixed layer depth.

Correlations of sea surface temperature and mixed layer depth along the entire track yield low values for the correlation coefficient (r). For the entire track, there is little correlation between sea surface temperature and mixed layer depth ($r = 0.17$). Mixed layer depth as a function of position, sea surface temperature, and gradient from the 100 meter thermocline is better ($r = 0.84$). However, along

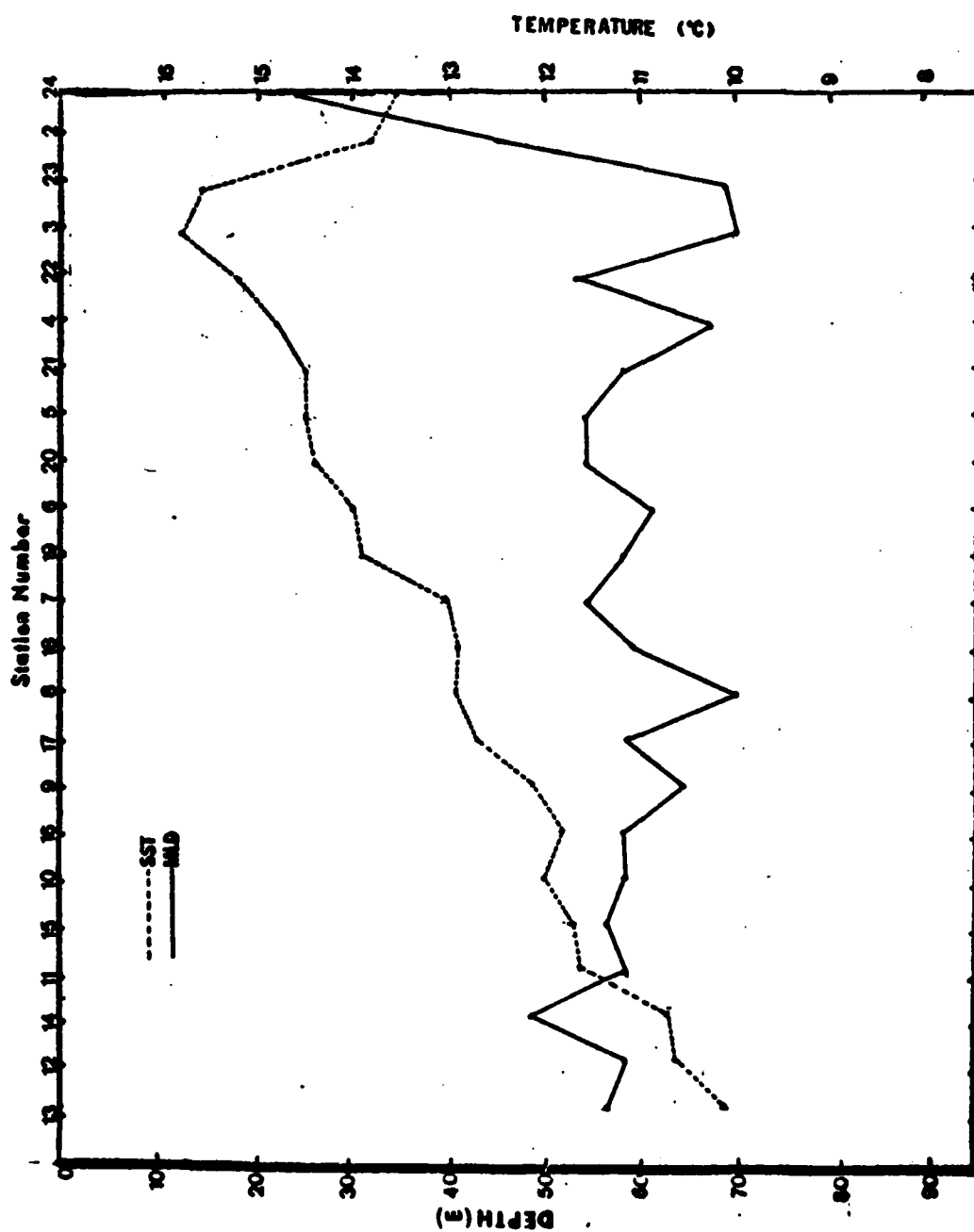


Figure 4.7 Mixed Layer Depth and Sea Surface Temperature (17 November).



Figure 4.8 NOAA-6 Image (17 November) [Ref. 60].

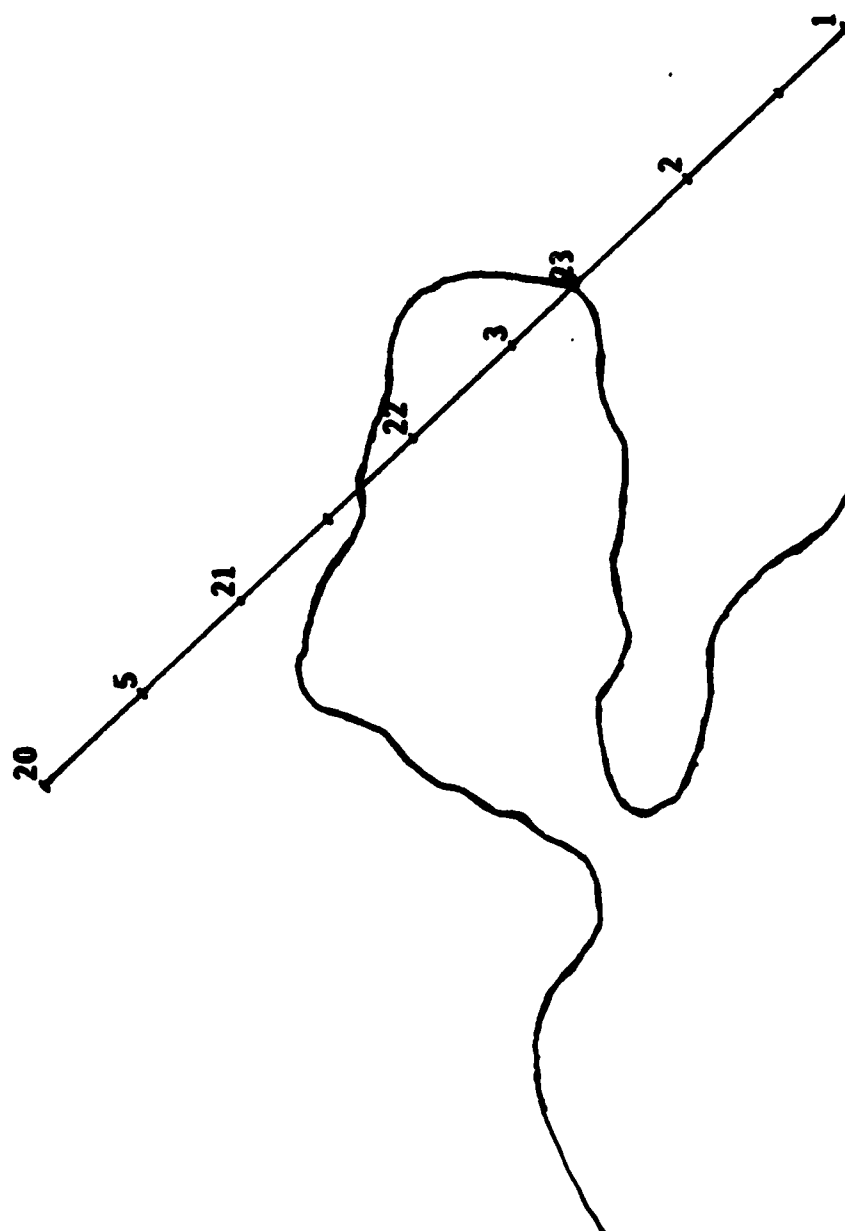


Figure 4.9 Flight Track, Buoy Numbers and Meander Location in Figure 4.8.

TABLE VI

MLD, SST and Gradients at the Thermocline, 17 November 1980.

Buoy	Position	MLD	SST	dT/5m	dT/15m	dT/50m	dT/100m
2	630	45	13.76	1.33	2.35	3.40	3.97
3	570	70	15.80	1.51	2.82	4.77	6.53
4	510	67	14.83	1.48	3.71	5.01	6.04
5	450	54	14.46	1.51	3.47	4.95	6.11
6	390	61	13.97	1.64	2.93	4.09	5.33
7	330	54	13.06	1.69	3.25	4.33	5.70
8	270	70	12.87	2.65	3.35	4.64	5.30
9	210	64	12.14	1.19	2.96	4.36	4.95
10	150	58	11.95	1.67	3.70	4.76	5.52
11	90	58	11.63	2.58	3.39	4.73	5.19
12	30	58	10.61	1.85	2.63	3.87	4.23
13	0	56	10.13	2.47	3.09	3.90	4.25
14	60	48	10.72	1.71	2.68	3.62	4.24
15	120	56	11.71	2.58	3.36	4.47	5.01
16	180	58	11.83	2.08	3.72	4.82	5.25
17	240	58	12.65	1.75	2.88	3.90	4.95
18	300	59	12.90	1.43	2.88	4.07	5.64
19	360	58	13.86	2.66	3.63	5.06	6.22
20	420	54	14.43	1.16	3.55	5.20	6.24
21	480	58	14.51	1.83	3.84	4.84	6.31
22	540	53	15.24	1.80	3.50	5.70	6.70
23	600	69	15.59	0.93	2.64	4.66	6.30
24	660	24	13.54	1.08	1.95	4.28	5.35

shorter track segments, and particularly across the meander, mixed layer depth and sea surface temperature show more correlation than for the entire track. Across the meander, the correlation coefficient for mixed layer depth vs. sea surface temperature is 0.86. This was not the case in either the Central Subarctic Domain ($r = 0.40$) or in the other part of the Transitional Domain ($r = -0.53$).

The mixed layer depth and sea surface temperature did not correlate to any significant degree on 17 November. Therefore, only two models are proposed for this flight track. As stated previously, breaking the track into segments yields a much higher correlation between otherwise uncorrelated parameters. Table VII presents the models for the entire track only.

TABLE VII

Models of MLD for 17 November.

Model Variables	Coefficient of Determination
SST, Position	0.615
SST, Position, Gradient (15)	0.627
SST, Position, Gradient (100)	0.707

Note:

1. Two gradient models were computed because the gradient from 15 meters appeared to be more highly correlated with track position than the gradient computed from the upper 100 meters of the thermocline.

The higher correlation between sea surface temperature and mixed layer depth in the warm meander may provide a means of estimating the depth of the mixed layer in such anomalies through observations of sea surface temperature.

During the interval between flight one and flight two, one storm had traversed the area and another had begun to approach the most western stations on the track. A slight deepening of the 10-degree through 11-degree isotherms occurred. The average mixed layer depth changed from 53.7 meters on 15 November to 57.0 meters on 17 November.

3. Flight Track Three

Figure 4.10 is the vertical cross-section associated with flight track three. Fourteen stations were used to construct this transect. Although there are some holes in the data along the track, this profile presents a picture similar to flight track two.

The gradient at the top of the thermocline diverges beginning at station nine, just as in the previous sections. Again, the gradient computed from the first five meters of the thermocline was inversely correlated with position ($r = -0.766$). The meander discussed for flight two still can be located in this profile between stations four and two.

The sea surface temperature and mixed layer depth variations with position are plotted in Figure 4.11. Table VIII lists the values for mixed layer depth, sea surface temperature, and gradients along the flight track. Between station nine and station six (Transitional Domain) both sea surface temperature and mixed layer depth vary almost linearly. Over the entire track length, however, the correlation between the two is negligible ($r = 0.10$). From station twenty-one to station one (across the meander) the correlation between mixed layer depth and sea surface temperature is much better ($r = 0.51$).

A front moved into the flight track area on 17 November, and became stationary over the area on 18 November. The stationary front caused poor conditions for satellite observations due to clouds. Small changes in sea surface temperature patterns could be expected from the front, but the basic structure remained unchanged from 17 November. The average mixed layer depth for 19 November remained at 57.0 meters. The position and structure of the meander along the track remained unchanged except for the development of a peak temperature exceeding 16 degrees Celsius at station three.

Table IX summarizes the models examined for flight track three. The correlation coefficient computed for sea surface temperature versus mixed layer depth was extremely low ($r = 0.01$). Therefore, the model equation for mixed layer depth as a function of sea surface temperature was

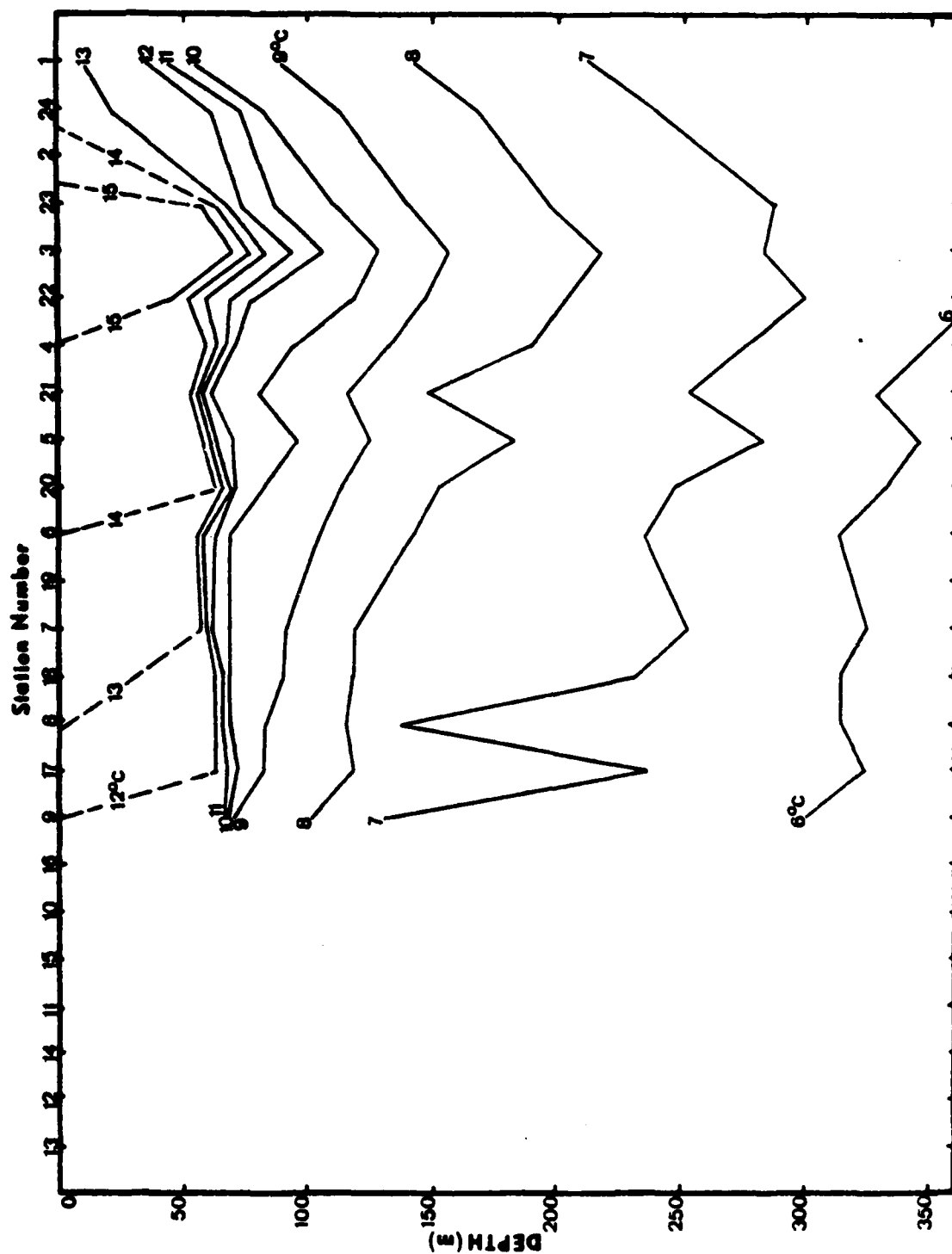


Figure 4.10 Vertical Temperature Cross-section
(19 November).

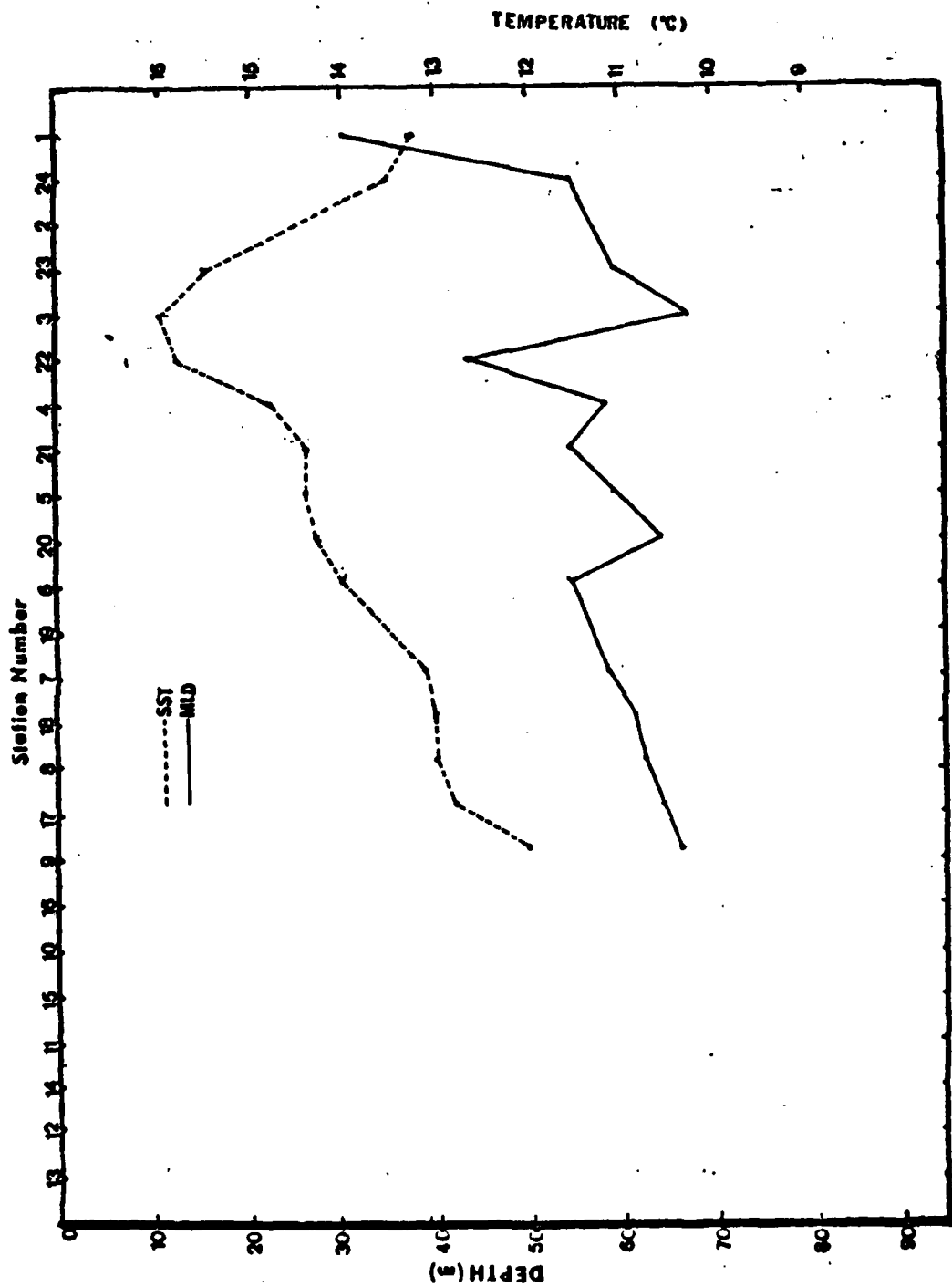


Figure 4.11 Mixed Layer Depth and Sea Surface Temperature (19 November) .

TABLE VIII

MLD, SST and Gradients at the Thermocline, 19 November 1980.

Buoy	Position	MLD	SST	dT/5m	dT/15m	dT/50m	dT/100m
1	480	30	13.17	1.15	2.86	3.90	4.65
3	360	67	16.04	1.41	2.69	4.62	5.92
4	300	58	14.81	1.13	3.14	5.35	6.22
5	240	59	14.43	1.56	2.58	4.01	5.06
6	180	54	13.95	1.70	3.64	5.27	6.49
7	120	58	13.14	2.52	3.36	4.22	5.52
8	60	62	13.00	1.94	3.33	4.49	5.66
9	0	66	11.98	2.48	3.04	4.01	5.30
17	30	64	12.79	2.67	3.66	4.74	5.49
18	90	61	12.95	1.99	2.88	4.09	4.79
20	210	64	14.32	1.15	2.86	3.90	4.65
21	270	54	14.35	1.41	2.69	4.62	5.92
22	330	43	15.80	1.13	3.14	5.35	6.22
23	390	59	15.48	1.56	2.58	4.01	5.06
24	450	54	13.51	1.70	3.64	5.27	6.49

omitted. Instead, a second gradient model was introduced as with flight track two. The gradient from 100 meters was continued as an element in a separate model because this gradient was either the most influential or second most influential of all gradients used in model equations.

The best fit of any model for mixed layer depth was the model based only on sea surface temperature and track position. Both surface temperature and track position are variables which can be derived from a satellite image of the sea surface.

4. Flight Track Four

The vertical cross-section of temperature for flight track four (Figure 4.12) was constructed from 21 stations. It is the most complete transect except for 17 November. A definite cooling has occurred between 17 November and this 1 December track. Surface temperatures dropped by about one degree Celsius (the average sea surface temperature dropped from 13.1 degrees Celsius on 17 November to 12.0 degrees

TABLE IX

Models of MLD for 19 November.

Model Variables	Coefficient of Determination
SST, Position	0.615
SST, Position, Gradient (5)	0.547
SST, Position, Gradient (100)	0.517

Note:

1. Two gradient models were computed because the gradient from 5 meters appeared to be more highly correlated with track position than the gradient computed from the upper 100 meters of the thermocline.

Celsius on 1 December). The gradient in the upper five to fifteen meters of the thermocline is not as strong as along the November flight tracks. Although still negatively correlated with track position, the correlation between gradient and track position is much weaker for this track ($r = -0.16$) than for similar gradients computed from the upper five meters of the thermocline. The meander is still recognizable, but its vertical profile is much less pronounced than during the November flights.

The gradient computed from the upper five meters of the thermocline showed the strongest correlation with position for all gradients computed along flight track four. As noted previously, the correlation between the five meter gradient and position has steadily decreased since the first flight. However, the five meter gradient is the most highly correlated of any gradient with position on each of the four flights.

Mixed layer depth doesn't show much relationship to track position. Sea surface temperature does increase along

the track, but the change across the meander is not as significant as in past flights. Figure 4.13 displays the variation with position for both mixed layer depth and sea surface temperature.

TABLE X

MLD, SST and Gradients at the Thermocline, 1 December 1980.

buoy position	MLD	SST	dT/5m	dT/15m	dT/50m	dT/100m
1	690	51	12.98	1.15	2.86	3.90
4	510	61	14.46	1.41	2.69	4.62
5	450	64	13.30	1.13	3.14	5.35
6	390	69	12.92	1.56	2.58	4.01
7	330	72	11.74	1.70	3.64	5.27
8	270	72	11.82	1.94	3.33	4.49
9	210	61	11.12	2.52	3.36	4.22
10	150	72	10.72	1.94	3.33	4.49
11	90	78	10.77	2.52	3.36	4.22
12	30	70	9.13	2.48	3.04	4.01
13	0	74	8.94	2.67	3.66	4.74
14	60	72	9.51	1.99	2.88	4.09
15	120	69	10.82	1.15	2.86	3.90
17	240	70	11.42	1.41	2.69	4.62
18	300	78	11.70	1.13	3.14	5.35
19	360	74	12.98	1.56	2.58	4.01
20	420	80	13.25	1.70	3.64	5.27
21	480	69	13.54	1.99	2.88	4.09
22	540	66	14.24	2.67	3.66	4.74
23	600	59	14.27	2.48	3.04	4.01
24	660	50	13.06	2.67	3.66	4.74

Table X lists the factors which were examined for flight four. This flight was unusual in that large changes from previous flights occurred in the correlations.

Both sea surface temperature and mixed layer depth had higher correlations with track position than on previous flights. The correlation of gradients with position declined in all four cases examined. Mixed layer depth was more highly correlated with sea surface temperature than on previous flights.

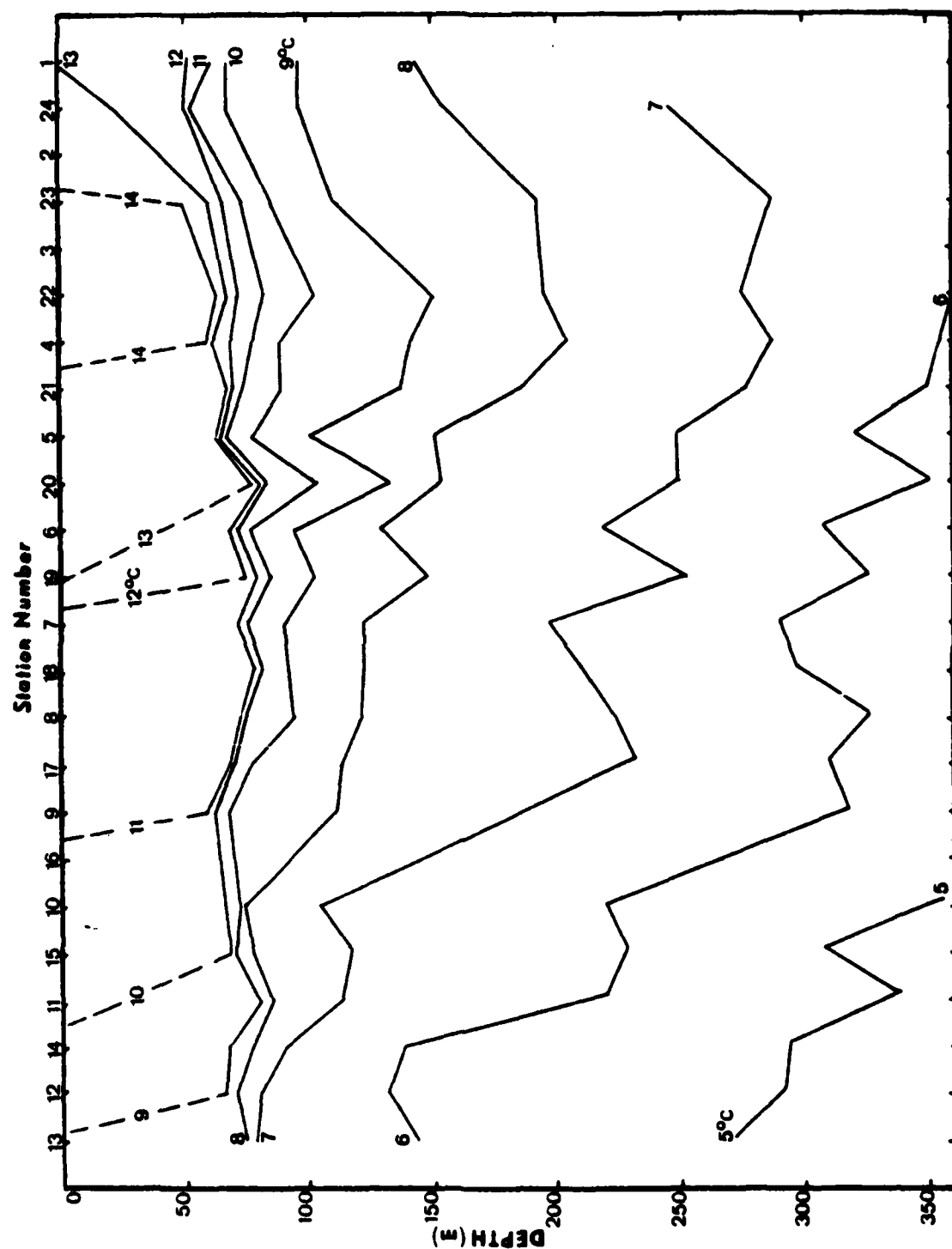


Figure 4.12 Vertical Temperature Cross-section
(1 December).

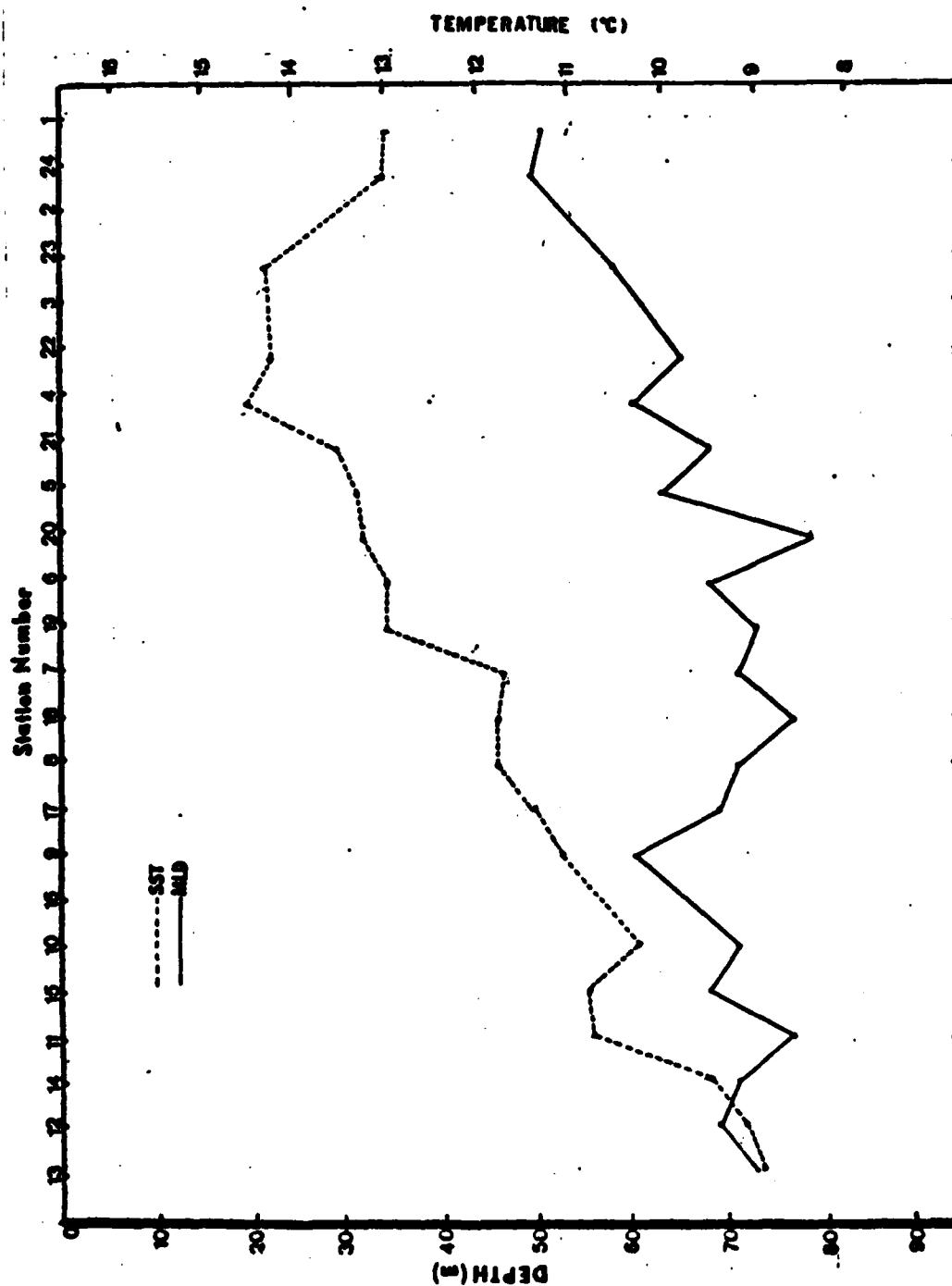


Figure 4.13 Mixed Layer Depth and Sea Surface Temperature (1 December).

Three models are presented for flight four and summarized in Table XI. Since the correlation of sea surface temperature and mixed layer depth was the highest observed of all flights, it is included as a model. Mixed layer depth as a function of track position, sea surface temperature and thermocline gradient showed the best correlation when the gradient computed from 100 meters was used.

TABLE XI

Models of MLD for 1 December.

Model Variables	Coefficient of Determination
SST	0.175
SST, Position	0.609
SST, Position, Gradient (100)	0.663

Note:

1. One gradient model was computed because the gradient from 100 meters appeared to be more highly correlated with track position than any other gradient.

5. Flight Track Five (Center and South)

The fifth flight added another dimension to the AXBT analysis. The southern track, offset by 60 nautical miles from the center track, provided additional information about the extent of the warm meander discussed previously. Figure 4.14, constructed from eleven stations, is the vertical Temperature Cross-section for the center track on 3 December. Figure 4.15, constructed from eight stations,

shows the profile for the southern track. Table XII lists the values for mixed layer depth, sea surface temperature, and gradients along the center flight track. Table XIII lists similar data for the southern track.

The vertical temperature profiles for the two tracks are similar in some respects. The meander is definitely present on the center track. The southern track displays some similar subsurface structure in the area where the meander should be located (between stations forty-one and forty-three). Although station forty-two should be inside the warm meander, the surface temperature at the station is 13.5 degrees Celsius, about one-half degree too low to be a part of the meander. The closed warm pocket of water is not present in the southern track (the center track has a closed pocket of 14 degree Celsius water).

The meander/eddy influence appears to be present to about 290 meters in both tracks. The southern track does not have the pronounced structure shown along the center track. Although some signs of the meander remain in the southern track, the meander appears to have formed a closed circulation.

Along the center flight track, sea surface temperature and mixed layer depth (Figure 4.16) are not highly correlated ($r = 0.38$). Across the eddy, however, the correlation coefficient for sea surface temperature versus mixed layer depth increases to 0.88. The southern track (Figure 4.17) also shows an excellent correlation between sea surface temperature and mixed layer depth ($r = 0.84$). The correlation between these two variables is less ($r = 0.66$) across the track segment which coincides with the eddy. It appears that the meander has formed into an eddy which does not extend to the southern track.

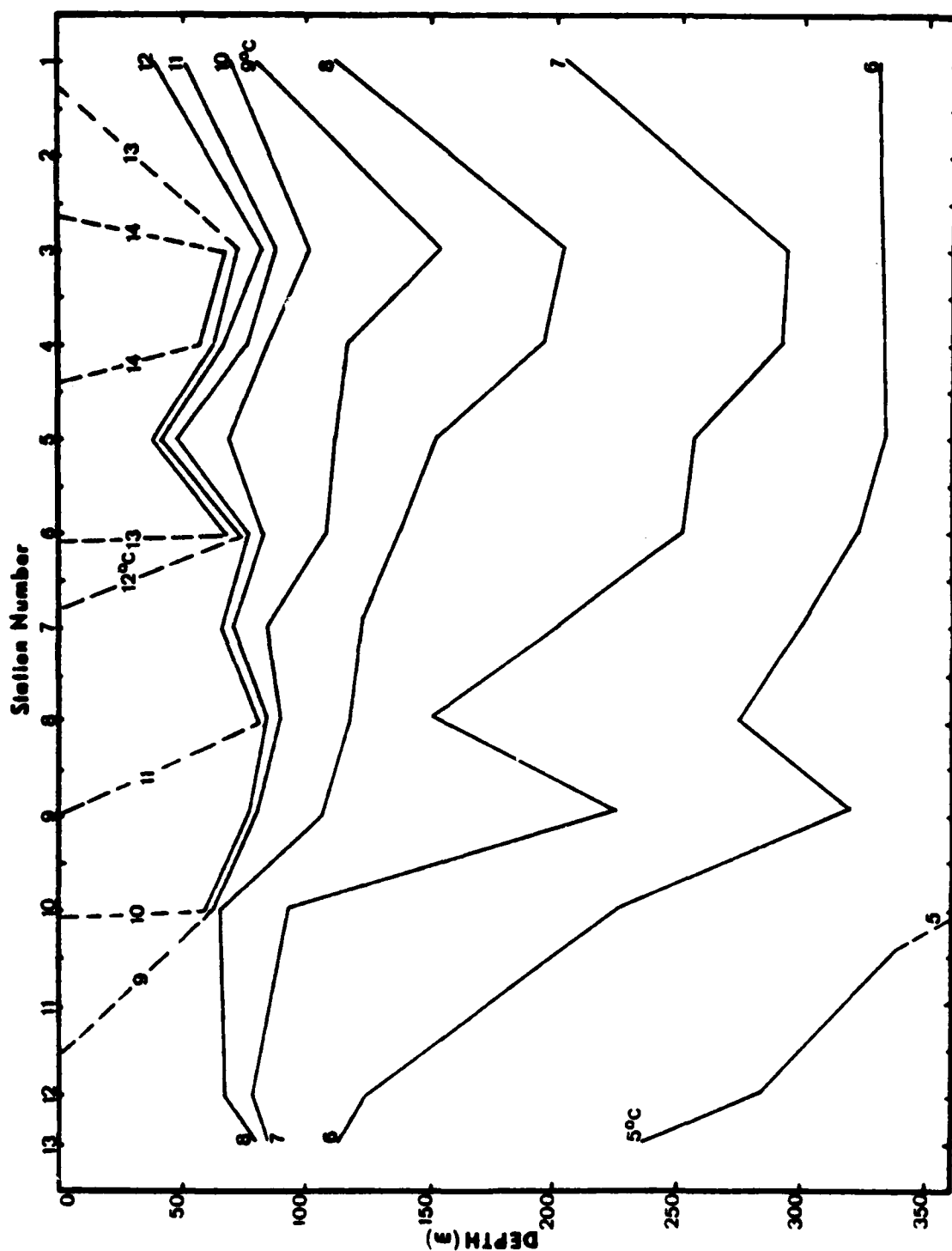


Figure 4.14 Vertical Temperature Cross-section (3 Dec, Center).

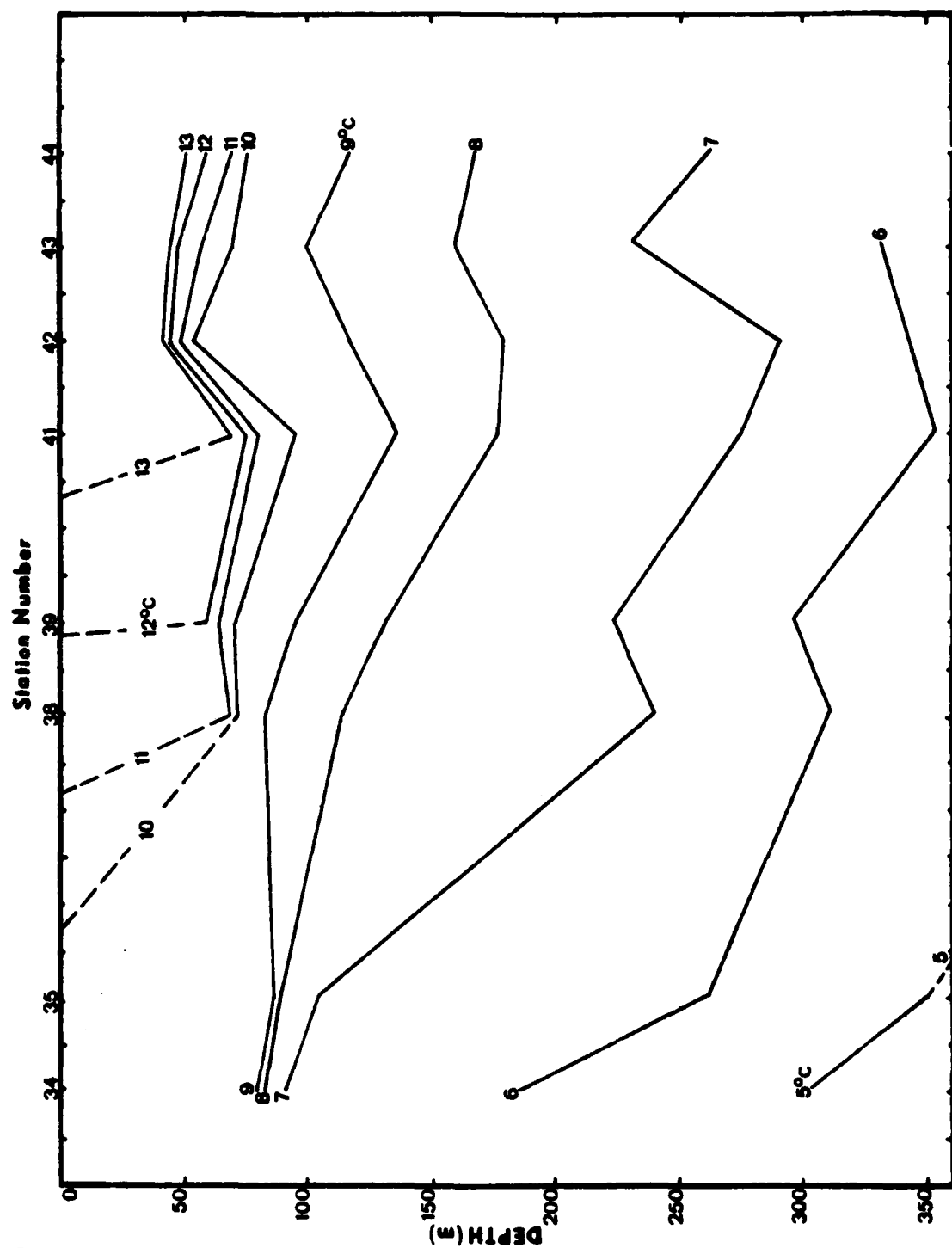


Figure 4.15 Vertical Temperature Cross-section
(3 Dec, South).

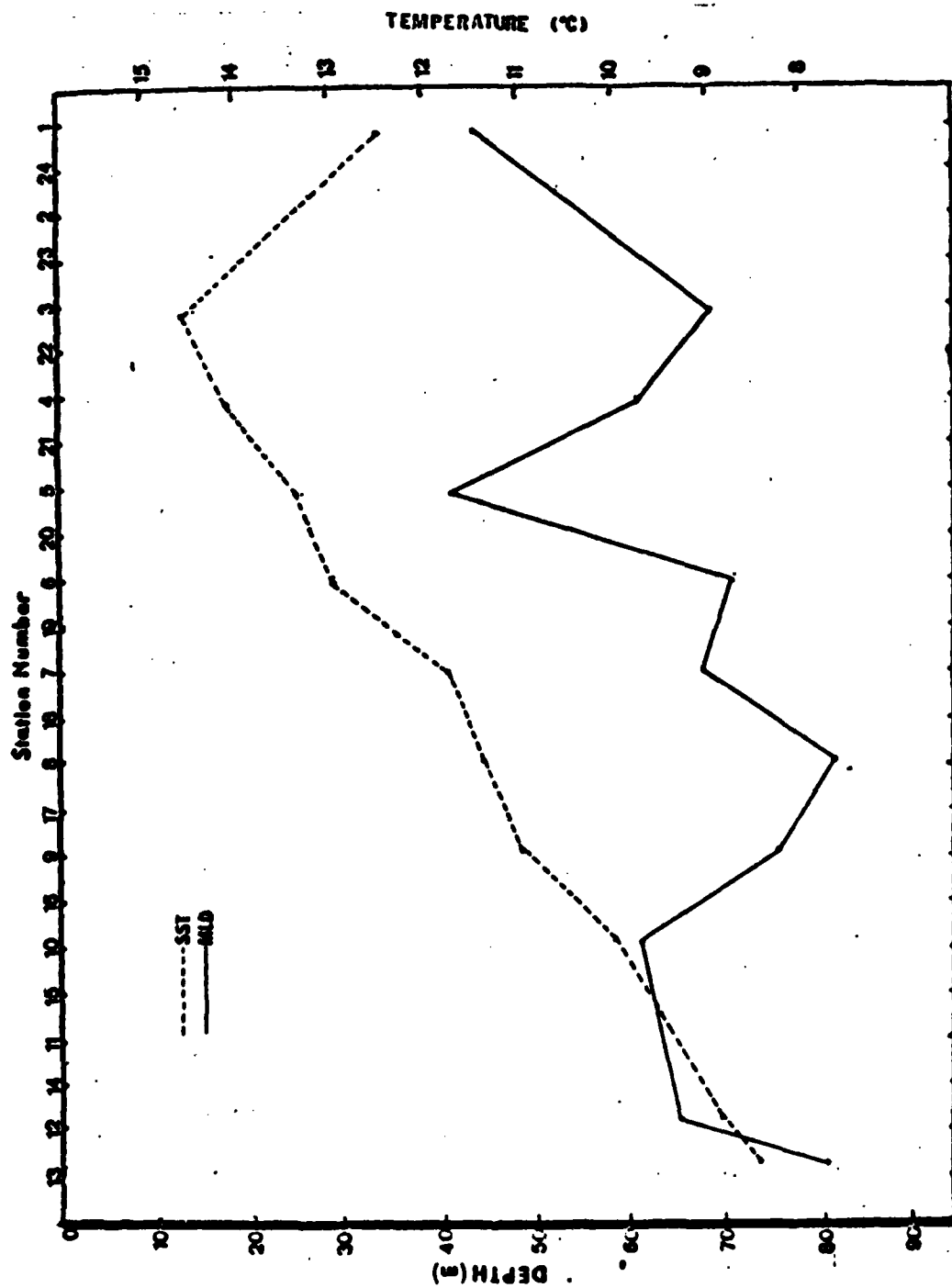


Figure 4.16 Mixed Layer Depth and Sea Surface Temperature (3 Dec, Center).

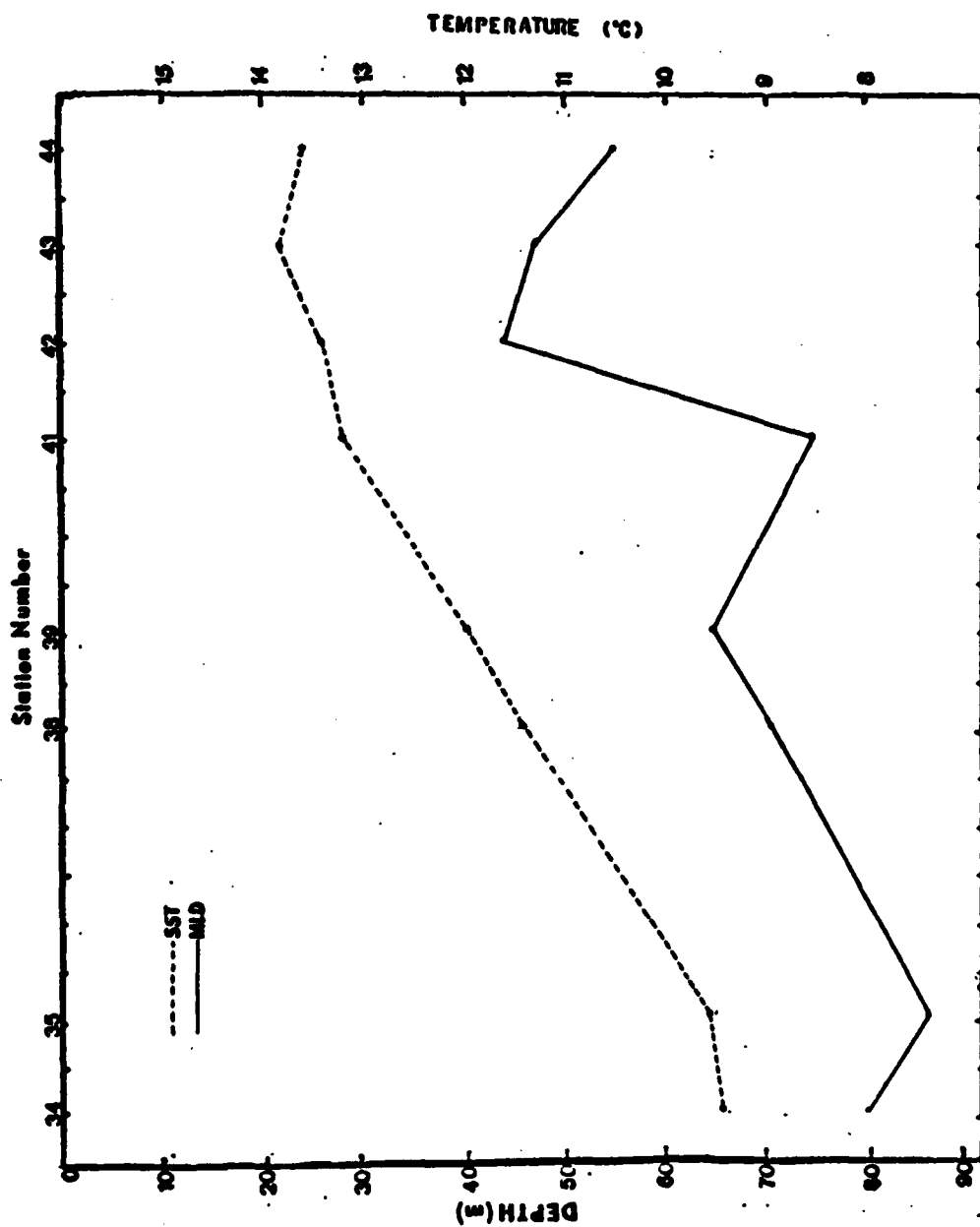


Figure 4.17 Mixed Layer Depth and Sea Surface Temperature (3 Dec, South).

Most of the southern track is in the Transitional Domain. The Central Subarctic Domain has influence up to station thirty-five, after which the track is under the influence of the Transitional Domain. Changes appear to be linear along the track within the Transitional Domain.

Winds increased from 11 meters/sec (24 kts) to 14-16 meters/sec (30-35 kts) on 1 December. These wind speeds were sustained through 2 December and through most of 3 December [Ref. 61]. These cold northwesterly winds lowered the sea surface temperature along the track, but caused no major changes to the vertical Temperature Cross-section.

The average mixed layer depth for the center track was 66.4 meters on 3 December. The southern track averaged 64.6 meters. There was a decrease in the average mixed layer depth along the track since the previous flight on 1 December. In comparing the two days, a large decrease in mixed layer occurred at station five (21 meter change). At first glance this appears to be an instrument error. However, the mixed layer depth profile for flight track one (Figure 4.5) is very similar to the profile for flight track five. On both days station five had a shallow mixed layer which deepened considerably across the eddy.

When overlaid, the mixed layer depth profiles and the sea surface temperature profiles for tracks one and five are remarkably similar. The mixed layer depth for flight five is deeper than for flight one, but the variations with position are very similar. Between stations ten and two, the sea surface temperature is highly correlated ($r = 0.98$) with position, and the mixed layer depth shows some correlation ($r = 0.54$).

Four model equations were used for each track on flight five. The models are summarized in Table XIV for the center track, and in Table XV for the southern track. On

TABLE XII

MLD, SST and Gradients at the Thermocline, 3 December 1980.

Buoy	Position	MLD	SST	dT/5m	dT/15m	dT/50m	dT/100m
46	(1) 690	45	12.47	0.04	1.28	3.58	4.48
3	570	70	14.64	1.05	2.39	4.67	5.97
4	510	62	14.16	1.35	2.73	4.87	5.46
5	450	42	13.38	1.41	2.17	3.35	4.51
6	390	72	13.06	1.42	2.44	4.20	5.20
7	330	69	11.77	0.81	2.07	3.01	4.14
8	270	83	11.42	1.53	2.66	3.71	4.36
9	210	77	10.99	1.80	2.26	3.24	3.37
10	150	62	10.02	2.28	2.71	3.30	3.82
12	30	66	8.86	0.78	1.43	2.24	2.43
13	0	82	8.46	1.42	1.88	2.20	2.49

TABLE XIII

MLD, SST and Gradients at the Thermocline, 3 December 1980
(South)

Buoy	Position	MLD	SST	dT/5m	dT/15m	dT/50m	dT/100m
34	0	80	9.40	1.23	2.56	3.23	3.42
35	60	86	9.53	1.43	1.70	2.40	2.62
38	240	70	11.44	1.69	1.88	3.08	3.55
39	300	64	12.04	1.00	2.53	3.34	4.61
41	420	74	13.27	0.92	2.60	3.48	4.89
42	480	43	13.46	1.79	3.61	4.20	4.76
43	540	46	13.89	1.62	2.56	4.20	5.12
44	600	54	13.65	1.07	2.10	4.09	5.22

the south track, the gradient computed from 100 meters produced the worst fit of any model of mixed layer as a function of sea surface temperature, track position and thermocline gradient. The gradient from 100 meters produced the best fit for the center track model. For comparison, the southern track model using the gradient computed from 100 meters is included.

TABLE XIV

Models of MLD for 3 December, Center Track.

Model Variables	Coefficient of Determination
SST	0.146
SST, Position	0.404
SST, Position, Gradient (15)	0.441
SST, Position, Gradient (100)	0.523

TABLE XV

Models of MLD for 3 December, South Track.

Model Variables	Coefficient of Determination
SST	0.703
SST, Position	0.716
SST, Position, Gradient (50)	0.861
SST, Position, Gradient (100)	0.716

6. Flight Track Six (Center and North)

Flight six examined both the center track (Figure 4.18) and a parallel track 60 nautical miles to the north (Figure 4.19) with eleven stations each. The values of mixed layer depth, sea surface temperature, and gradient associated with each station are given in Table XVI for the center track, and Table XVII for the northern track. The temperature structure along the center track resembles

previous flight tracks. The isotherms begin to diverge after station nine. The gradient computed from the upper five meters of the thermocline is negatively correlated with position ($r = -0.27$).

The eddy seems to have diminished both in length along the center track and in depth. The northern track does not appear to traverse the eddy.

The sea surface temperature and mixed layer depth variation with position along the center track (Figure 4.20) show the best correlation in any flight along the center track. Both sea surface temperature and mixed layer depth varied linearly with position up to station three. Sea surface temperature correlation with position along the entire track was better ($r = 0.92$) than along the shorter track across the eddy ($r = -0.80$), or along any previous center flight track. Mixed layer depth was more highly correlated with position across the eddy ($r = -0.95$) than along the entire track ($r = -0.83$).

Across the eddy on the center track, sea surface temperature and mixed layer depth again are highly correlated ($r = 0.90$). Over the entire track length, the relationship between sea surface temperature and mixed layer depth is not as strong ($r = -0.55$). Of all flights, this was the best overall correlation of sea surface temperature and mixed layer depth for the center track.

The northern track (Figure 4.21) shows a relationship similar to that along the center track between sea surface temperature and mixed layer depth. The eddy is not apparent in the sea surface temperature profile, but does present a familiar profile of mixed layer depth. Across the eddy position on the north track, mixed layer depth is highly correlated with position ($r = -0.97$). This same relationship holds true for the center track ($r = -0.95$).

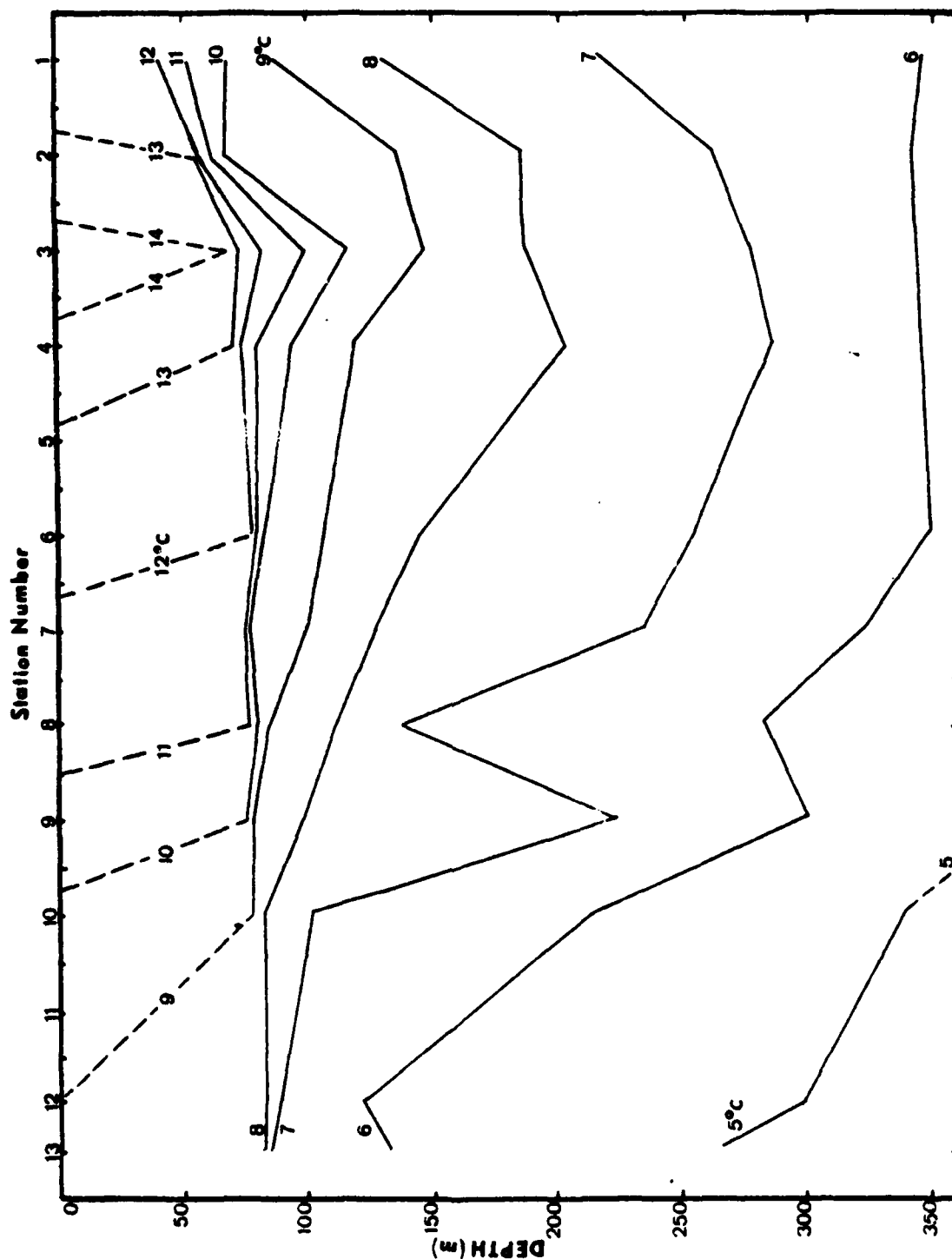


Figure 4.18 Vertical Temperature Cross-section
(5 Dec, Center).

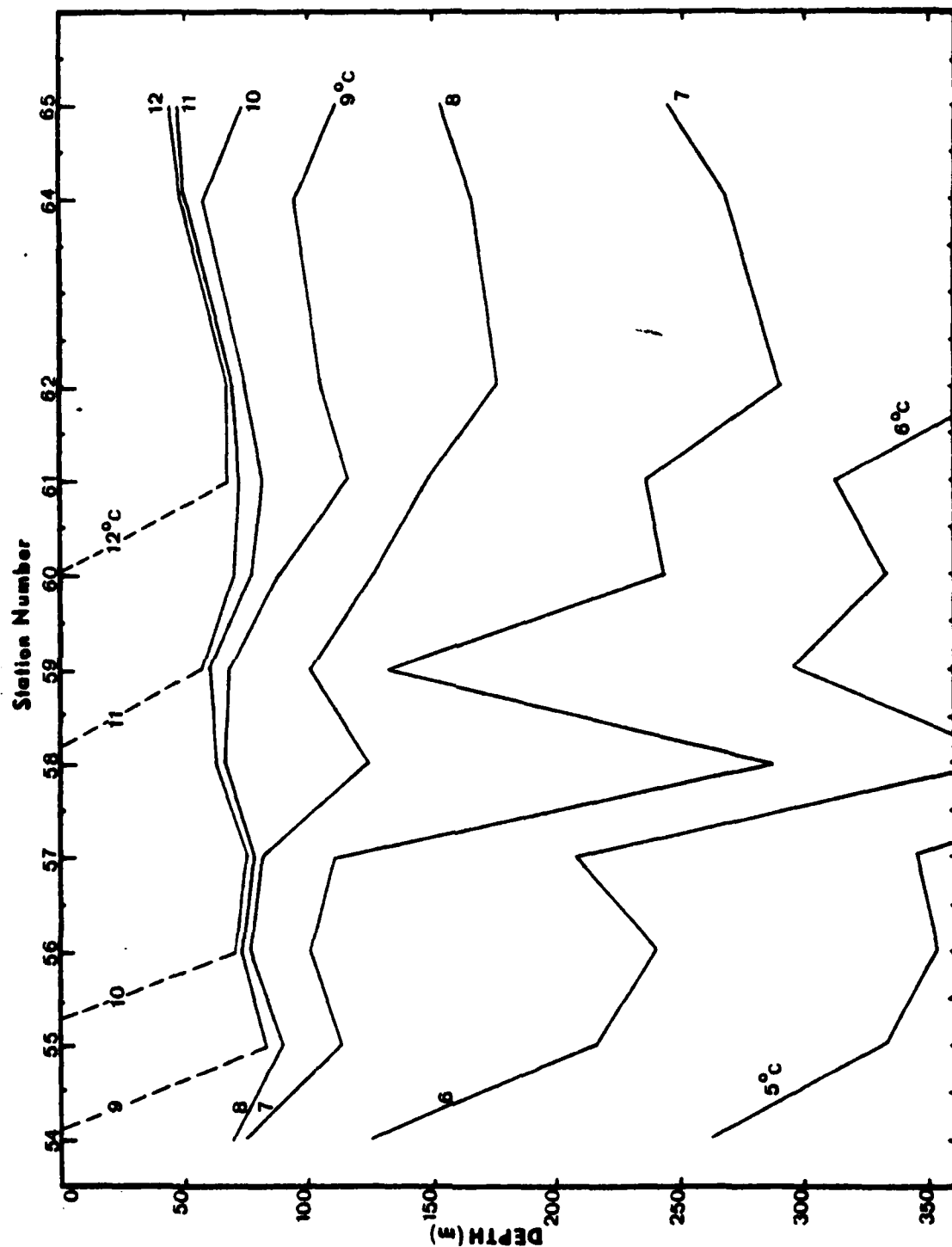


Figure 4.19 Vertical Temperature Cross-section
(5 Dec, North).

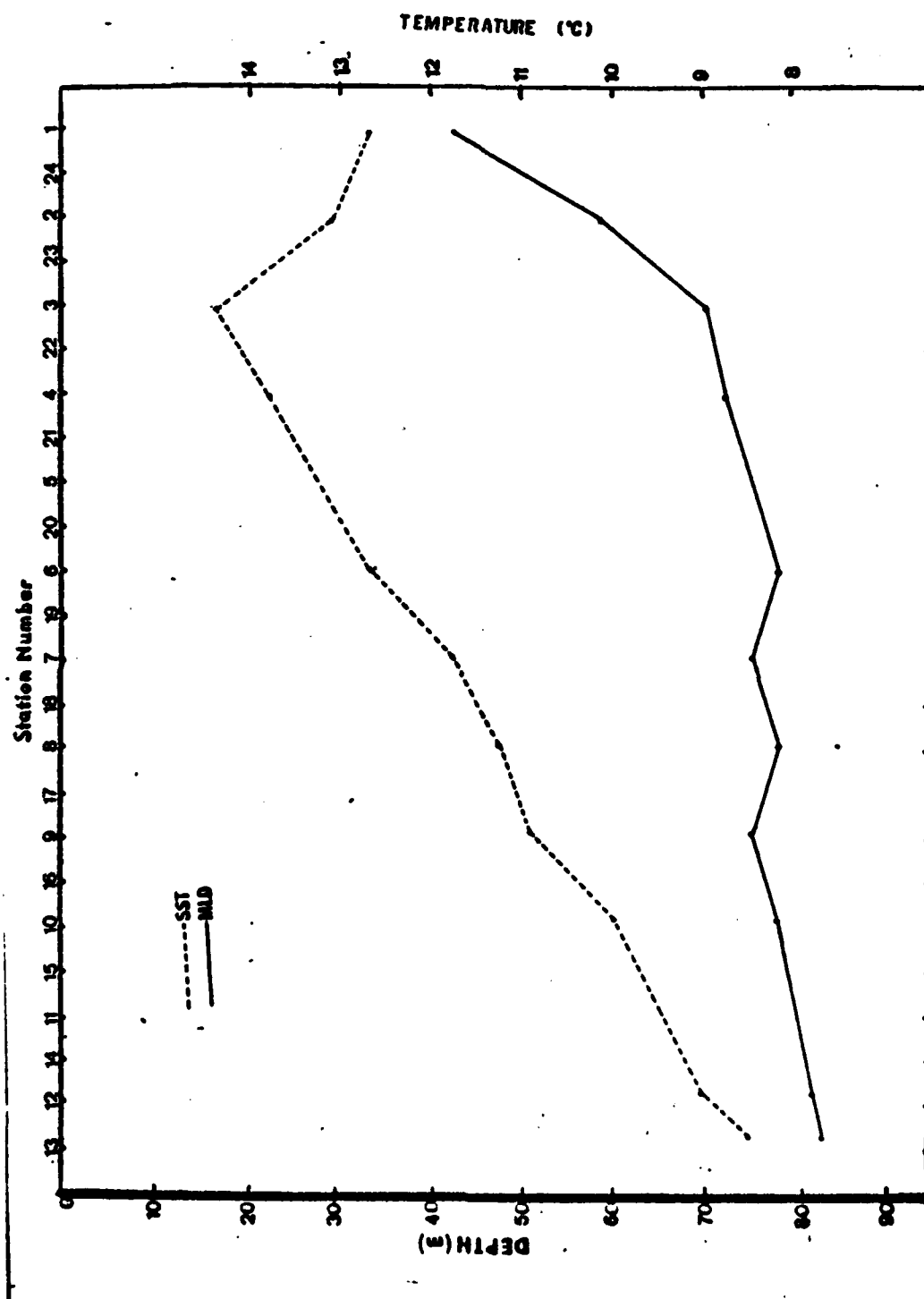


Figure 4.20 Mixed Layer Depth and Sea Surface Temperature (5 Dec, Center).

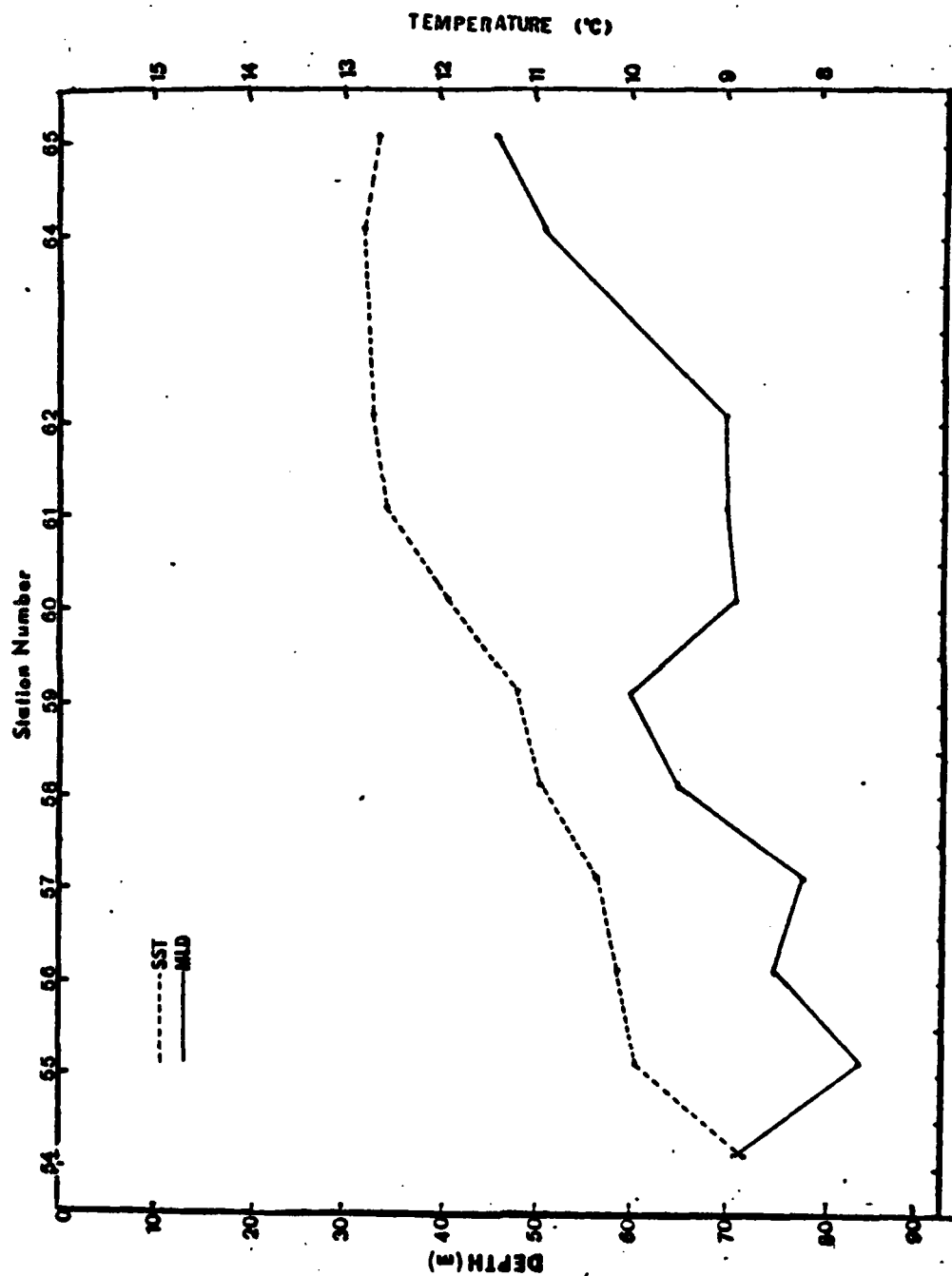


Figure 4.21 Mixed Layer Depth and Sea Surface Temperature (5 Dec, North).

A subsurface feature developed over the course of the experiment, and became very obvious in the northern track on 5 December. At station 58, the isotherms reach a maximum depth. A corresponding excursion to depth for the same isotherms (6 and 7 degree Celsius) occurs along the center track at station nine. In looking back through the previous flight cross-sections, this same excursion is found to occur on flights four and five.

Lundell [Ref. 62] reported a submerged sound channel in the vicinity of station nine. The Kilonski digitized bathythermographs indicated a slight inversion in this area (of the order 0.3 degrees Celsius). This unusual structure occurs at the boundary between two Domains: the Central Subarctic and Transitional. Along the center track, the maximum depth excursion of the six and seven degree isotherms shifted to the west between flight two and flight six.

This submerged feature is not driven by surface conditions as it occurs well below both thermocline and halocline. This appears to be some type of shift in lower domain boundaries. A time series over one or two months, between stations seven and ten, might have provided some insight into the lower layer variability at this domain boundary.

As with the southern track on flight five, the northern track data on flight six showed the worst fit by a model using the gradient computed from 100 meters. The gradient from fifty meters produced the best fit on this track. The gradient from five meters produced the best fit on the center track. The model parameters and coefficients of determination are presented in Tables XVIII and XIX.

TABLE XVI

MLD, SST and Gradients at the Thermocline, 5 December 1980.

Buoy	Position	MLD	SST	dT/5m	dT/15m	dT/50m	dT/100m
1	690	42	12.68	0.84	1.17	3.19	4.21
2	630	58	13.11	1.77	3.17	3.79	4.40
3	570	70	14.40	0.89	2.10	4.25	5.88
4	510	72	13.81	1.79	3.05	4.60	5.44
6	390	78	12.68	1.77	3.05	4.00	4.83
7	330	75	11.77	1.10	2.18	3.40	4.30
8	270	78	11.23	1.39	2.45	3.67	4.25
9	210	75	10.88	1.11	2.46	3.42	3.42
10	150	78	9.94	1.76	2.57	3.47	3.75
12	30	82	8.97	1.60	2.26	2.91	2.83
13	0	83	8.43	1.46	1.83	2.02	2.32

Note:

1. A slight inversion existed at station 12 between 135 meters and 200 meters.

TABLE XVII

MLD, SST and Gradients at the Thermocline, 5 December 1980
(North)

Buoy Position	MLD	SST	dT/5m	dT/15m	dT/50m	dT/100m
54	0	70	8.81	1.22	1.59	2.37
55	60	83	9.94	1.36	2.32	3.69
56	120	74	10.15	2.03	2.68	3.77
57	180	77	10.37	2.24	2.89	4.23
58	240	64	10.96	0.91	2.16	2.69
59	300	59	11.20	1.70	2.31	4.49
60	360	70	11.93	0.95	1.97	3.52
61	420	69	12.60	0.92	2.28	4.89
62	480	69	12.73	1.64	3.42	4.62
64	600	50	12.84	1.86	3.01	4.71
65	660	45	12.68	1.12	1.44	3.59

E. DYNAMIC HEIGHT COMPARISONS, 17 NOVEMBER

Emery and O'Brien [Ref. 63] proposed a method of inferring salinity from temperature or depth in the North Pacific Ocean. The method relies on mean salinity values computed

TABLE XVIII

Models of MLD for 5 December, Center Track.

Model Variables	Coefficient of Determination
SST	0.298
SST, Position	0.962
SST, Position, Gradient (5)	0.977
SST, Position, Gradient (100)	0.963

TABLE XIX

Models of MLD for 5 December, North Track.

Model Variables	Coefficient of Determination
SST	0.370
SST, Position	0.846
SST, Position, Gradient (50)	0.872
SST, Position, Gradient (100)	0.854

by five degree squares. In the test region, the mean salinity curves are nearly constant. Bernstein et al. [Ref. 64] used this method to estimate dynamic heights in the Western North Pacific with good success. It was decided to employ both a single recent salinity sounding in the area (from a CTD cast), and a Fleet Numerical Oceanographic Center salinity climatology for November, as a basis for calculating and comparing dynamic heights for flight track two (17 November).

TABLE XX

Dynamic Heights Relative to 350 meters (17 Nov).

BOUY	POSITION	CONST-S	FNOC-S
13	0.	0.618	0.629
12	30.	0.643	0.650
14	60.	0.638	0.644
11	90.	0.654	0.658
15	120.	0.654	0.658
10	150.	0.656	0.657
16	180.	0.665	0.663
9	210.	0.696	0.690
17	240.	0.705	0.698
8	270.	0.713	0.698
18	300.	0.717	0.690
7	330.	0.714	0.681
19	360.	0.742	0.699
6	390.	0.741	0.761
20	420.	0.743	0.753
5	450.	0.759	0.768
21	480.	0.766	0.774
4	510.	0.777	0.779
22	540.	0.763	0.747
3	570.	0.821	0.821
23	600.	0.817	0.816
2	630.	0.737	0.735
24	660.	0.704	0.697

Notes:

1. Heights in dynamic meters.
2. Const-S refers to single salinity profile for entire area.
3. FNOC-S refers to November salinity climatology from the Fleet Numerical Oceanographic Center.

Consideration then was given to plotting the dynamic topography along the track. Since only one salinity profile was used to calculate the dynamic height at all stations, the resulting variations in dynamic heights along the track were due to temperature variations only. The reference level was selected as 350 meters because this depth represented the useful limit of temperature data available from the digitized report.

As a means of comparing dynamic height variation with position and other factors of interest such as temperature gradient at the thermocline or mixed layer depth, the Fleet Numerical Oceanographic Center climatology for the flight

track was used in calculations of dynamic heights. The results are shown in Figure 4.22 and Table XX.

The variation of dynamic height along the track was low (0.19 meters/kilometer). Across the eddy the height change was 0.1 meters per 150 kilometers. This height signal would be too small for the SEASAT altimeter to detect accurately. However, future generations of satellite altimeters should be able to detect the magnitude of the signal from this eddy.

The temperature gradient in the thermocline can be an important factor in a model of mixed layer depth. This gradient cannot be predicted accurately from sea surface temperature observations. Therefore, a correlation between thermocline gradient and dynamic height was investigated. The gradient from one hundred meters showed the strongest correlation with dynamic height. The possibility exists, then, to predict the gradient from measured values of dynamic heights along the track.

F. OVERALL OBSERVATIONS

1. An Eddy on the Southeastern Part of the Track

A warm eddy formed in the observation area. It began as an intrusion of warm water (the meander imaged by satellite on 17 November) and eventually appeared to form a closed circulation. Based on the November image, the eddy appeared to have a 90-nautical-mile (165 kilometer) major axis and a 60-nautical-mile (110 kilometer) minor axis. By the end of the experiment, the major axis had decreased to about 60 nautical miles, while the minor axis did not decrease significantly.

The sea surface temperature and mixed layer depth were highly correlated across the eddy. The southeast

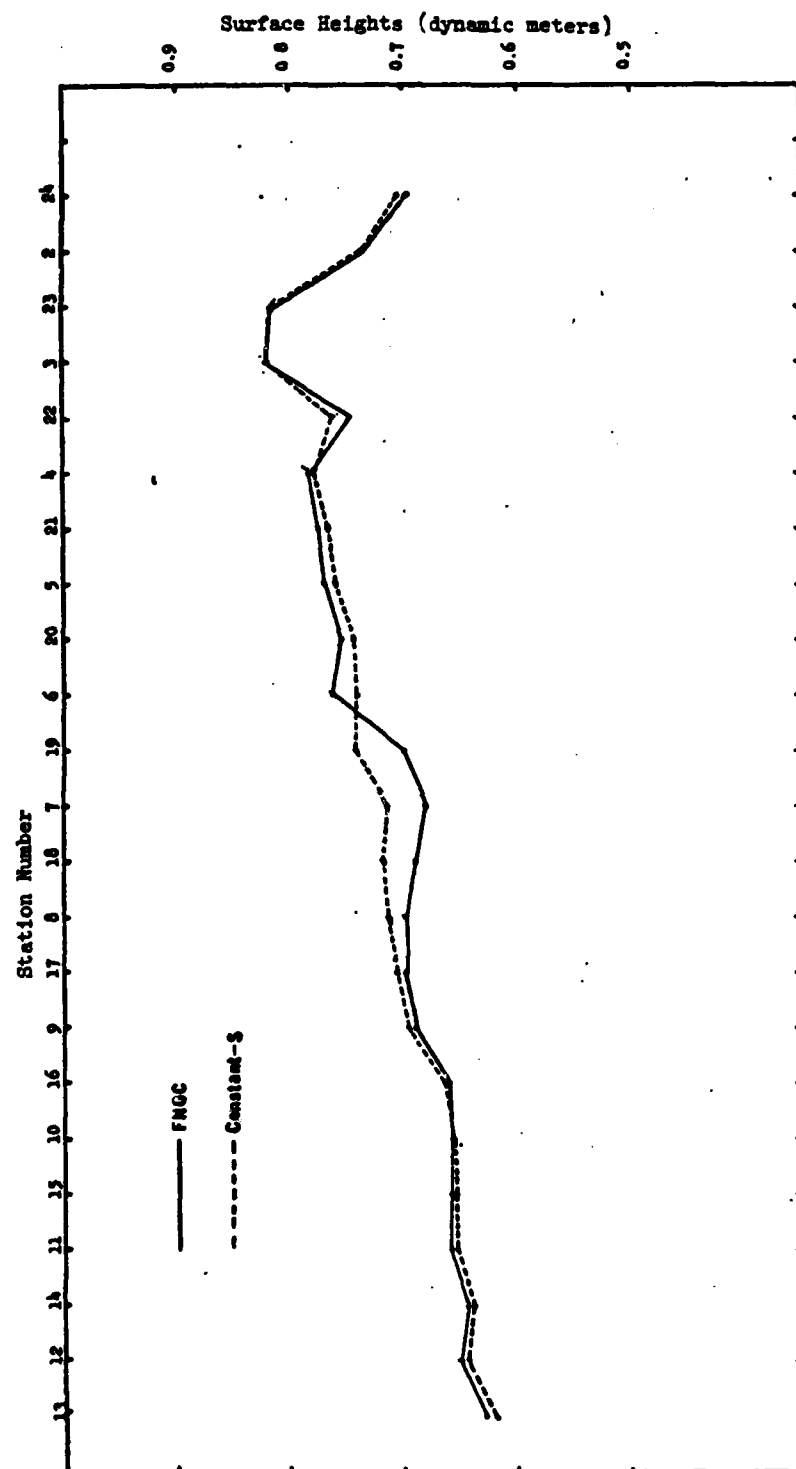


Figure 4.22 Dynamic Heights Along the Center Track
(17 Nov) 0/350.

"wall" of this eddy displayed sharp gradients of both sea surface temperature and mixed layer depth. The correlation was consistently strong enough to infer that the influence of the eddy was confined to the vertical area directly below the surface thermal manifestation, that is, the front which existed between the eddy water and the surrounding water had a slope which approached ninety degrees, especially to the southeast of the eddy.

2. Gradients in the Thermocline

The gradient computed from the first five meters of the thermocline showed a negative correlation with position in seven of eight flight tracks. The gradient was strongest to the east of station nine. Station nine lies near the boundary between the Central Subarctic Domain and the Transitional Domain.

The gradient computed from five meters was more correlated with position in November than in December. Table XXI lists the correlation coefficients for the gradient from five meters.

Of the gradients computed, the gradient from five meters and the gradient from one hundred meters generally had the best correlation with position. Attempts to model mixed layer depth were generally more successful using the gradient computed from 100 meters. This is to be expected as the gradient computed from 100 meters tends to smooth errors introduced by an arbitrary starting point (the strength of the five meter gradient could vary by as much as twenty percent depending on what depth was selected as the top of the thermocline. Table XXII lists the two gradients, by flight track, which exhibited the largest magnitude correlation with position on the flight track.

TABLE XXI

Correlation Coefficient (r) for Gradient from 5 meters
vs. Position

FLIGHT	DATE	CORRELATION COEFFICIENT (r)
1	15 Nov	-0.818
2	17 Nov	-0.583
3	19 Nov	-0.766
4	1 Dec	-0.159
5	3 Dec	-0.478
5 (south)	3 Dec	+0.012
6	5 Dec	-0.266
6 (north)	5 Dec	-0.129

TABLE XXII

Gradients Most Correlated with Position (by Flight).

FLIGHT	DATE	GRADIENT	(r)
1	15 Nov	5	-0.818
		15	-0.412
2	17 Nov	5	-0.583
		100	+0.575
3	19 Nov	5	-0.766
		50	+0.282
4	1 Dec	5	-0.159
		50	+0.115
5	3 Dec	100	+0.842
		5	-0.478
5 (S)	3 Dec	100	+0.919
		50	+0.859
6	5 Dec	100	+0.781
		50	+0.642
6 (N)	5 Dec	100	+0.524
		5	-0.129

Note:

1. Track five south indicated by 5(S) and track six north indicated by 6(N).

3. Sea Surface Temperature

The sea surface temperature correlated with position on all flight tracks. This is due in part to the system of specifying positions on the line. It is still interesting to note that the sea surface temperature increased almost linearly along the track until reaching the eddy. There, a second order fit with position was more appropriate. Table XXIII lists the correlation coefficient computed for sea surface temperature vs. position for each track.

TABLE XXIII

Correlation Coefficient (r) for SST vs. Track Position.

FLIGHT	DATE	ENTIRE TRACK	EDDY LOCATION
1	15 Nov	0.856	-0.125
2	17 Nov	0.909	-0.416
3	19 Nov	0.569	-0.480
4	1 Dec	0.909	-0.648
5	3 Dec	0.894	-0.476
5 (S)	3 Dec	0.982	0.764
6	5 Dec	0.917	-0.795
6 (N)	5 Dec	0.954	0.491

Notes:

1. Eddy location is the along track correlation between buoys that would define the eddy boundaries (stations 4 to 24 on 17 November).

The objective of this study was not the formulation of a predictor for sea surface temperature. Observed sea surface temperature patterns did show when deviations from the expected climatology occurred. The sea surface temperature gradients, in particular, provided very good information for defining frontal conditions at the eddy. Although values of sea surface temperature did not imply corresponding values of mixed layer depth with any reliability, the sharp gradients of surface temperature

AD-A125 027

SATELLITE APPLICATIONS TO ACOUSTIC PREDICTION SYSTEMS
(U) NAVAL POSTGRADUATE SCHOOL MONTEREY CA S A COX
OCT 82 NPS68-82-005

2/2

UNCLASSIFIED

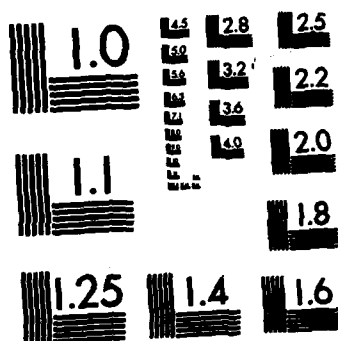
F/G 8/10

NL

END

FILMED

DATE



MICROCOPY RESOLUTION TEST CHART
NATIONAL BUREAU OF STANDARDS-1963-A

along the track did occur in conjunction with similar gradients of mixed layer depth.

Satellite-derived sea surface temperature gradients, then, can be used to modify sound velocity profiles when water mass discontinuities are observed. As a first guess, a single bathythermograph could provide temperatures, while satellite-derived surface temperatures could be used to modify the measured vertical structure at another location. The sea surface temperature gradients would be useful as a decision aid for predicting the changes occurring in the mixed layer depth. A vertical temperature structure along the proposed track could be worked out in this manner.

TABLE XXIV

Correlation Coefficient (r) - MLD vs. Track Position.

FLIGHT	DATE	ENTIRE TRACK	EDDY LOCATION
1	15 Nov	-0.149	-0.231
2	17 Nov	-0.164	-0.607
3	19 Nov	-0.641	-0.544
4	1 Dec	-0.655	-0.931
5	3 Dec	-0.569	-0.018
5 (S)	3 Dec	-0.845	-0.527
6	5 Dec	-0.827	-0.954
6 (N)	5 Dec	-0.787	-0.972

Note: Eddy location is the same as in the previous table.

4. Mixed Layer Depth

The mixed layer depth varied along each track. Sometimes it would correlate with position, but seldom would the correlation be as high as for sea surface temperature. The correlation was always negative, that is the mixed layer shallowed toward the coast. This is to be expected from the

climatological description of the area. The Transitional Domain is characterized by a weakening of the halocline, warmer water, and shallower isothermal surface layers.

The sea surface temperature indicated the presence of a warm meander or eddy. The satellite image from 17 November shows the thermal signature of warm water entrained in a cold area. Even so, the sea surface temperature generally did not show as strong a correlation with position in the eddy as did mixed layer depth. Table XXIV shows the correlation coefficients for mixed layer depth vs. track position, both for the entire track and the eddy only. This may provide a means of estimating mixed layer depth in warm eddies. Satellites can be used to define the surface boundaries of a warm eddy. Then mixed layer depth across the eddy could be predicted as a function of position in the eddy.

TABLE XXIV

Correlation Coefficients (r) for MLD vs. SST.

Flight	r (entire track)	r (eddy)
1	0.334	0.970
2	0.170	0.858
3	-0.101	0.509
4	-0.418	0.601
5	-0.382	0.881
6 (S)	-0.838	-0.662
6 (N)	-0.546	-0.898
	-0.608	-0.433

Note: The eddy column refers to correlations of data gathered only from stations along the track which include the eddy.

5. Mixed Layer Depth and Sea Surface Temperature Correlations

Mixed layer depth and sea surface temperature showed little correlation in November, but the December flight tracks showed a strong increase in the correlation coefficient for the entire track. The eddy displayed a strong mixed-layer-depth sea-surface-temperature correlation in November, decreasing somewhat in December. Table XXV summarizes the correlation coefficients for mixed layer depth and sea surface temperature for each day of observations.

V. CONCLUSIONS AND RECOMMENDATIONS

A. CONCLUSIONS

Satellites can be used to map sea surface conditions, particularly sea surface temperature. For ASTREX data, knowledge of sea surface temperature and position along the flight track was used to model mixed layer depth. This model correlated poorly with in situ observations. When gradient in the thermocline was added to the model, the correlation increased significantly.

The gradient in the thermocline may be predicted (with low confidence) from satellite altimeter measurements of the ocean surface. A useful relationship between thermocline gradient and the dynamic topography variations may exist.

The most striking result of this study was the strong correlation observed between sea surface temperature and mixed layer depth across a warm eddy. Satellite imagery provided the location of the eddy boundaries with a high degree of accuracy. The strength of this surface thermal front is an indication of mixed layer depth variability in the area. Qualitatively, a large thermal gradient at the surface indicates a correspondingly large change in mixed layer depth. Across the southeastern boundary of the warm eddy, the sea surface temperature and mixed layer depth changed significantly in the same sense (both increased together when tracked from the northwest to the southeast).

Uncorrected satellite temperatures in the area displayed the same variations along the track as did observed AXBT sea surface temperatures. The variations of sea surface temperature (thermal gradients at the surface) contain the information needed to locate anomalies such as the warm eddy

observed in the southeastern part of the flight tracks. The NOAA-6/7 satellites can resolve 0.5 degree Kelvin temperatures at one-kilometer resolution. Frontal areas can be identified and accurately located. The AXBT's provided temperature values at 55-kilometer intervals, which were sufficient to observe that the eddy did exist, but were not sufficient to pinpoint the eddy boundaries. Satellite imagery, providing temperature values at one-kilometer intervals, can be used to specify the boundaries of a front or eddy more accurately.

B. RECOMMENDATIONS

In future experiments in the ASTREX region, consideration should be given to investigating satellite located-anomalies such as the warm eddy observed during ASTREX. Until a satellite altimeter becomes available, dynamic heights must be calculated indirectly from other observed variables. Therefore, the salinity should be measured in any future test area.

Various models of mixed layer depth must be explored. In addition to modeling the mixed layer as a function of position, sea surface temperature and gradient in the thermocline, additional factors should be added. These factors should include wind mixing in the mixed layer based on observed wind speeds in the area, dynamic heights associated with tracks examined, and possibly observed sea state in the area.

Another model which could prove very useful would include the effects of wind speed and duration on the mixed layer depth. Wind was not used as a factor in this study, but it is an important element in the formation of the mixed layer. Between the November and December flights, wind speed increased and so did mixed layer depth. Instruments

such as the SMHR on NIMBUS-7 can provide scalar wind fields for an area. The formulation of mixed layer depth as a function of magnitude and duration of wind, sea surface temperatures, and other factors may provide the best model of mixed layer depth.

APPENDIX A

VARIATION OF THERMOCLINE GRADIENTS WITH POSITION FOR NOVEMBER

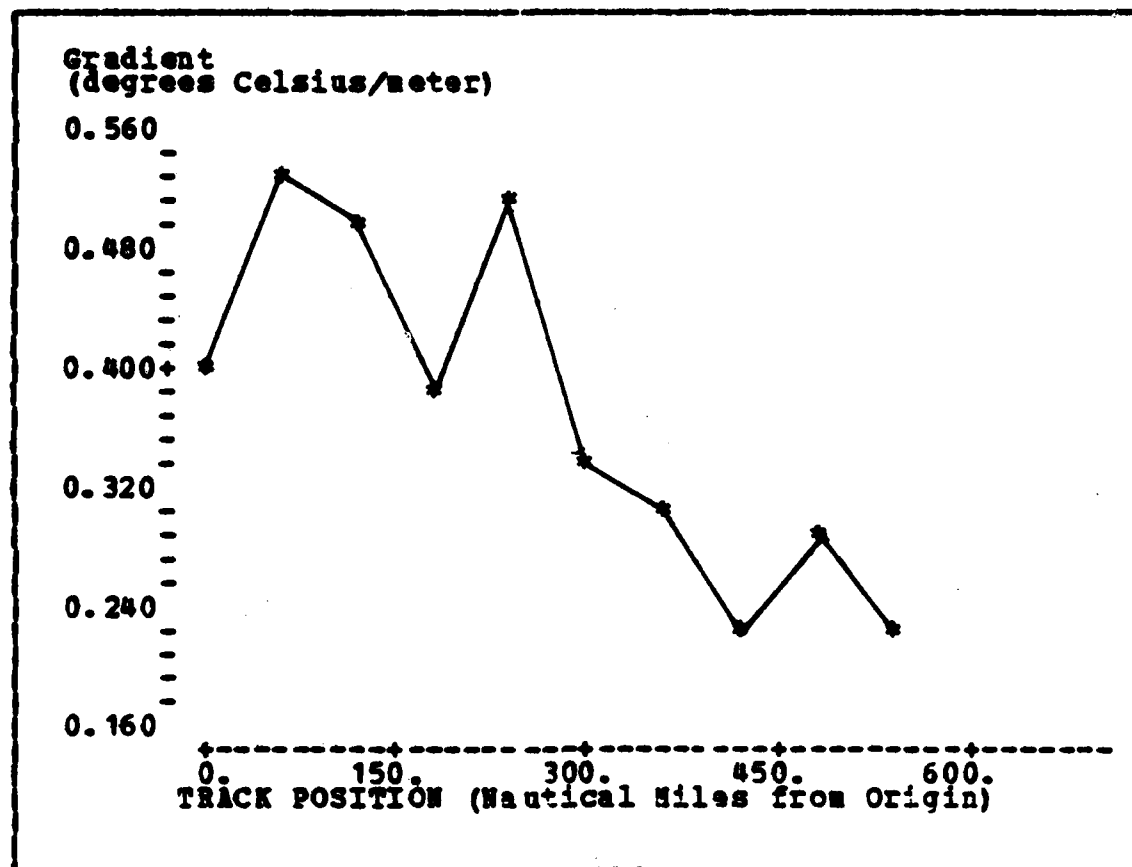


Figure A.1 Gradient from 5 meters vs. Position (15 Nov).

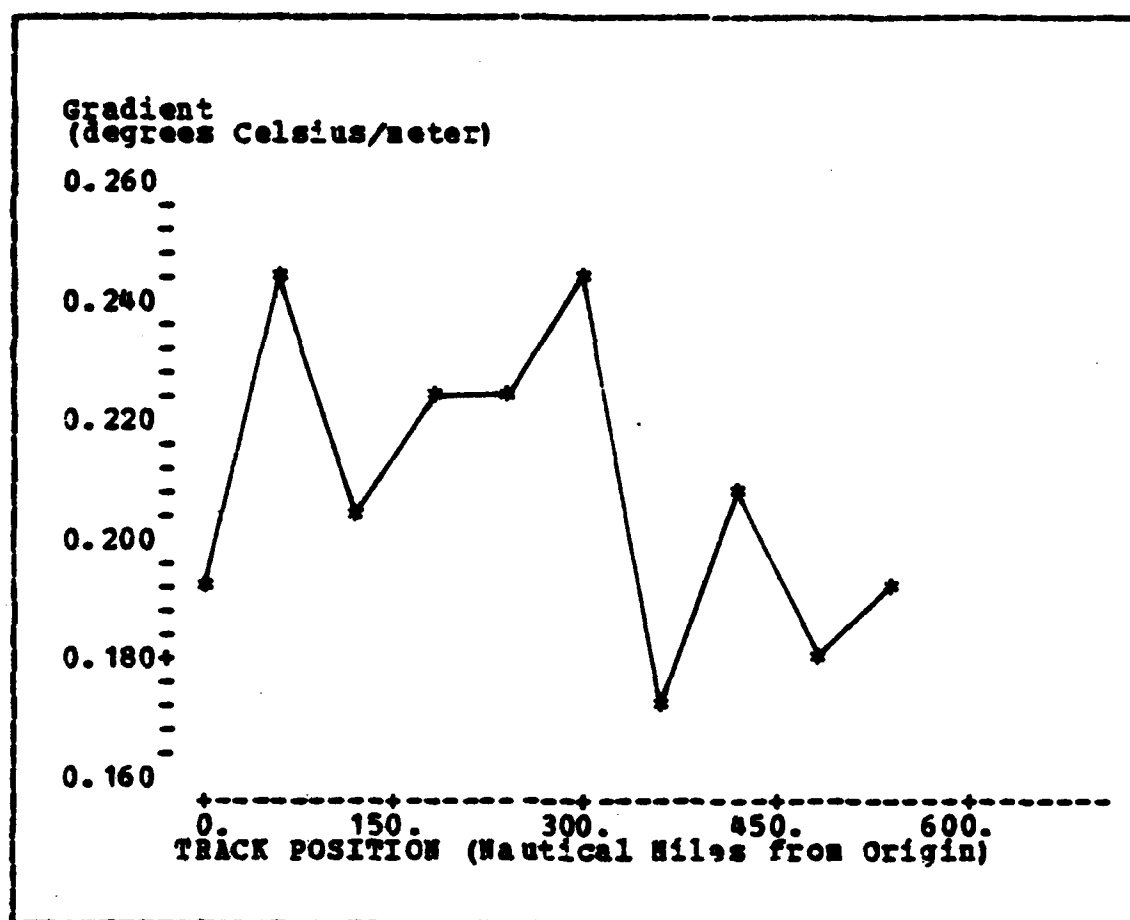


Figure A.2 Gradient from 15 meters vs. Position (15 Nov).

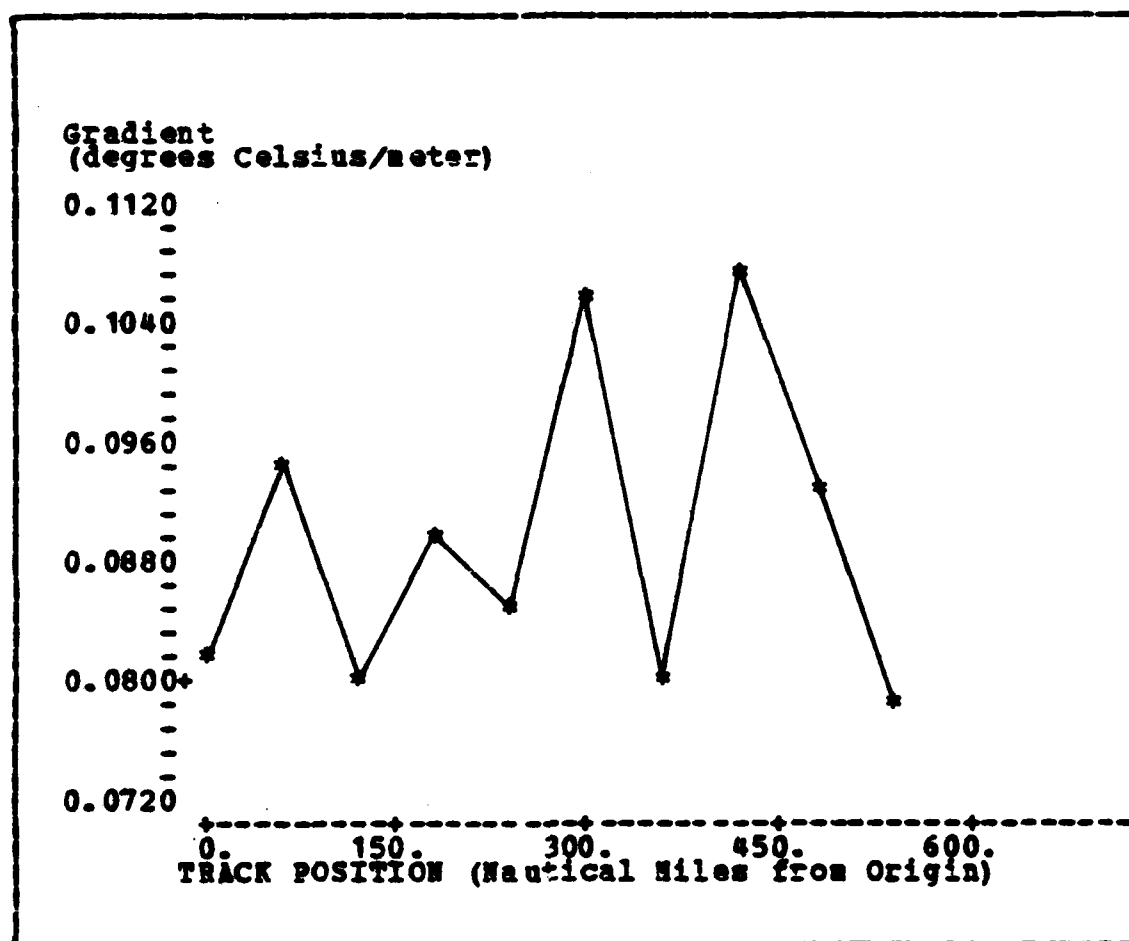


Figure A.3 Gradient from 50 meters vs. Position (15 Nov).

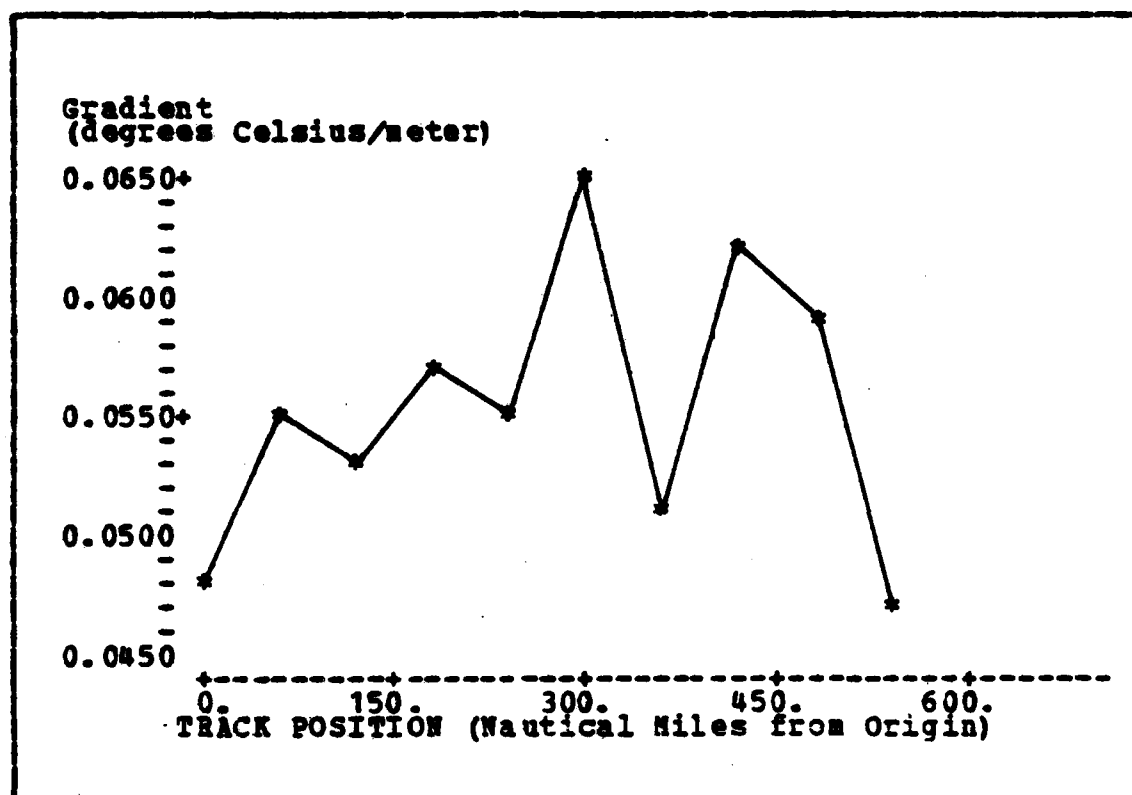


Figure A.4 Gradient from 100 meters vs. Position (15 Nov).

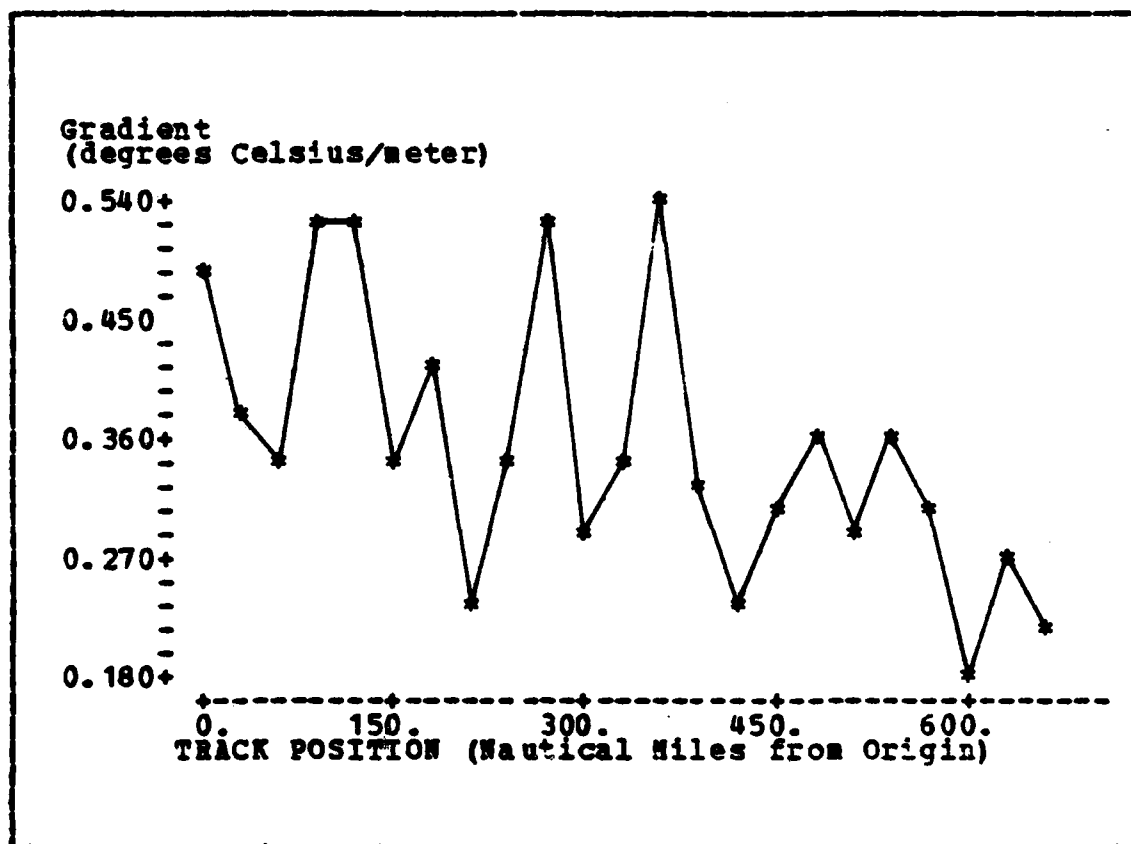


Figure A.5 Gradient from meters vs. Position (17 Nov).

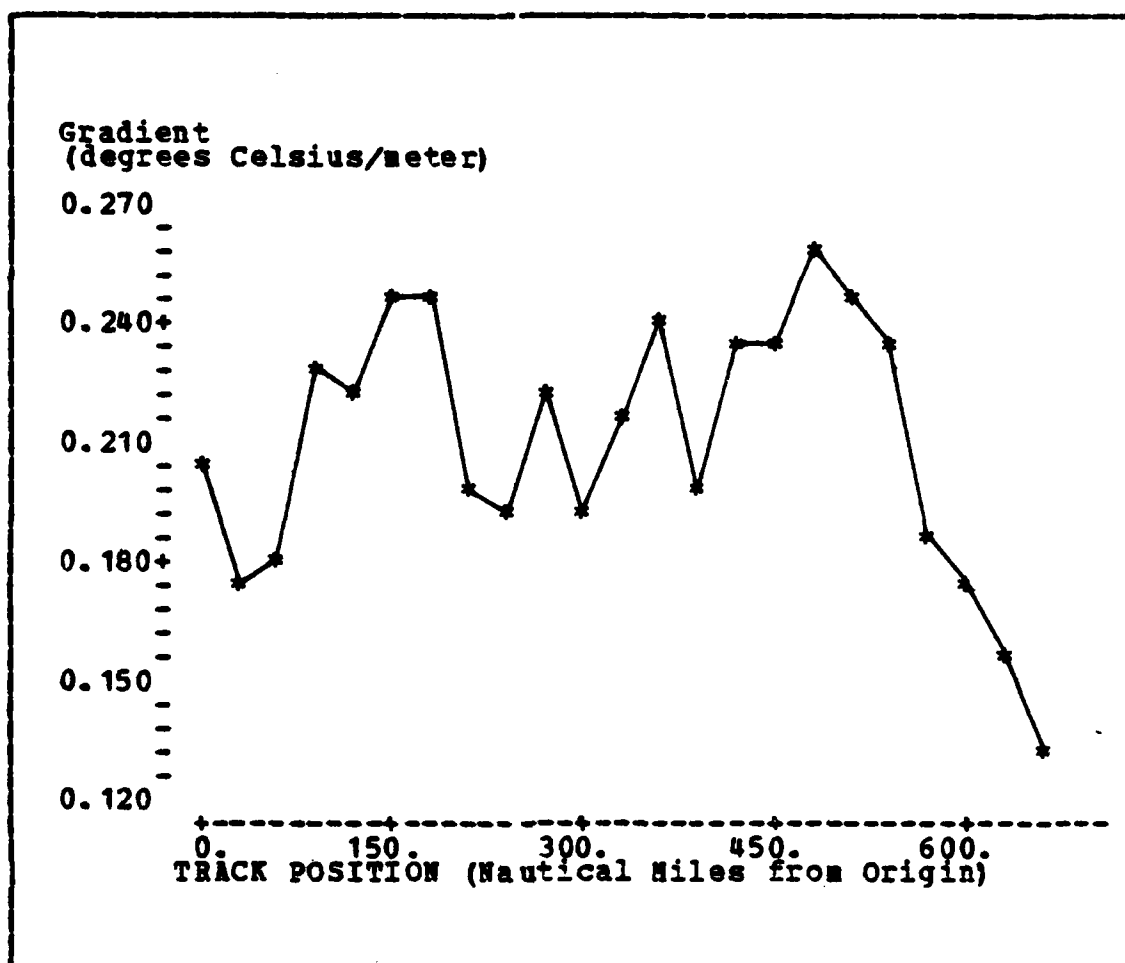


Figure A.6 Gradient from 15 meters vs. Position (17 Nov).

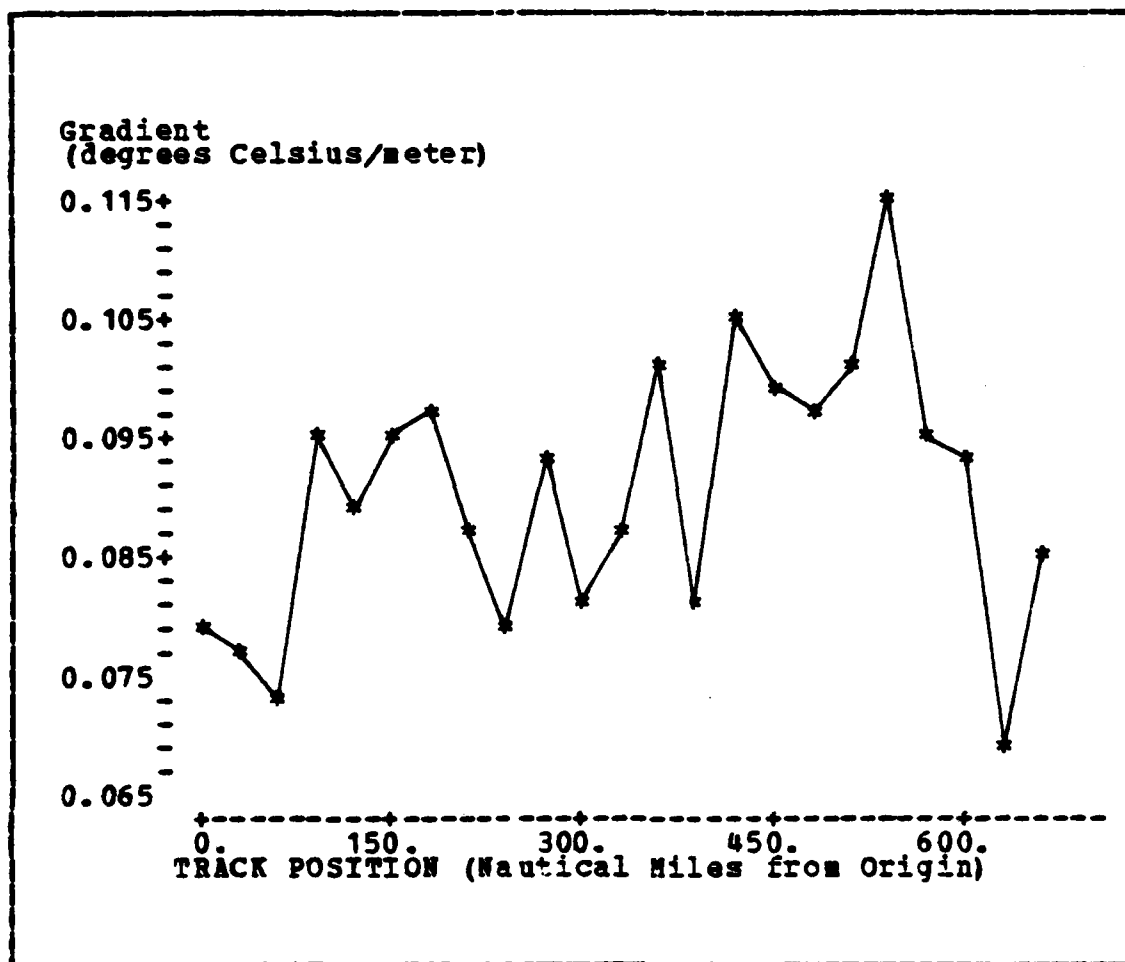


Figure A.7 Gradient from 50 meters vs. Position (17 Nov).

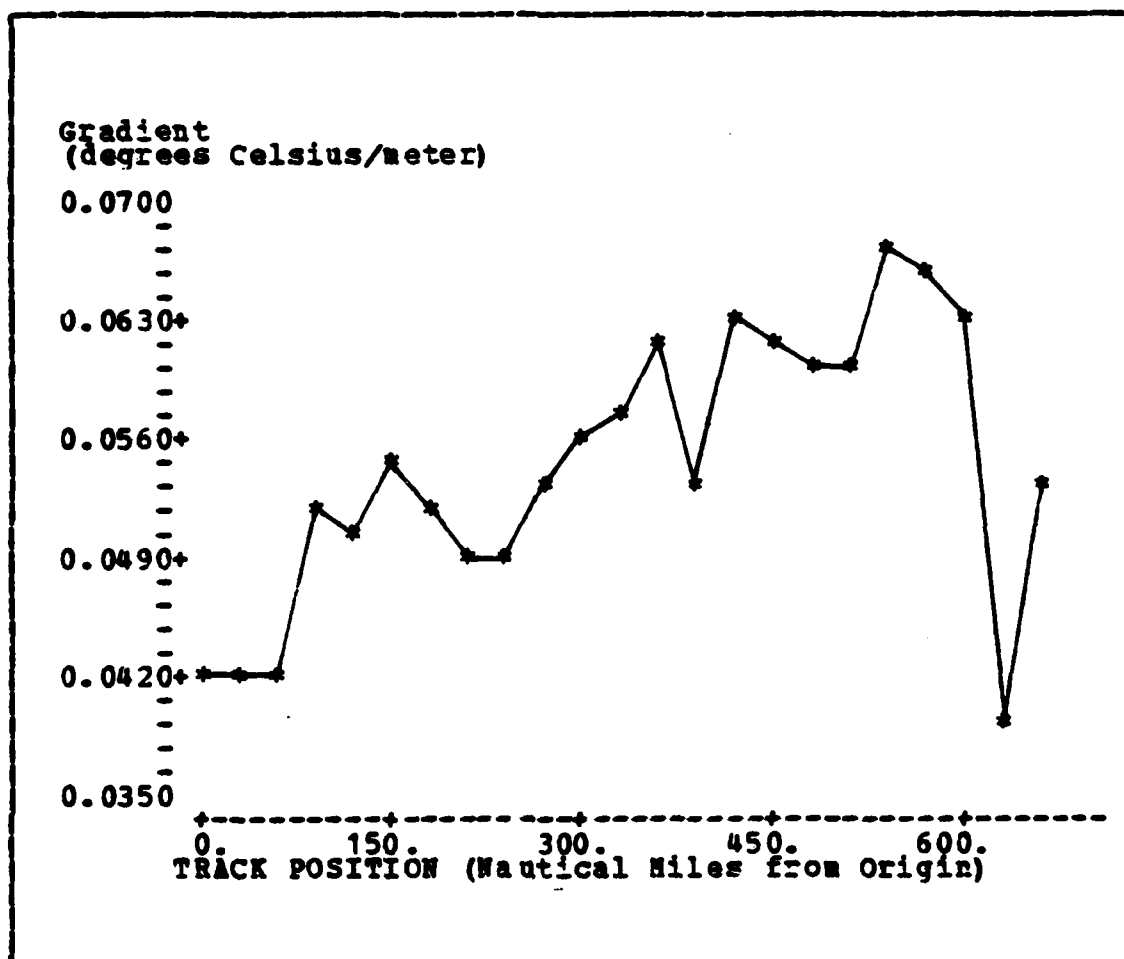


Figure A.8 Gradient from 100 meters vs. Position (17 Nov).

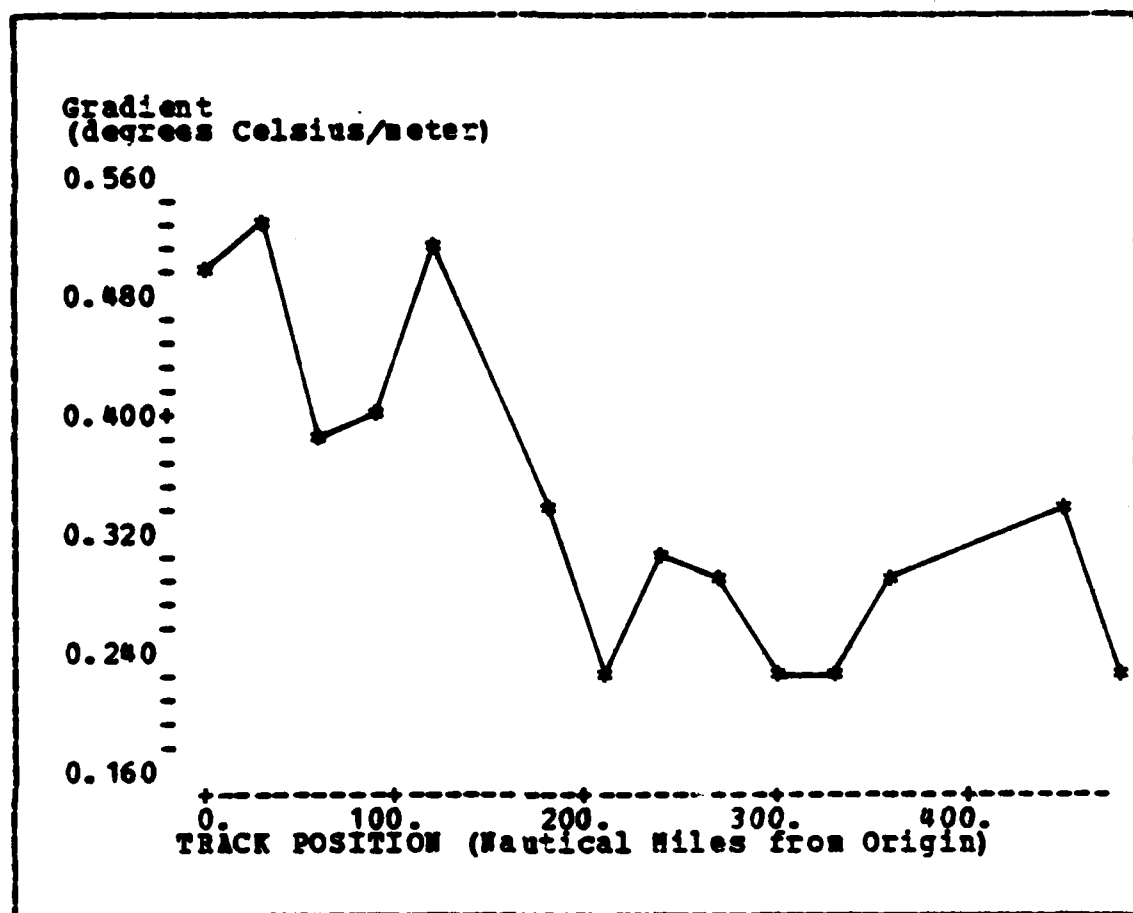


Figure A.9 Gradient from 5 meters vs. Position (19 Nov).

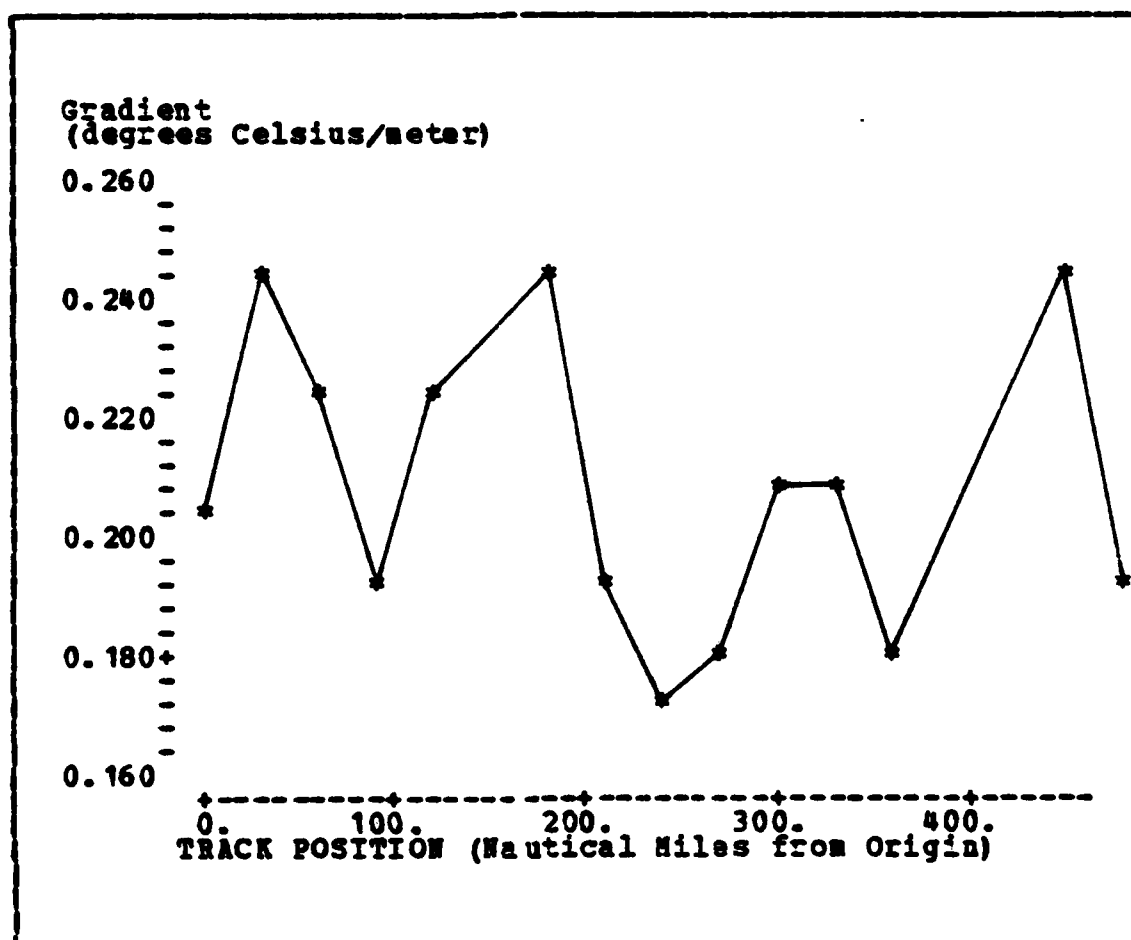


Figure A.10 Gradient from 15 meters vs. Position (19 Nov).

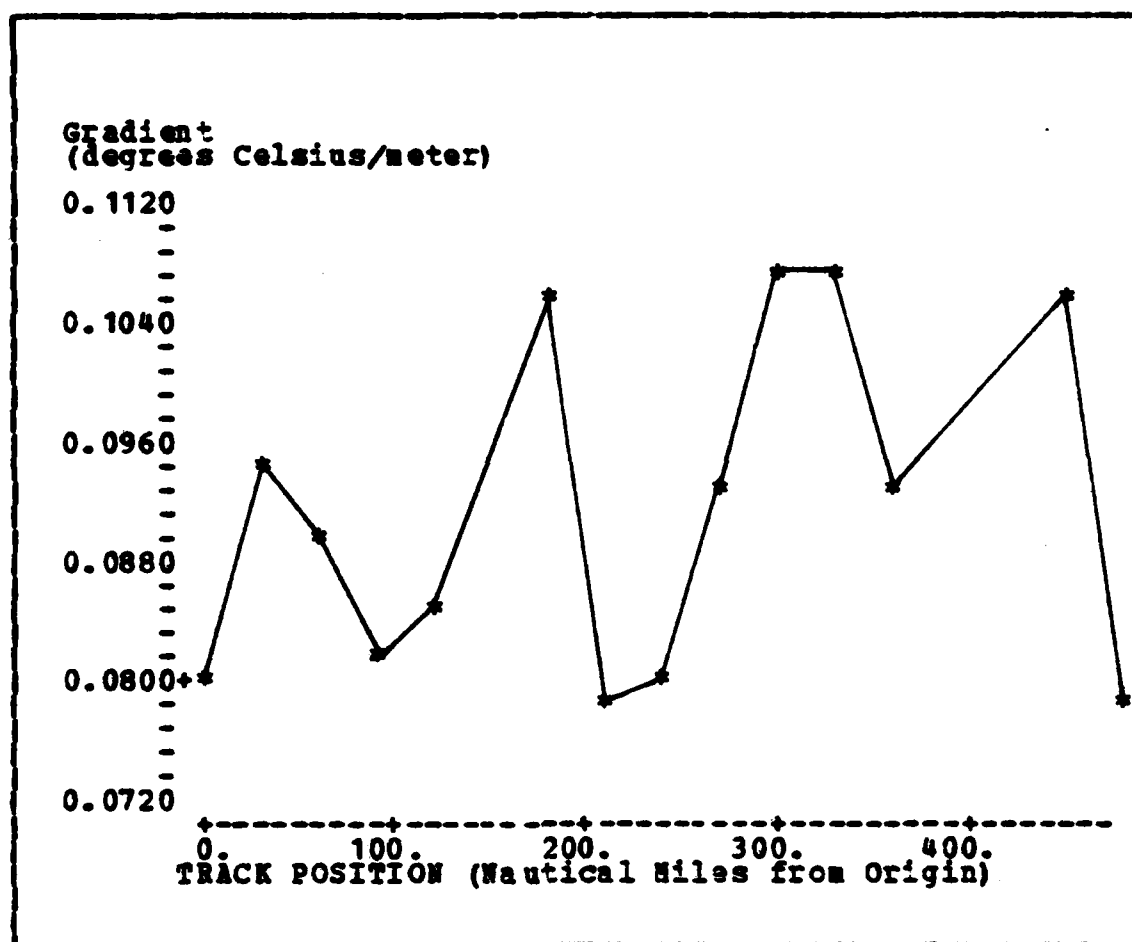


Figure A.11 Gradient from 50 meters vs. Position (19 Nov).

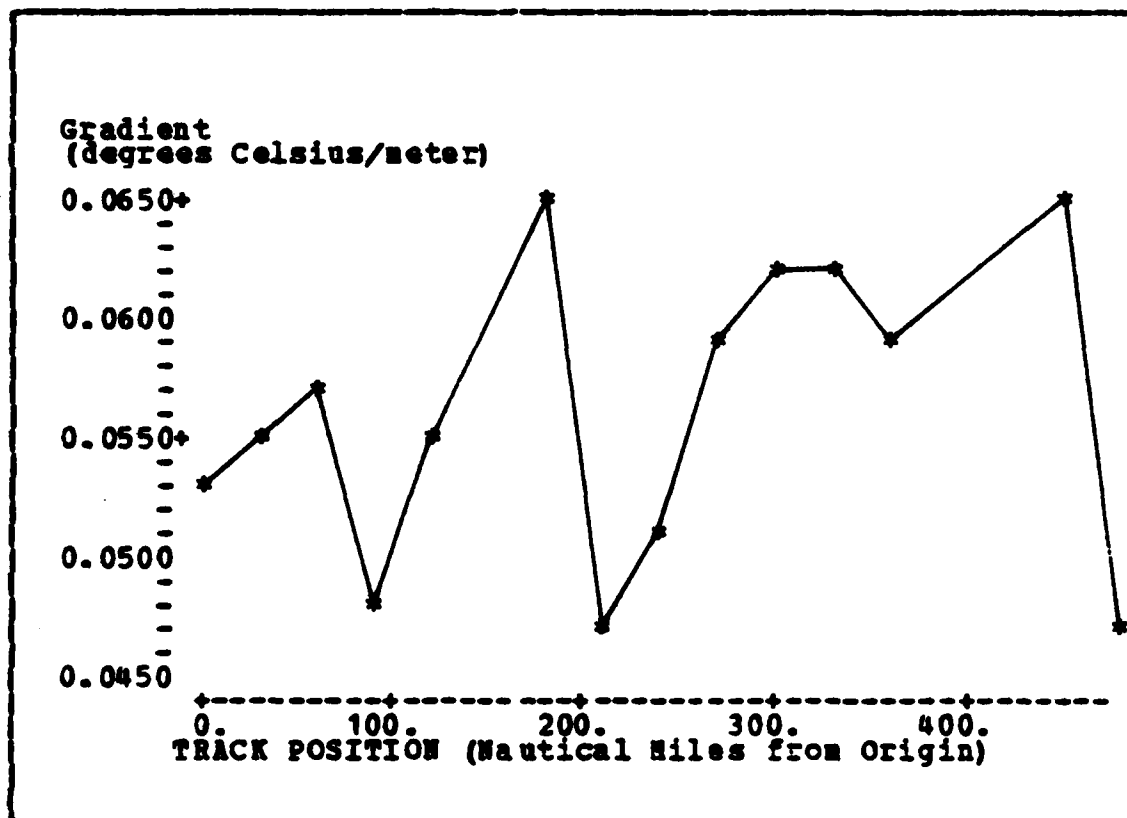


Figure A.12 Gradient from 100 meters vs. Position (19 Nov).

APPENDIX B

VARIATION OF THERMOCLINE GRADIENTS WITH POSITION FOR DECEMBER

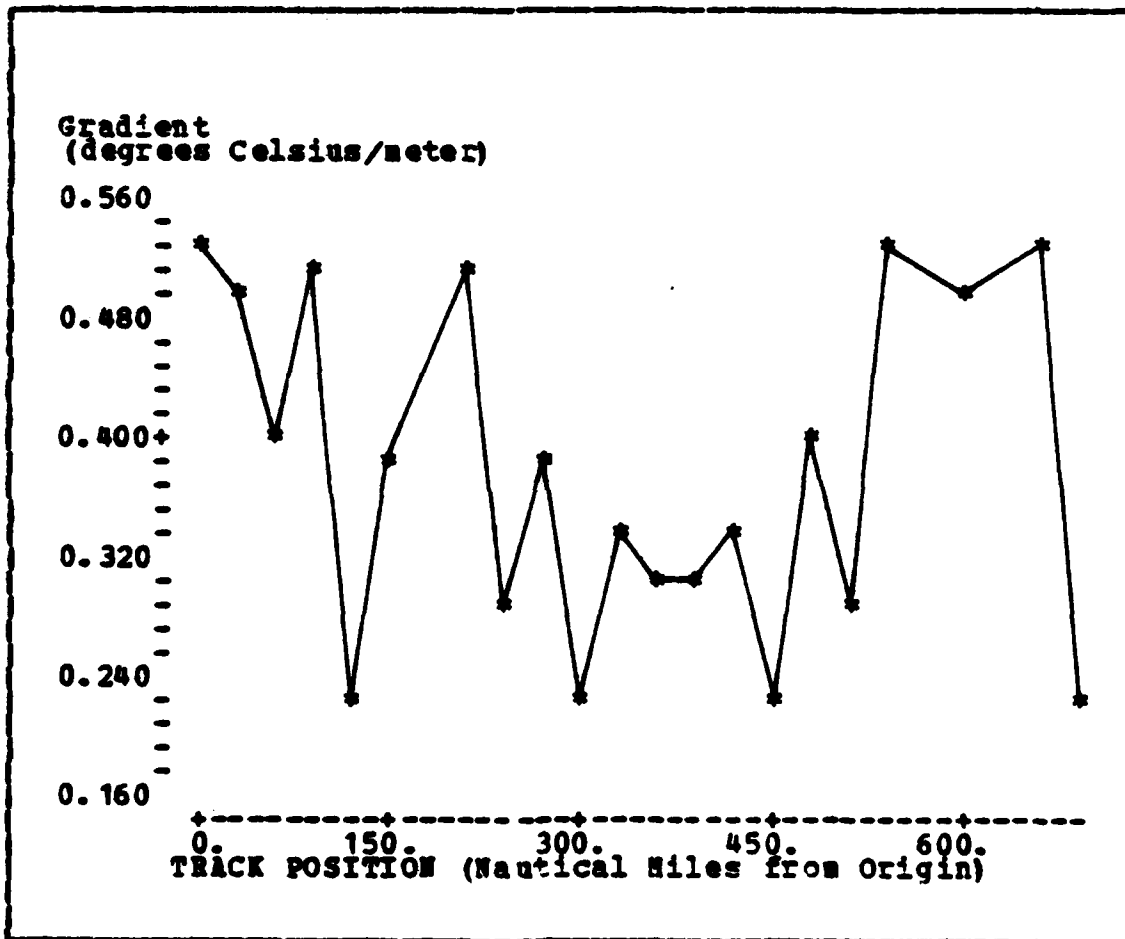


Figure B. 13 Gradient from 5 meters vs. Position (1 Dec).

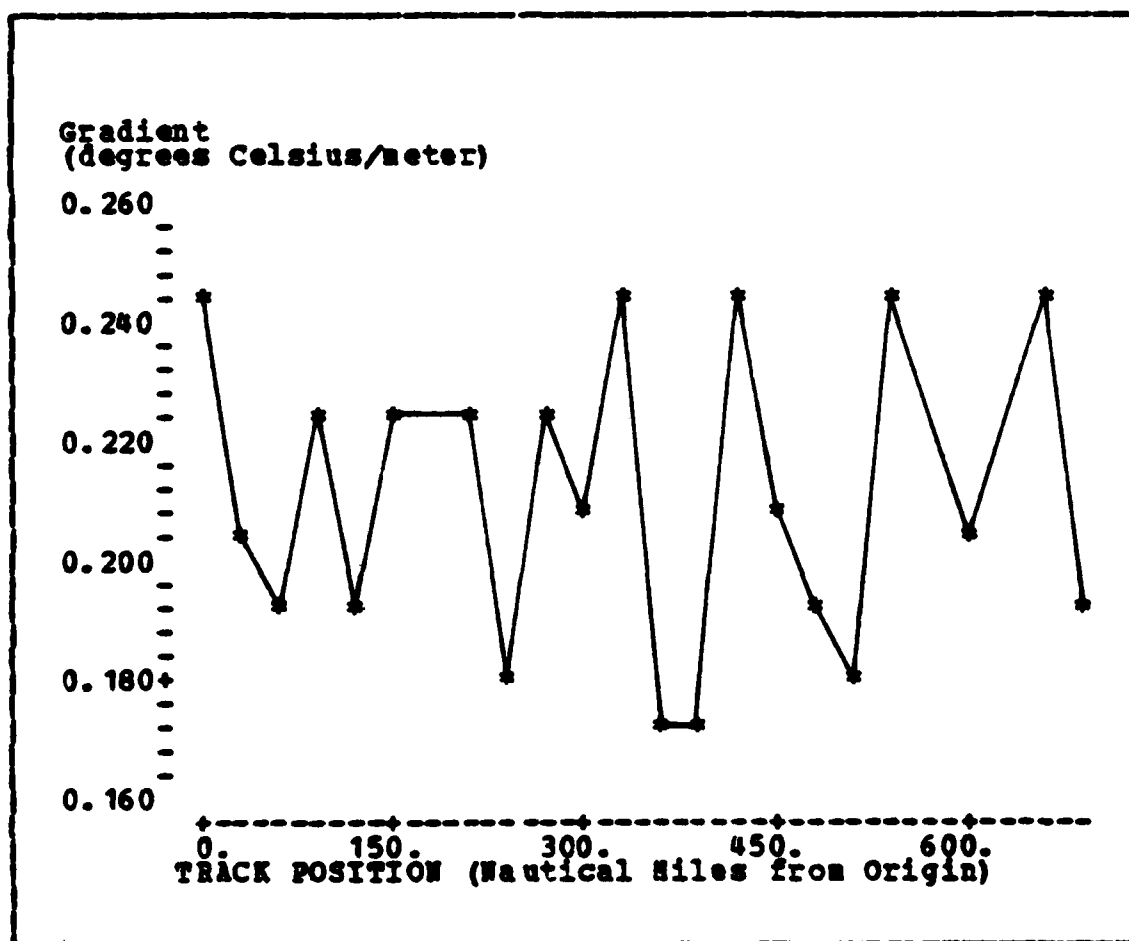


Figure B. 14 Gradient from 15 meters vs. Position (1 Dec).

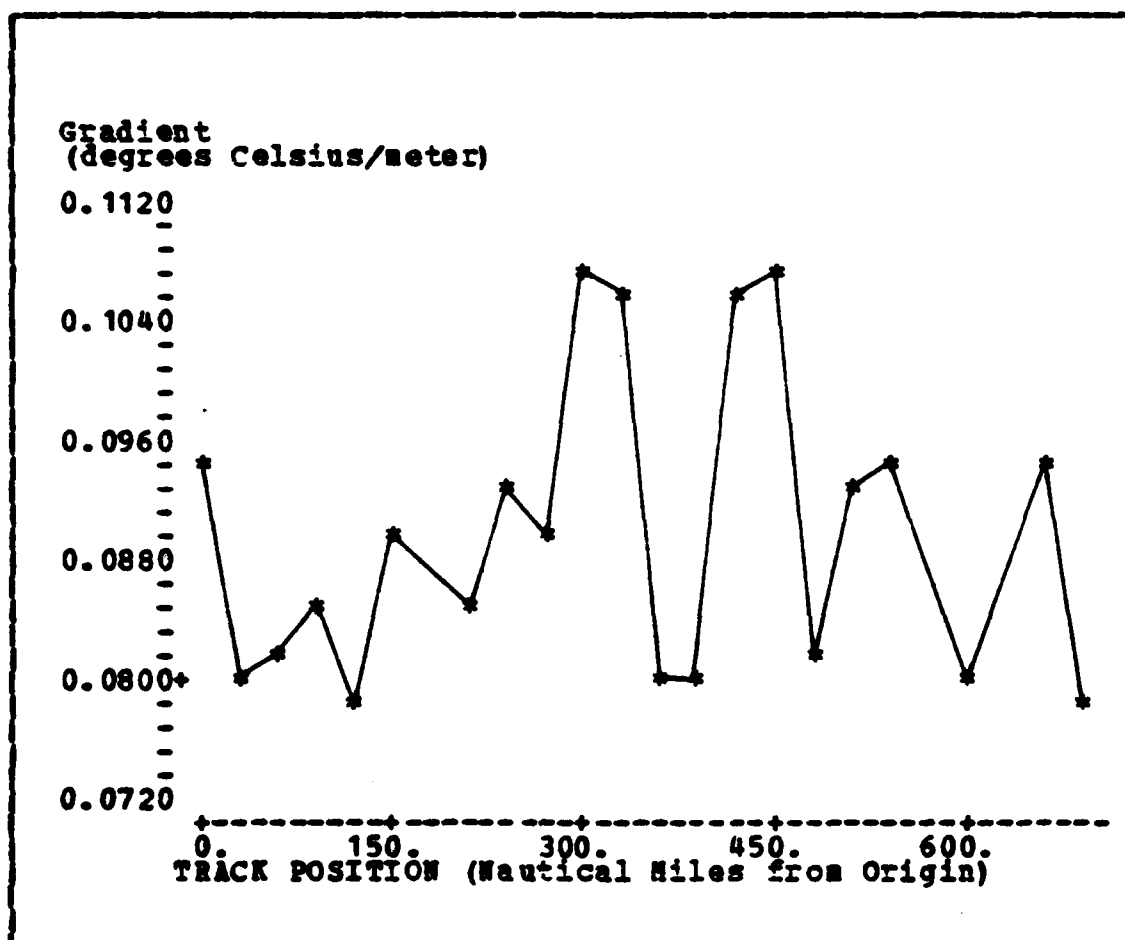


Figure B.15 Gradient from 50 meters vs. Position (1 Dec).

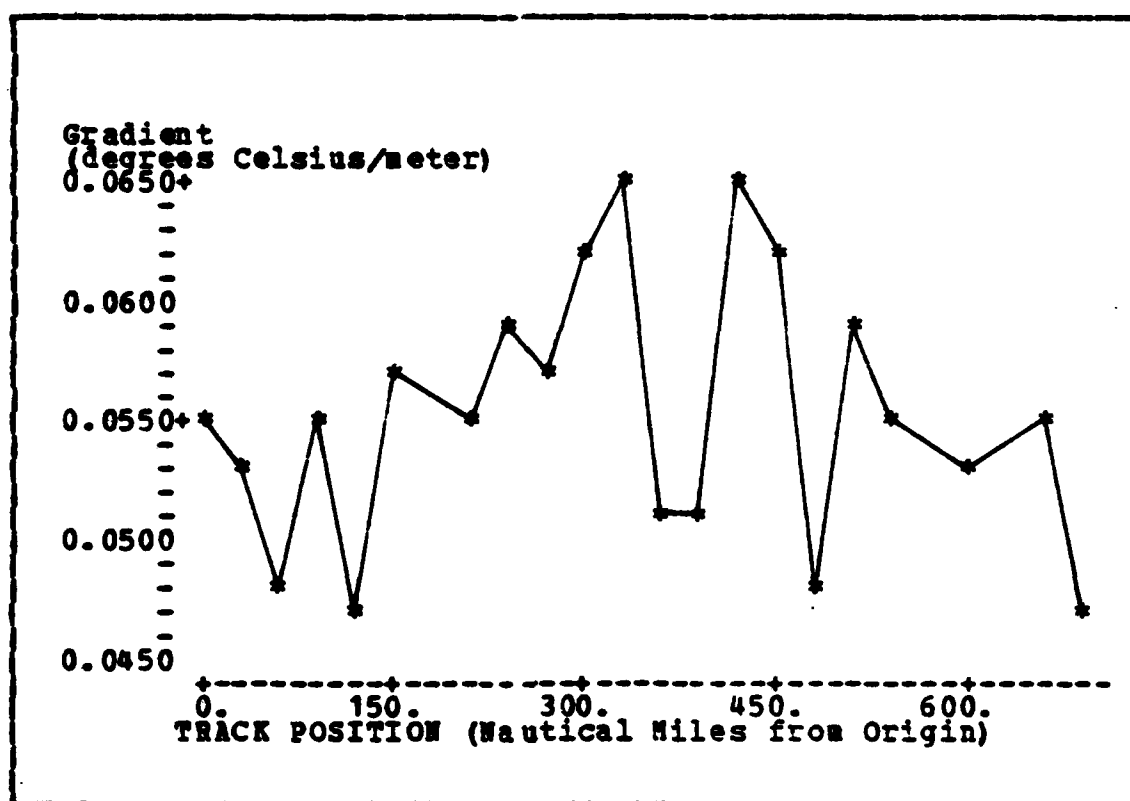


Figure B.16 Gradient from 100 meters vs. Position (1 Dec).

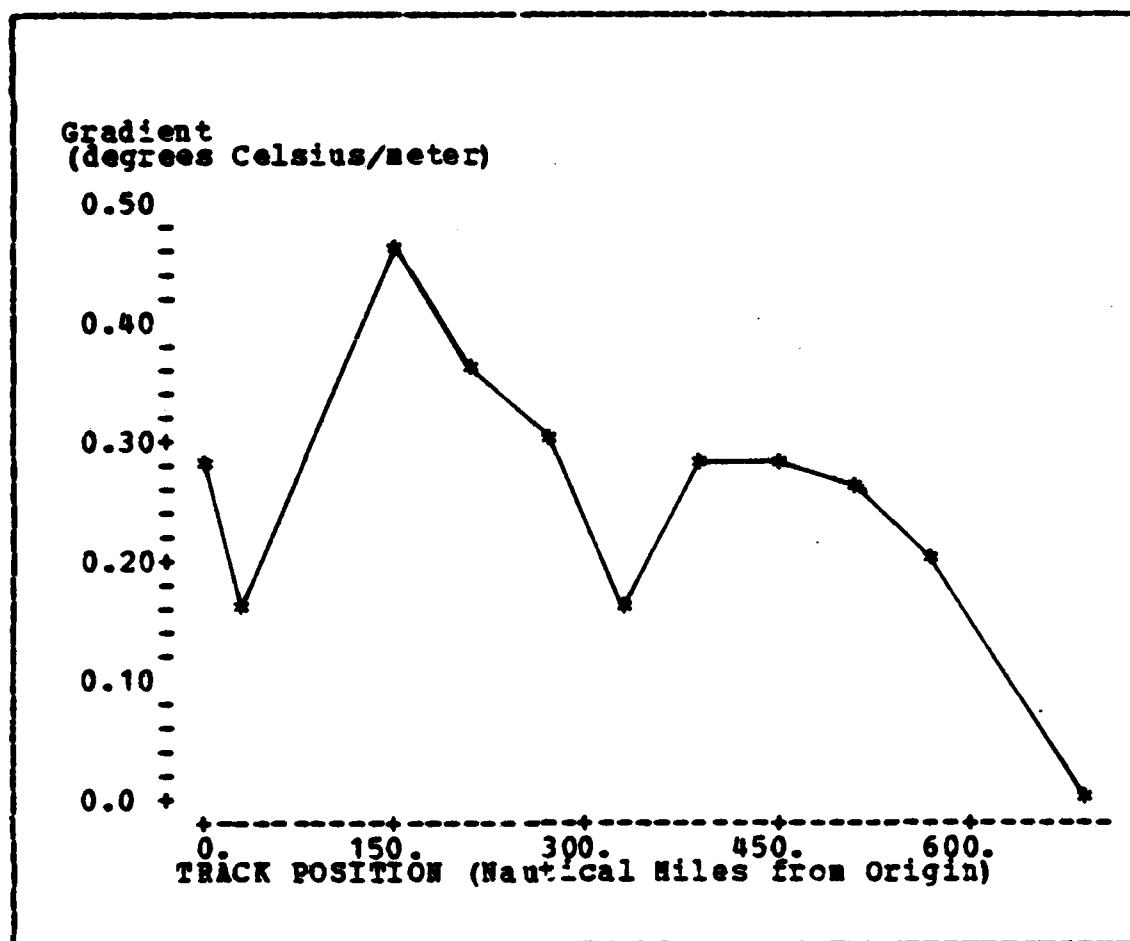


Figure B.17 Gradient from 5 meters vs. Position (3 Dec).

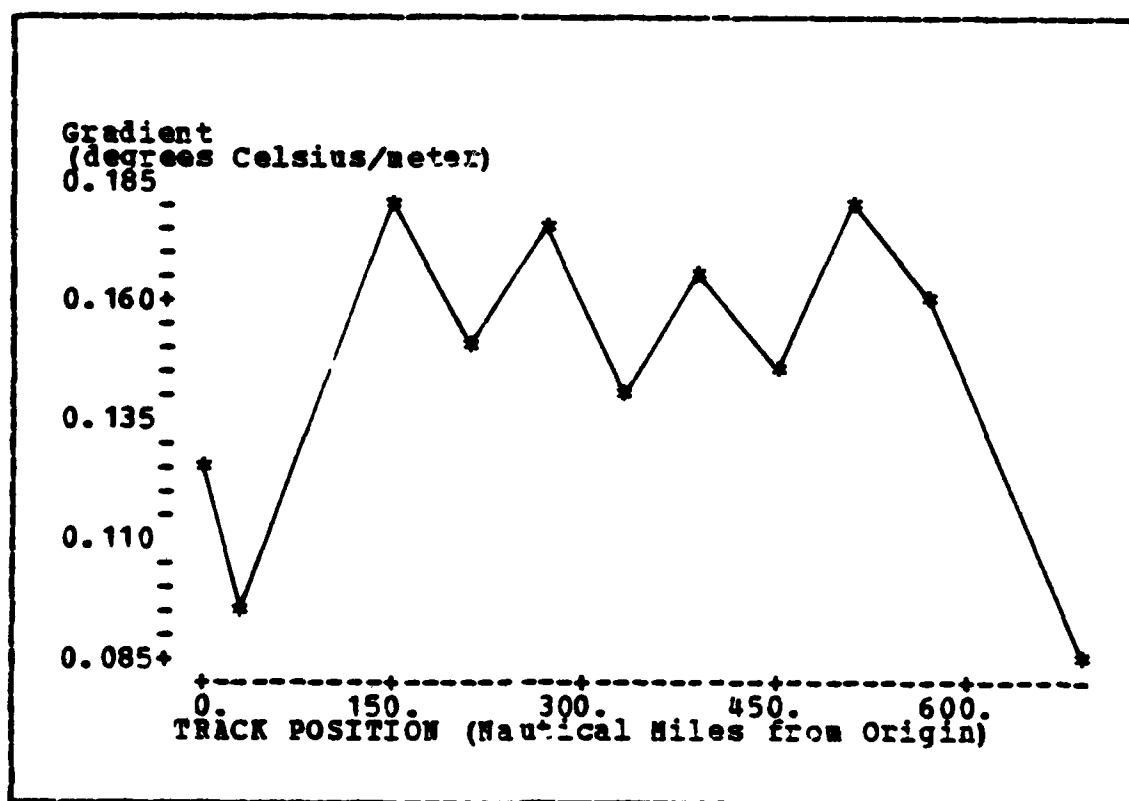


Figure B.18 Gradient from 15 meters vs. Position (3 Dec).

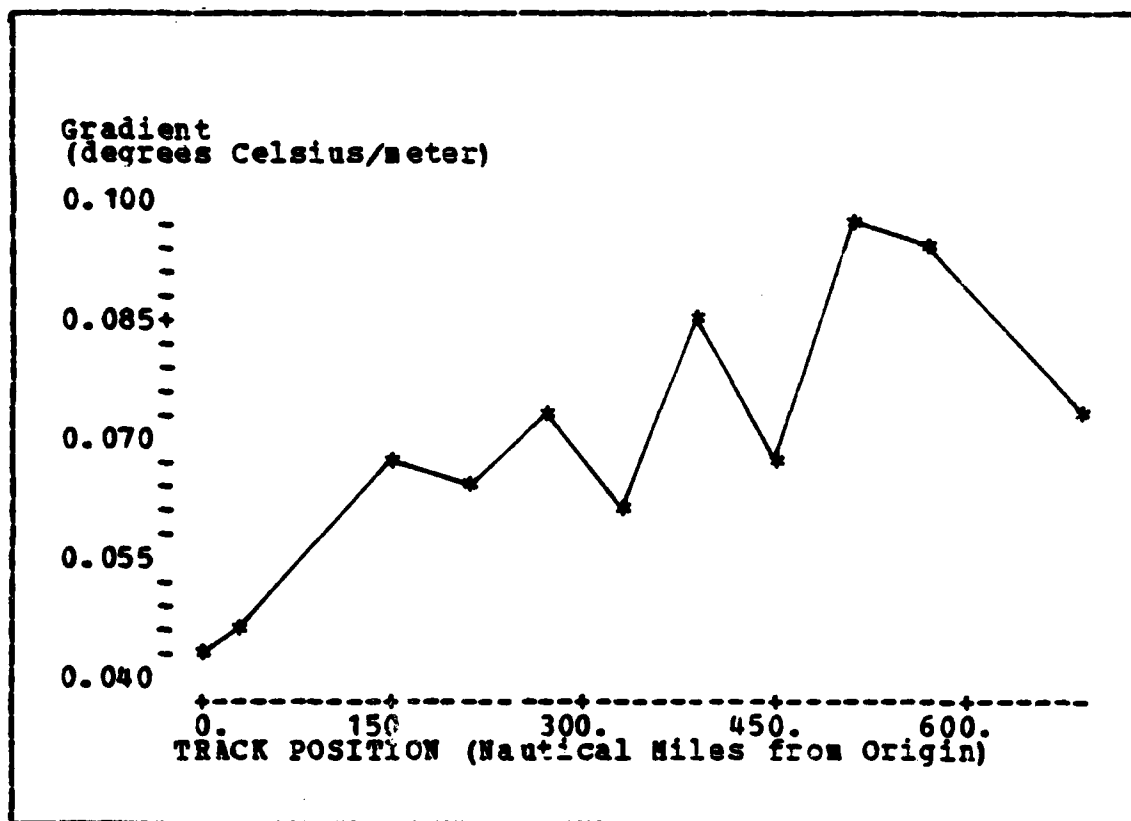


Figure B.19 Gradient from 50 meters vs. Position (3 Dec).

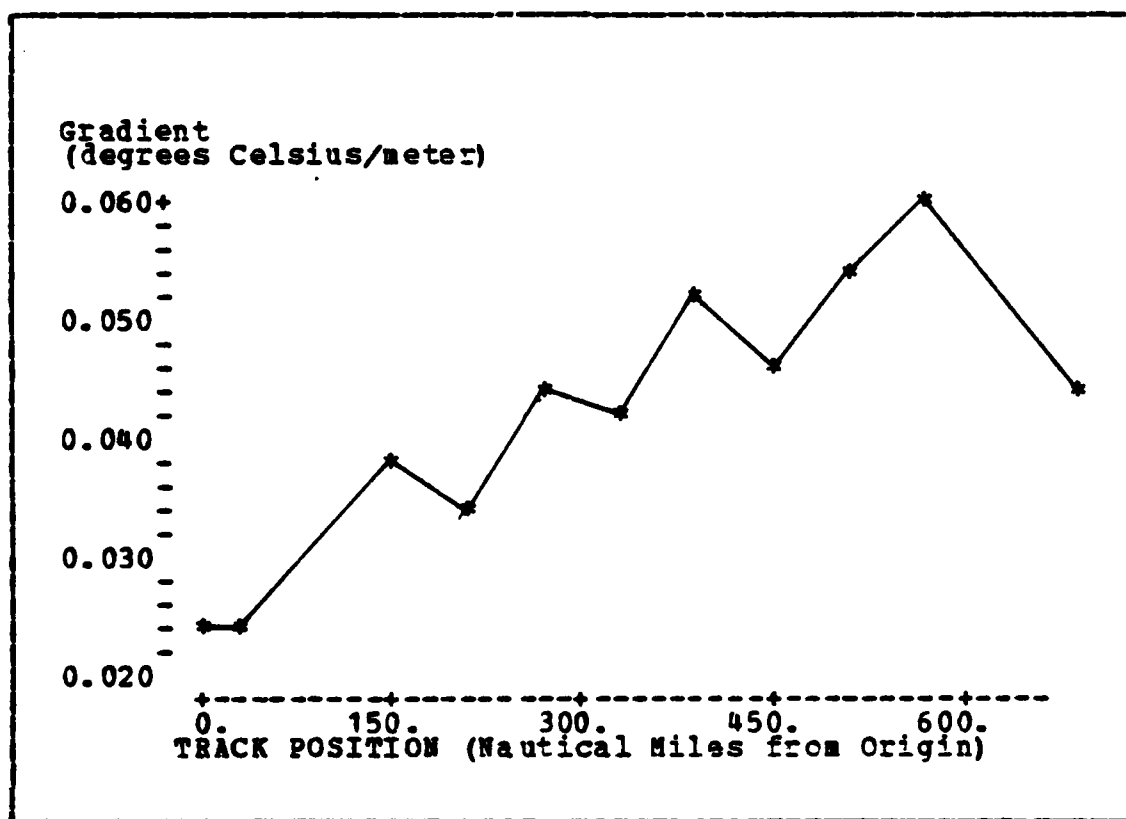


Figure B.20 Gradient from 100 meters vs. Position (3 Dec).

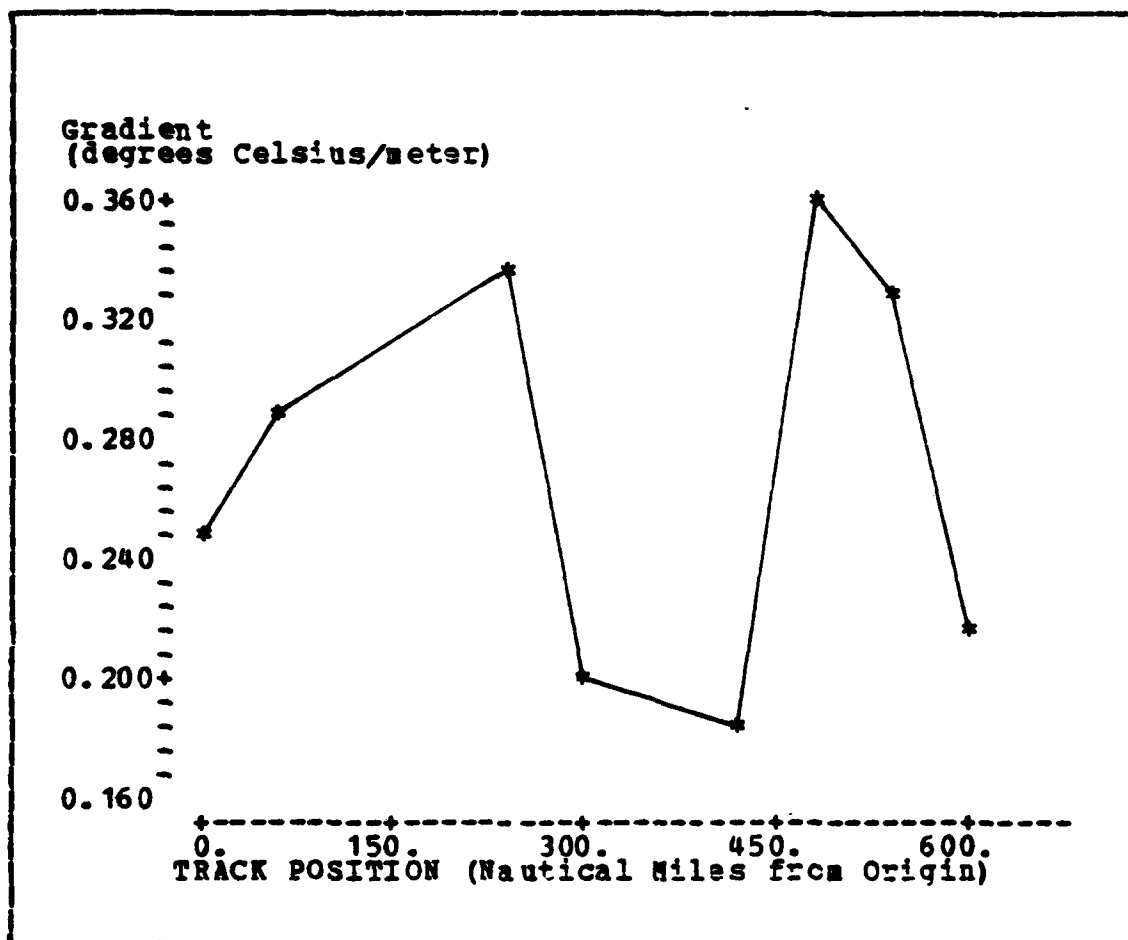


Figure B.21 Gradient from 5 meters vs Position (3 Dec - South).

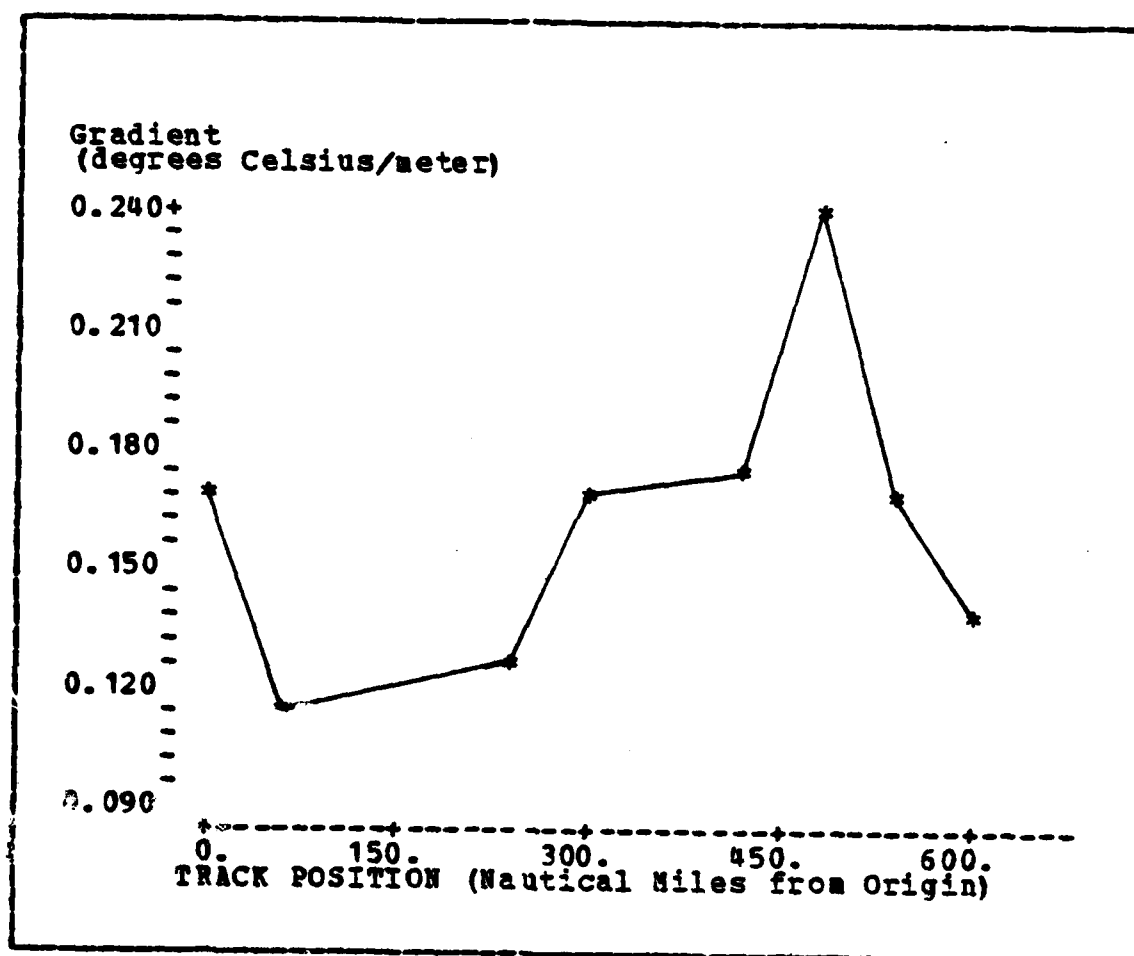


Figure B.22 Gradient from 15 meters vs Position (3 Dec - South).

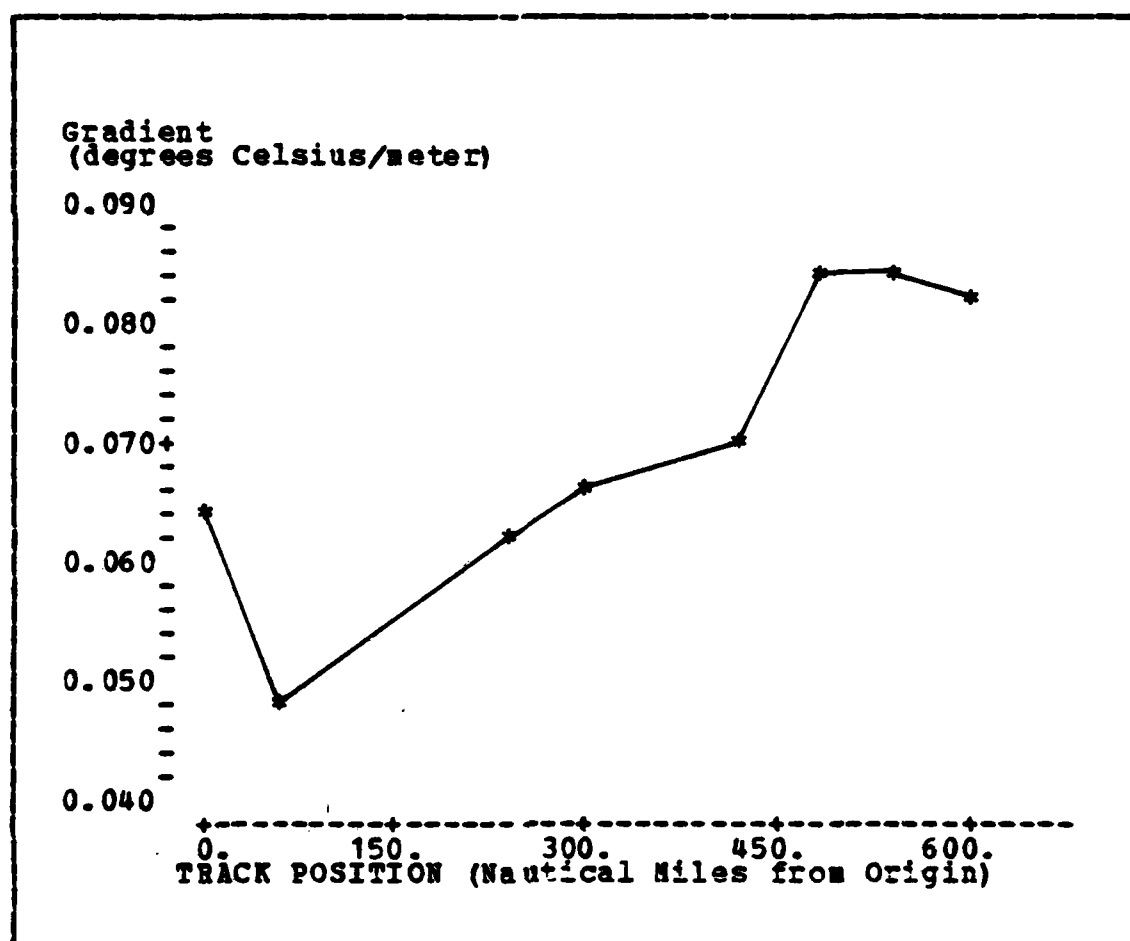


Figure B.23 Gradient from 50 meters vs Position (3 Dec - South).

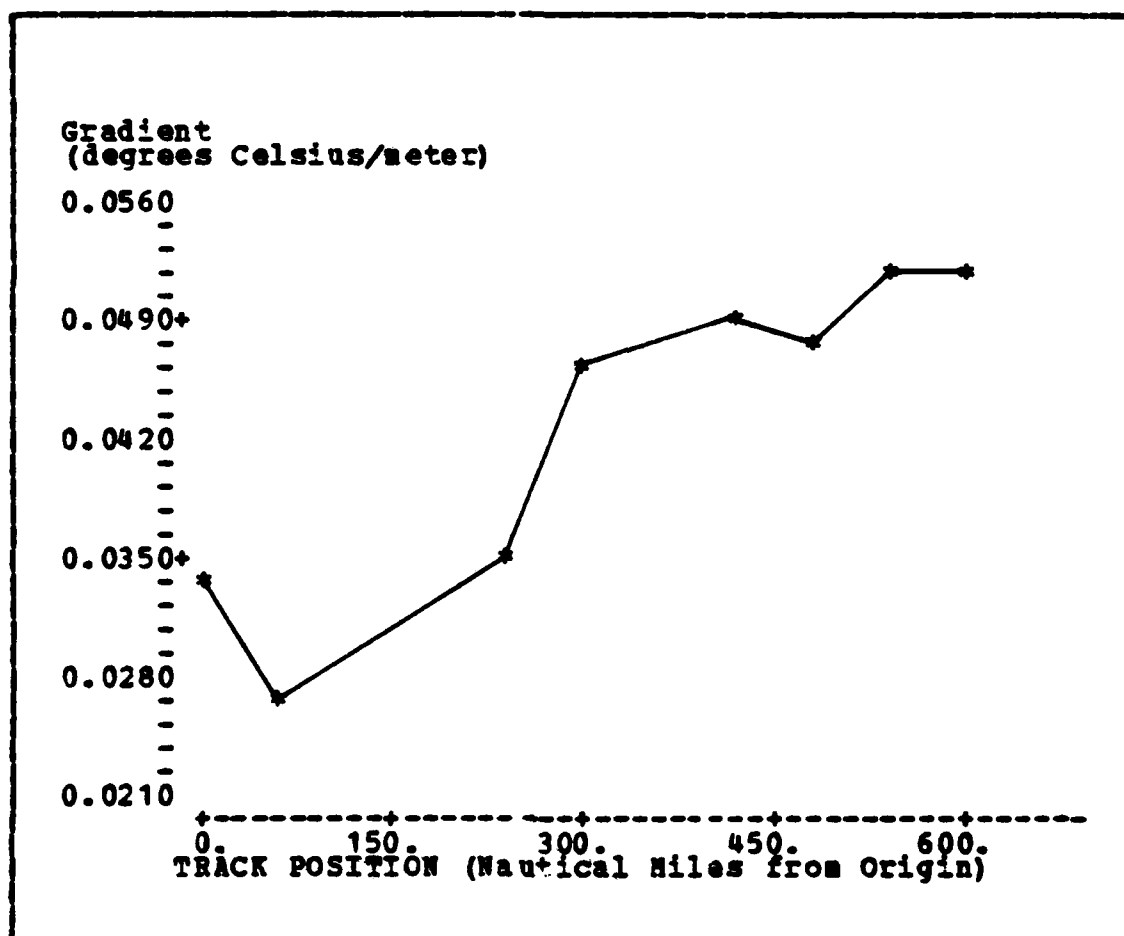


Figure B.24 Gradient from 100 meters vs Position (3 Dec - South).

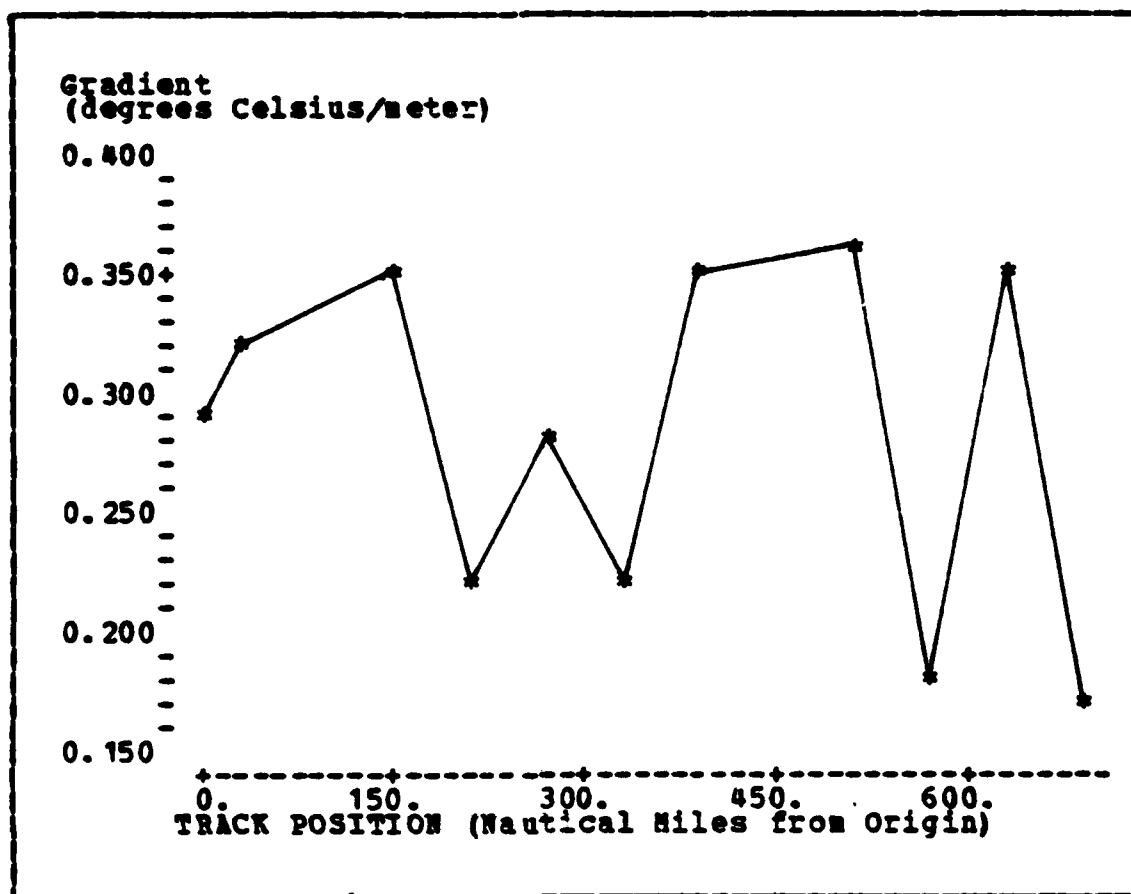


Figure B.25 Gradient from 5 meters vs. Position (5 Dec).

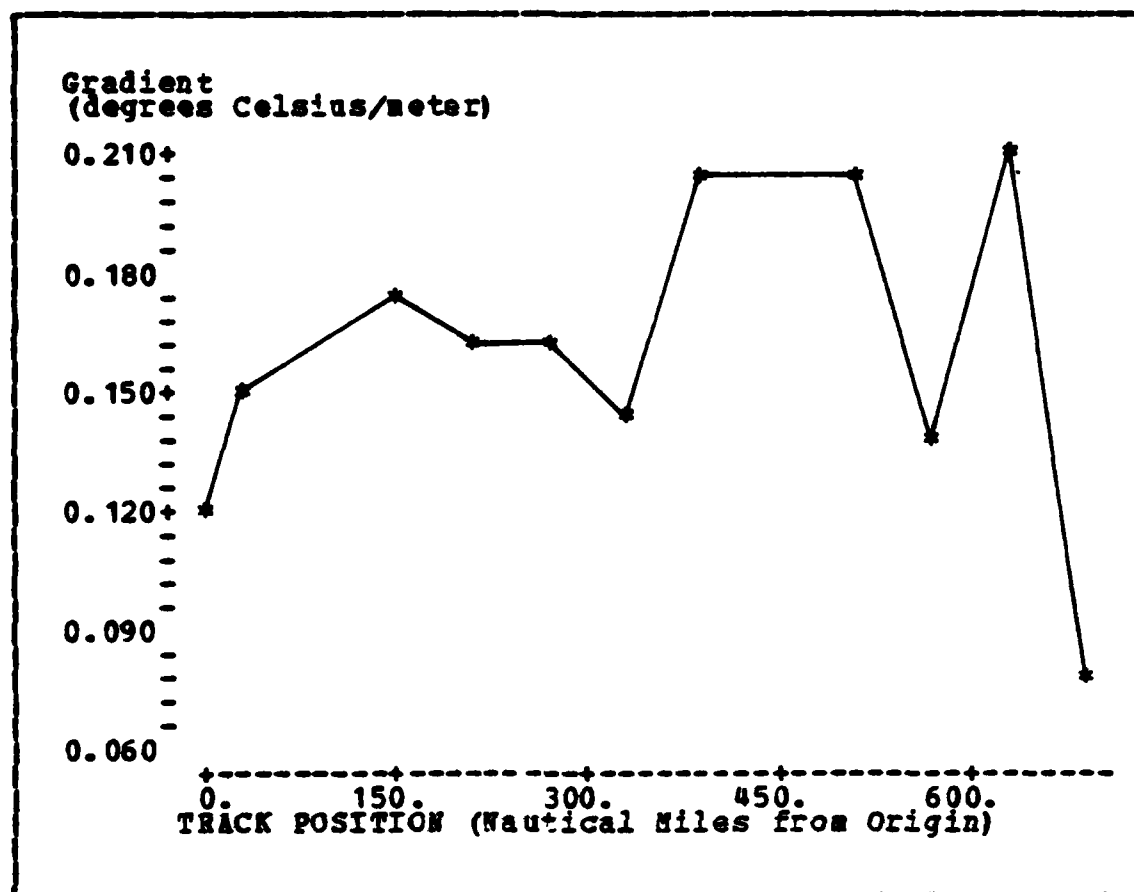


Figure B.26 Gradient from 15 meters vs. Position (5 Dec).

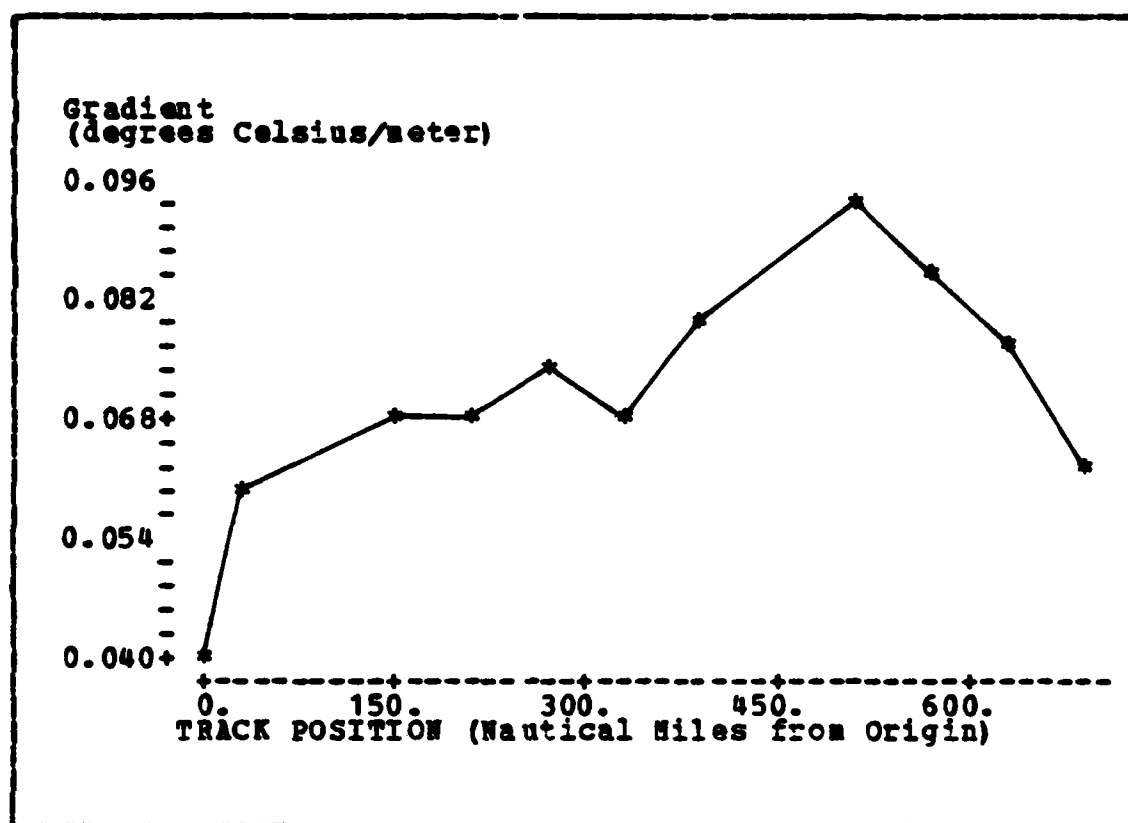


Figure B.27 Gradient from 50 meters vs. Position (5 Dec).

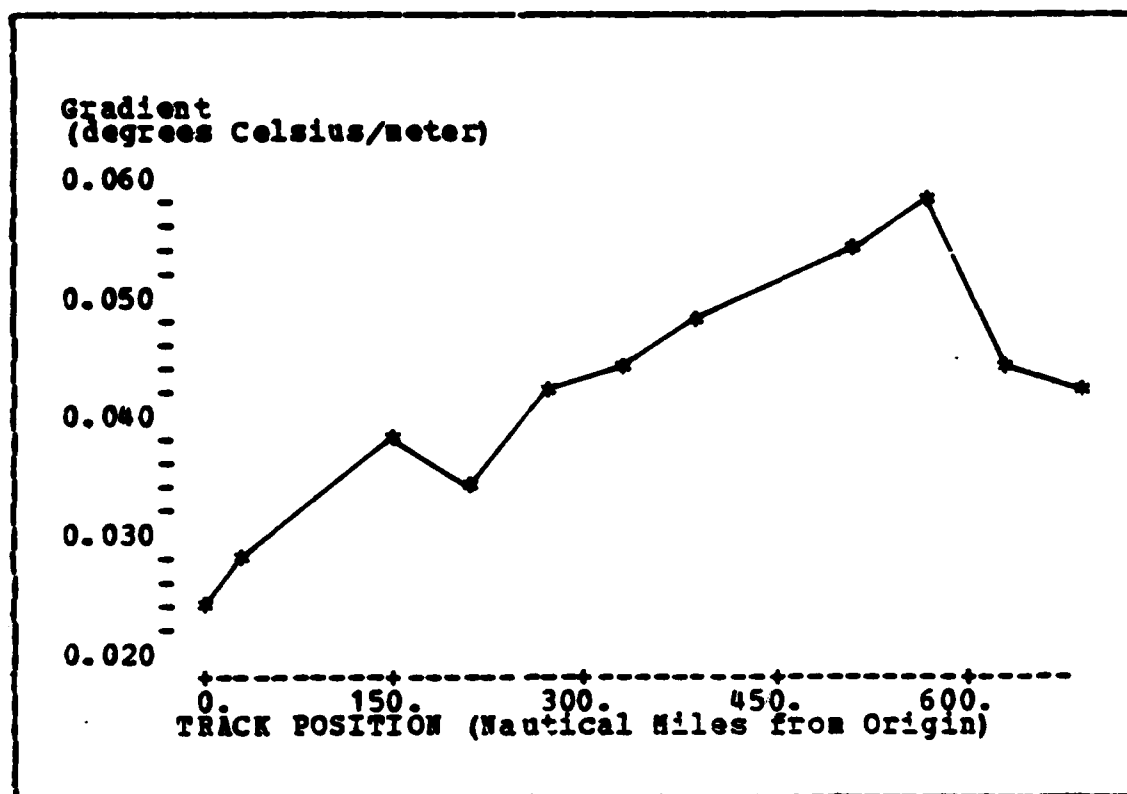


Figure B.28 Gradient from 100 meters vs. Position (5 Dec).

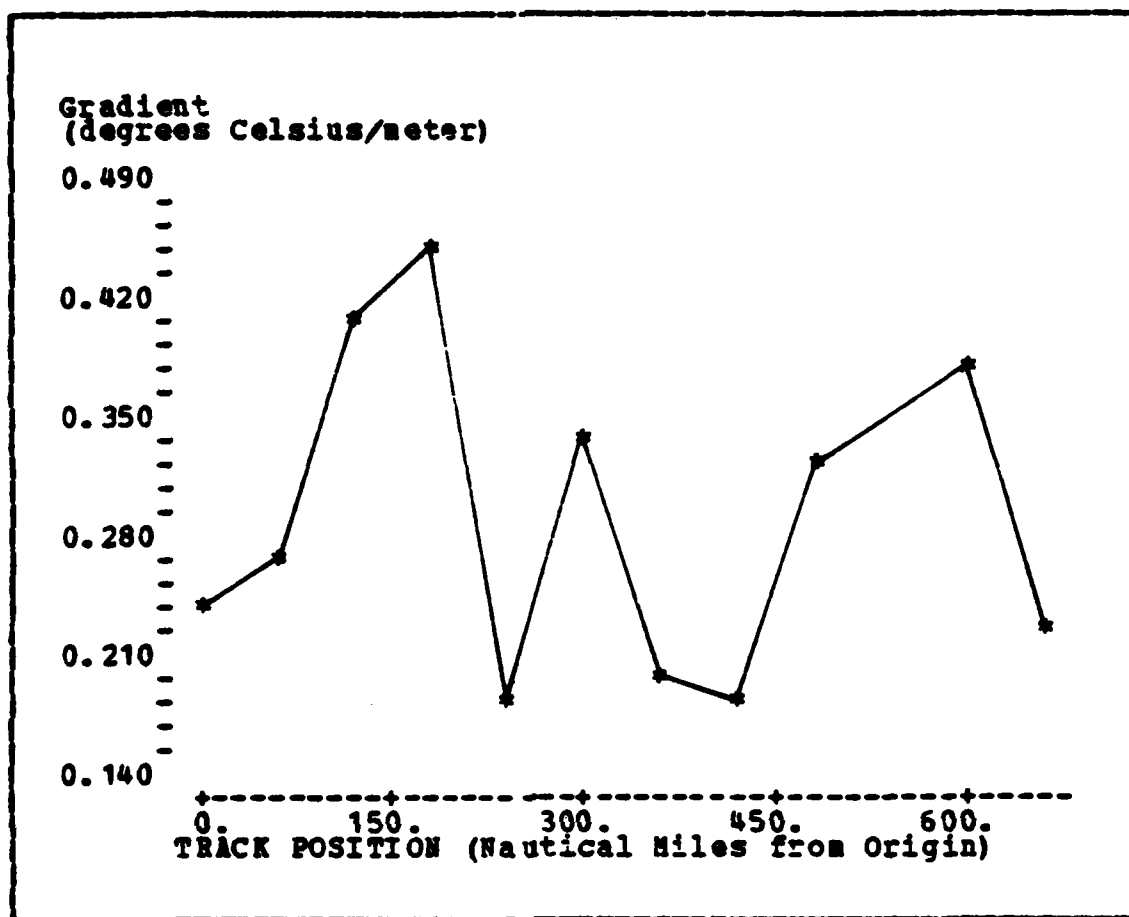


Figure B.29 Gradient from 5 meters vs. Position (5 Dec - North).

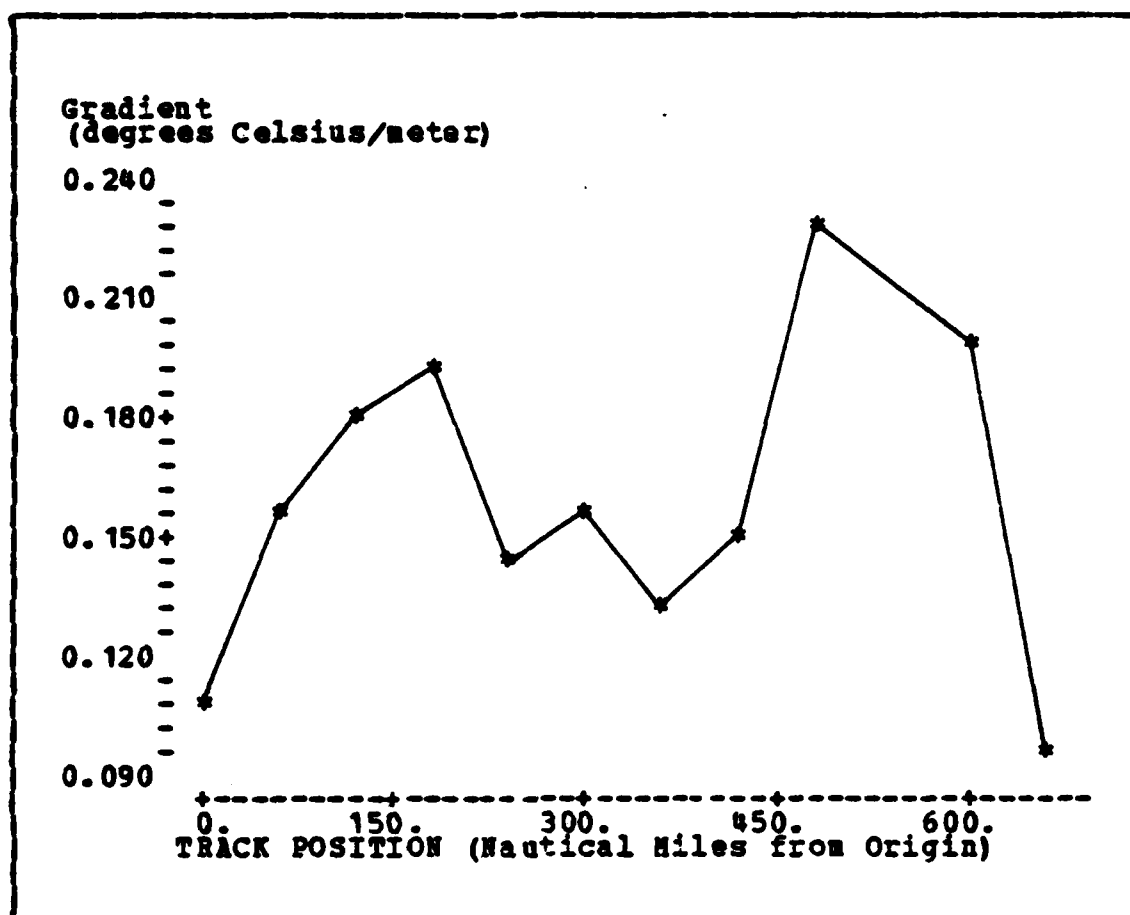


Figure B.30 Gradient from 15 meters vs. Position (5 Dec - North).

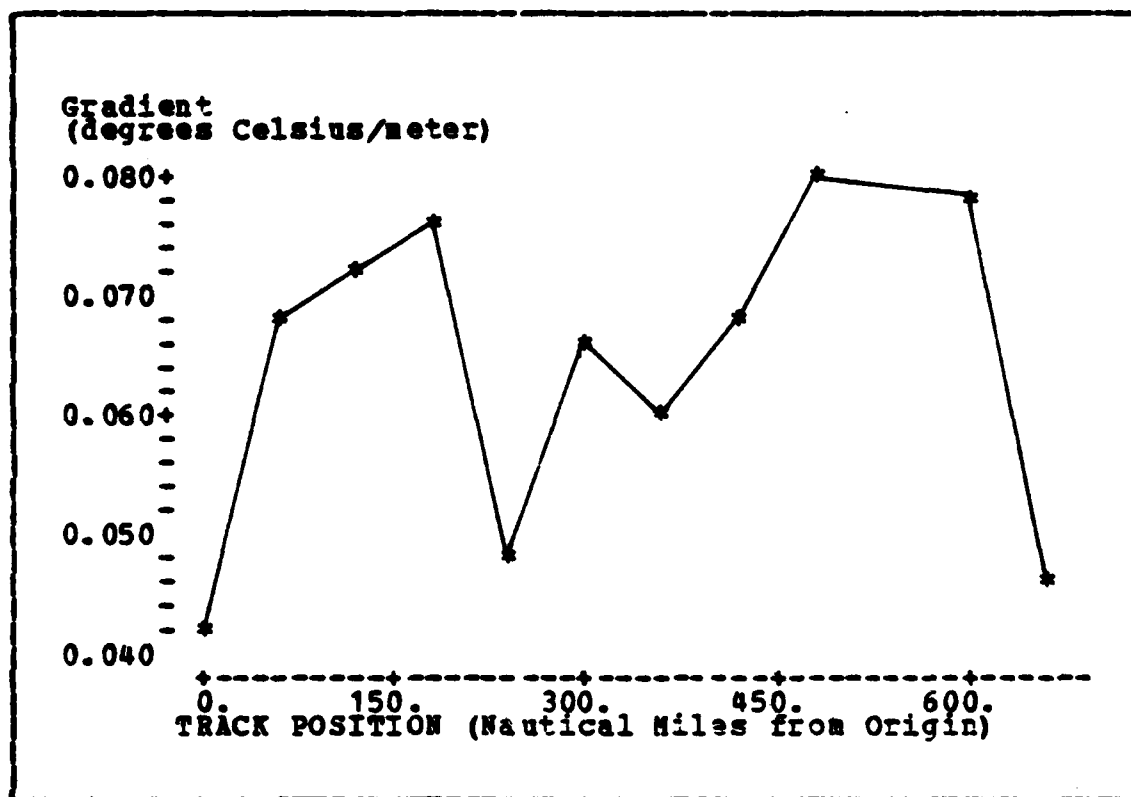


Figure B.31 Gradient from 50 meters vs. Position (5 Dec - North).

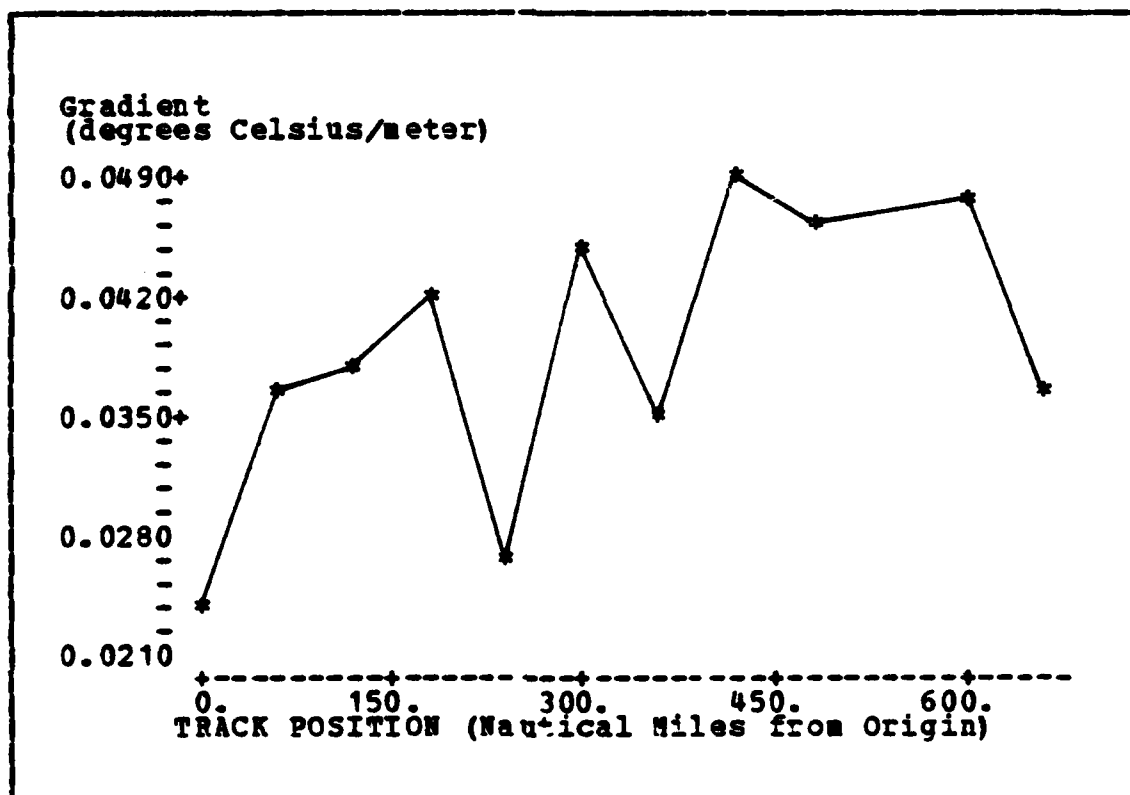


Figure B.32 Gradient from 100 meters vs. Position (5 Dec - North).

APPENDIX C

TABLES OF NORMALIZED GRADIENTS IN THE THERMOCLINE

TABLE XXVI

Normalized Gradients for Flight Track One.

5 meter	15 meter	50 meter	100 meter
0.3980	0.1920	0.0818	0.0479
0.5340	0.2440	0.0948	0.0549
0.4960	0.2027	0.0802	0.0530
0.3880	0.2220	0.0898	0.0566
0.5040	0.2240	0.0844	0.0552
0.3400	0.2427	0.1054	0.0649
0.3120	0.1720	0.0802	0.0506
0.2260	0.2093	0.1070	0.0622
0.2820	0.1793	0.0924	0.0592
0.2300	0.1907	0.0780	0.0465

Note:

1. Gradients were computed from the temperature change over the distance specified in the column heading.

TABLE XXVII

Normalized Gradients for Flight Track Two.

5 meter	15 meter	50 meter	100 meter
0.4940	0.2060	0.0780	0.0425
0.3700	0.1753	0.0774	0.0423
0.3420	0.1787	0.0724	0.0424
0.5160	0.2260	0.0946	0.0519
0.5160	0.2240	0.0894	0.0501
0.3340	0.2467	0.0952	0.0552
0.4160	0.2480	0.0964	0.0525
0.2380	0.1973	0.0872	0.0495
0.3500	0.1920	0.0780	0.0495
0.5300	0.2233	0.0928	0.0530
0.5380	0.1920	0.0814	0.0564
0.3380	0.2167	0.0866	0.0570
0.5320	0.2420	0.1012	0.0622
0.3280	0.1953	0.0818	0.0533
0.3200	0.2367	0.1040	0.0624
0.3020	0.2313	0.0990	0.0611
0.3660	0.2560	0.0968	0.0601
0.2960	0.2473	0.1002	0.0604
0.3600	0.2333	0.1140	0.0670
0.3020	0.1880	0.0954	0.0653
0.1860	0.1760	0.0932	0.0630
0.2660	0.1567	0.0680	0.0397
0.2160	0.1300	0.0856	0.0535

TABLE XXVIII

Normalized Gradients for Flight Track Three.

5 meter	15 meter	50 meter	100 meter
0.4960	0.2027	0.0802	0.0530
0.5340	0.2440	0.0948	0.0549
0.3880	0.2220	0.0898	0.0566
0.3980	0.1920	0.0818	0.0479
0.5040	0.2240	0.0844	0.0552
0.3400	0.2427	0.1054	0.0649
0.2300	0.1907	0.0780	0.0465
0.3120	0.1720	0.0802	0.0506
0.2820	0.1793	0.0924	0.0592
0.2260	0.2093	0.1070	0.0622
0.2260	0.2093	0.1070	0.0622
0.2820	0.1793	0.0924	0.0592
0.3400	0.2427	0.1054	0.0649
0.2300	0.1907	0.0780	0.0465

TABLE XXIX

Normalized Gradients for Flight Track Four.

5 meter	15 meter	50 meter	100 meter
0.5340	0.2440	0.0948	0.0549
0.4960	0.2027	0.0802	0.0530
0.3980	0.1920	0.0818	0.0479
0.5040	0.2240	0.0844	0.0552
0.2300	0.1907	0.0780	0.0465
0.3880	0.2220	0.0898	0.0566
0.5040	0.2240	0.0844	0.0552
0.2820	0.1793	0.0924	0.0592
0.3880	0.2220	0.0898	0.0566
0.2260	0.2093	0.1070	0.0622
0.3400	0.2427	0.1054	0.0649
0.3120	0.1720	0.0802	0.0506
0.3120	0.1720	0.0802	0.0506
0.3400	0.2427	0.1054	0.0649
0.2260	0.2093	0.1070	0.0622
0.3980	0.1920	0.0818	0.0479
0.2820	0.1793	0.0924	0.0592
0.5340	0.2440	0.0948	0.0549
0.4960	0.2027	0.0802	0.0530
0.5340	0.2440	0.0948	0.0549
0.2300	0.1907	0.0780	0.0465

TABLE XXX

Normalized Gradients for Flight Track Five (Center).

5 meter	15 meter	50 meter	100 meter
0.2840	0.1253	0.0440	0.0249
0.1560	0.0953	0.0448	0.0243
0.4560	0.1807	0.0660	0.0382
0.3600	0.1507	0.0648	0.0337
0.3060	0.1773	0.0742	0.0436
0.1620	0.1380	0.0602	0.0414
0.2840	0.1627	0.0840	0.0520
0.2820	0.1447	0.0670	0.0451
0.2700	0.1820	0.0974	0.0546
0.2100	0.1593	0.0934	0.0597
0.0080	0.0853	0.0716	0.0448

TABLE XXXI

Normalized Gradients for Flight Track Five (South).

5 meter	15 meter	50 meter	100 meter
0.2460	0.1707	0.0646	0.0342
0.2860	0.1133	0.0480	0.0262
0.3380	0.1253	0.0616	0.0355
0.2000	0.1687	0.0668	0.0461
0.1840	0.1733	0.0696	0.0489
0.3580	0.2407	0.0840	0.0476
0.3240	0.1707	0.0840	0.0512
0.2140	0.1400	0.0818	0.0522

TABLE XXXII

Normalized Gradients for Flight Track Six (Center).

5 meter	15 meter	50 meter	100 meter
0.2920	0.1220	0.0404	0.0232
0.3200	0.1507	0.0582	0.0283
0.3520	0.1713	0.0694	0.0375
0.2220	0.1640	0.0684	0.0342
0.2780	0.1633	0.0734	0.0425
0.2200	0.1553	0.0680	0.0430
0.3540	0.2033	0.0800	0.0483
0.3580	0.2033	0.0920	0.0544
0.1780	0.1400	0.0850	0.0588
0.3540	0.2113	0.0758	0.0440
0.1680	0.0780	0.0638	0.0421

TABLE XXXIII

Normalized Gradients for Flight Track Six

(North).

5 meter	15 meter	50 meter	100 meter
0.2440	0.1060	0.0428	0.0237
0.2720	0.1547	0.0678	0.0369
0.4060	0.1787	0.0730	0.0377
0.4480	0.1927	0.0758	0.0423
0.1820	0.1440	0.0478	0.0269
0.3400	0.1540	0.0656	0.0449
0.1900	0.1313	0.0606	0.0352
0.1840	0.1520	0.0686	0.0489
0.3280	0.2280	0.0792	0.0462
0.3720	0.2007	0.0774	0.0471
0.2240	0.0960	0.0456	0.0359

APPENDIX D

MODEL EQUATIONS FOR EACH FLIGHT

TABLE XXXIV

Model Equations for MLD (15 November).

Model Variables	Equations
SST	MLD =
SST, Position	MLD = - 122 - 0.0918 (Position) + 14.6 (SST)
SST, Position, Gradient (100)	MLD = - 105 - 0.0718 (Position) + 10.5 (SST) + 62.3 (GRAD(100))

Notes:

1. SST is sea surface temperature.
2. Position refers to station position relative to the most seaward station.
3. GRAD (100) refers to the gradient computed from the upper 100 meters of the thermocline.

TABLE XXXV

Model Equations for MLD (17 November).

Model Variables	Equations
SST	$MLD = + 43.7 + 1.01 (SST)$
SST, Position	$MLD = - 57.7$ $- 0.0865 (Position)$ $+ 10.9 (SST)$
SST, Position, Gradient (15)	$MLD = + 62.8$ $- 0.098 (Position)$ $+ 12.3 (SST)$ $- 43.1 (GRAD(15))$
SST, Position, Gradient (100)	$MLD = - 88.2$ $- 0.115 (Position)$ $+ 17.3 (SST)$ $+ 8.18 (GRAD(100))$

TABLE XXXVI

Model Equations for MLD (19 November).

Model Variables	Equations
SST	$MLD = + 68.7 - 0.86 (SST)$
SST, Position	$MLD = + 17.9$ $- 0.0551 (Position)$ $+ 3.71 (SST)$
SST, Position, Gradient (5)	$MLD = - 7.46$ $- 0.045 (Position)$ $+ 4.58 (SST)$ $+ 31.2 (GRAD(5))$
SST, Position, Gradient (100)	$MLD = + 18.2$ $- 0.055 (Position)$ $+ 3.72 (SST)$ $- 8.62 (GRAD(100))$

TABLE XXXVII

Model Equations for MLD (1 December).

Model Variables	Equations
SST	$MLD = + 92.5 - 2.03 (SST)$
SST, Position	$MLD = + 28.9$ $- 0.061 (Position)$ $+ 4.93 (SST)$
SST, Position, Gradient (50)	$MLD = + 11.3$ $- 0.06 (Position)$ $+ 4.62 (SST)$ $+ 235. (GRAD (50))$
SST, Position, Gradient (100)	$MLD = + 16.3$ $- 0.057 (Position)$ $+ 4.28 (SST)$ $+ 344 (GRAD (100))$

TABLE XXXVIII

Model Equations for MLD (3 December, Center).

Model Variables	Equations
SST	$MLD = + 95.5 - 2.48 (SST)$
SST, Position	$MLD = + 40.61$ $- 0.0683 (Position)$ $+ 4.10 (SST)$
SST, Position, Gradient (15)	$MLD = + 52.0$ $- 0.043 (Position)$ $+ 0.95 (SST)$ $+ 118.2 (GRAD (15))$
SST, Position, Gradient (100)	$MLD = + 71.7$ $- 0.064 (Position)$ $- 3.61 (SST)$ $+ 1384 (GRAD (100))$

TABLE XXXIX

Model Equations for MLD (3 December, South).

Model Variables	Equations
SST	$MLD = + 95.5 - 2.48 (SST)$
SST, Position	$MLD = + 40.61$ $- 0.0683 (Position)$ $+ 4.10 (SST)$
SST, Position, Gradient (50)	$MLD = + 127$ $- 0.021 (Position)$ $+ 0.85 (SST)$ $- 936.6 (GRAD (50))$
SST, Position, Gradient (100)	$MLD = + 102$ $- 0.044 (Position)$ $- 1.530 (SST)$ $+ 103.0 (GRAD (100))$

TABLE XL

Model Equations for MLD (5 December, Center).

Model Variables	Equations
SST	$MLD = + 111 - 3.38 (SST)$
SST, Position	$MLD = + 12.40$ $- 0.103 (Position)$ $+ 8.18 (SST)$
SST, Position, Gradient (5)	$MLD = + 8.23$ $- 0.10 (Position)$ $+ 7.92 (SST)$ $+ 20.9 (GRAD (5))$
SST, Position, Gradient (100)	$MLD = + 20.2$ $- 0.099 (Position)$ $+ 6.70 (SST)$ $+ 187.4 (GRAD (100))$

TABLE XLI

Model Equations for MLD (5 December, North).

Model Variables	Equations
SST	$MLD = + 123 - 5.01 (SST)$
SST, Position	$MLD = - 43.7$ $- 0.12 (Position)$ $+ 13.1 (SST)$
SST, Position, Gradient (5)	$MLD = + 8.23$ $- 0.10 (Position)$ $+ 7.92 (SST)$ $+ 20.9 (GRAD(5))$
SST, Position, Gradient (100)	$MLD = - 34.0$ $- 0.114 (Position)$ $+ 11.42 (SST)$ $+ 174.7 (GRAD(100))$

LIST OF REFERENCES

1. Miyake, M., STREX Storm Transfer and Response Experiment Operation Plan, (draft), p. I-V, June 20, 1980.
2. Tabata, S., "Characteristics of Water and Variations of Salinity, Temperature, and Dissolved Oxygen Content of the Water at Ocean Weather Station 'P' in the Northeast Pacific Ocean", Journal of the Fisheries Research Board of Canada, v. 17(3), p. 353, 1960.
3. Ibid., p. 356.
4. Dodimead, A.J., Favorite, P., and Hirano, T., Review of Oceanography of the Subarctic Pacific Region, v. 1, p. 44, paper prepared for the International North Pacific Fisheries Commission, 1 October 1962.
5. Sverdrup H.U., Johnson, M.W., and Fleming, R.H., The Oceans, Their Physics, Chemistry, and General Biology, p. 740, Prentice-Hall, 1942.
6. Kibblewhite, A.C., Bedford, M.L. and Mitchell, S.K., "Regional Dependence of Low-Frequency Attenuation in the North Pacific Ocean", Journal of the Acoustical Society of America, v. 61(5), pp. 1169-1177, May 1977.
7. Tabata, S., "Variability of Oceanographic Conditions at Ocean Station 'P' in the Northeast Pacific Ocean", Transactions of the Royal Society of Canada, v. 3, series 4, p. 369, June 1965.
8. Dodimead et al., op. cit., p. 4.
9. Roden, G.I., "On North Pacific Temperature, Salinity, Sound Velocity and Density Fronts and Their Relation to Wind and Energy Flux Fields", Journal of Physical Oceanography, v 5., n.4, p. 560, October 1975.
10. Tabata, S., op. cit., p. 369, 1965.
11. Dodimead et al., op. cit., p. 66.
12. Tabata, S., op. cit., p. 372, 1965.
13. Dodimead et al., op. cit., p. 62.
14. Dodimead et al., op. cit., Figures 216 & 225.

15. Tully, J. P., "Oceanographic Regions and Assessment of Temperature Structure in the Seasonal Zone of the North Pacific Ocean", Journal of the Fisheries Research Board of Canada, v. 21 (5), p. 955, 1964.
16. Naval Oceanographic Office Reference Publication 2 Atlas of North Pacific Ocean Monthly Mean Temperatures and Mean Salinities of the Surface Layer, by H. K. Robinson and R. A. Bauer, 1976.
17. Dodimead et al., op. cit., p. 62.
18. Tully op. cit., p. 960.
19. Dodimead et al., op. cit., p. 63.
20. Dodimead et al., op. cit., Figure 216.
21. Dodimead et al., op. cit., p. 63.
22. Tabata, S., "Temporal Changes of Salinity, Temperature, and Dissolved Oxygen Content of the Water at Station "P" in the Northeast Pacific Ocean, and Some of Their Determining Factors", Journal of the Fisheries Research Board of Canada, v. 18 (6), p. 1090, 1961.
23. Uda, Michitake, "Oceanography of the Subarctic Pacific Ocean", Journal of the Fisheries Research Board of Canada, v. 20 (1), p. 131, 1963.
24. Dodimead et al., op. cit., p. 68.
25. Tully, J. P. and Giovando, L. F., "Seasonal Temperature Structure in the Eastern Subarctic Pacific Ocean", Marine Distributions, The Royal Society of Canada Special Publication No. 5, p. 10, 1963.
26. Dodimead et al., op. cit., Figure 37.
27. Dodimead et al., op. cit., Figure 225.
28. Uda, op. cit., p. 132.
29. Dodimead et al., op. cit., pp. 68-69.
30. Tabata, S., op. cit., pp. 376-378, 1965.

31. Tully and Giovando, op. cit., p. 13.
32. Tully and Giovando, op. cit., p. 13.
33. NAVAIR 50-1C-529, U.S. Navy Marine Climatic Atlas of the World, v. 2 (North Pacific Ocean), March, 1977.
34. Maul, G. A. and Sidran, M., "Atmospheric Effects on Ocean Surface Temperature Sensing from NOAA Satellite Scanning Radiometer," Journal of Geophysical Research, v. 78(12), p. 1911, 20 APR 1973.
35. Stewart, R.H., "Satellite Oceanography: The Instruments", Oceanus, v. 24, Fall 1981.
36. NEPREP Technical Report 80-07 Navy Tactical Applications Guide, Volume 3, North Atlantic and Mediterranean Weather Analysis and Forecast Applications, by R. W. Fett and W. A. Bohan, p. 1B-7, March 1981.
37. National Oceanic and Atmospheric Administration Technical Memorandum NESS 109, National Environmental Satellite Service Catalog of Products, by D.C. Dismack, K.L. Booth and J.A. Leese, p. 3, April 1980.
38. Fett and Bohan, op. cit., p. 1B-14.
39. RCA Corporation, Electro-Optics Handbook, pp. 83-83, 1974.
40. Fett and Bohan, op. cit., p. 1A-5.
41. Deschamps, P. Y. and Phulpin, F. "Measurements of Sea Surface Temperature Using Channels at 3.7, 11 and 12 μm ", Passive Radiometry of the Ocean, D. Reidel Publishing Company, p. 140, 1980.
42. Leitao, C. D., Huang, N. E. and Parra, C. G., "A Note on the Comparison of Radar Altimetry with IR and In Situ Data for the Detection of the Gulf Stream Surface Boundaries", Journal of Geophysical Research, v. 84, p. 3970, 30 July 1979.
43. Maul, G. A., "Recent Progress in the Remote Sensing of Ocean Surface Currents", Marine Technology Society Journal, v. 11(1), p. 6, 1977.

44. NIMBUS-7 SMNR GDR Processing System Test Results, Contract No. NAS5-25346, Systems and Applied Science Corporation, 15 January 1981.
45. Lipes, R. G., "Description of SEASAT Radiometer Status and Results", Journal of Geophysical Research, vol 87 (C5), p. 3386, 30 April 1982.
46. Wilheit, T. T., NASA Goddard Space Flight Center, Greenbelt, Maryland, Interview, November 1981.
47. Njoku, E. G., Christensen, E. J. and Cofield, R. E., "The SEASAT Scanning Multichannel Microwave Radiometer (SMNR): Antenna Pattern Corrections - Development and Implementation", IEEE Journal of Oceanic Engineering, vol. OE-5(2), 1980.
48. Naval Research Lab Memorandum Report 4205, On the Measurement of Geostrophic Ocean Currents by (Nadir) Satellite Altimeter, by D. T. Chen, V. E. Noble and S. L. Smith, p. 1, 10 April 1980.
49. Leitao et al., op. cit., p. 3971.
50. Legeakis, R. and Gordon, A.L., "Satellite Observations of the Brazil and Falkland Currents - 1975 to 1976 and 1978", Deep Sea Research, v. 29, p.396, March 1982.
51. Blackstone, F.A. and Whritner, R.H., A Method of Locating and Determining Intensities of Sea Surface Temperature Gradients Utilizing Defense Meteorological Satellite Imagery, Naval Weather Service Facility, San Diego, p. 27, December 1976.
52. Leitao et al., op. cit., p. 3973.
53. Lundell, G. W., Rapid Oceanographic Data Gathering: Some Problems in Using Remote Sensing to Determine the Horizontal and Vertical Thermal Distributions in the Northeast Pacific Ocean, Master's Thesis, Naval Postgraduate School, Monterey, 1981.
54. Kilonski, B., ASTREX Data Package, Environmental Acoustics Research Group Internal Document, Naval Postgraduate School, Monterey, CA., June 1981.
55. Ibid.

56. Miyake, M. and Recker, E. E., Storm Transfer and Response Experiment Field Phase Report (partial preliminary draft), p. III-10, April 16, 1981.
57. Kilonski, op. cit., 1980.
58. Ryan, T. A., Joiner, B. L., and Ryan, B. F., MINITAB Reference Manual, The Pennsylvania State University, 15 January 1981.
59. Miller, I. and Freund, J. E., Probability and Statistics for Engineers, Prentice-Hall, Inc., p. 322, 1977.
60. Lundell, G.W., op. cit., p. 121.
61. The BDM Corporation Report BDM/M-TR-0004-81 STREX A Preliminary Report of Naval Postgraduate School Data, by D. E. Spiel, pp. B-16, B-17, 15 March 1981.
62. Lundell, G.W., op. cit., p. 140.
63. Emery, W. J. and O'Brien, A., "Inferring Salinity from Temperature or Depth for Dynamic Height Computations in the North Pacific", Atmosphere-Ocean, v. 16, p. 348, 1978.
64. Bernstein, R. L., Born, G. H. and Whritner, R. H., "SEASAT Altimeter Determination of Ocean Current Variability", Journal of Geophysical Research, v. 87 (C5), pp. 3262-3264, 30 April 1982.

INITIAL DISTRIBUTION LIST

	No. Copies
1. Defense Technical Information Center Cameron Station Alexandria, Virginia 22314	2
2. Library, Code 0142 Naval Postgraduate School Monterey, California 93940	2
4. Superintendent Attn: Code 68Jg Naval Postgraduate School Monterey, California 93940	2
5. Superintendent Attn: Code 68Du Naval Postgraduate School Monterey, California 93940	2
6. Commander Naval Electronics Systems Command Attn: PME-124-60 Naval Electronic Systems Command Headquarters Washington D.C. 20360	1
7. Commander Oceanographic System, Pacific Box 1390 Pearl Harbor, HI 96860	1
8. Commander Attn: Code 531 Naval Ocean Systems Center San Diego, CA 92152	1
9. Chief of Naval Operations Attn: OP951P Navy Department Washington, D.C. 20350	1
10. LCDR S. A. Cox Amphibious Squadron ONE FPO San Francisco, California 96601	1
11. Commanding Officer Attn: Seas Program Officer, Code 520 Naval Ocean Research and Development Activity NSTL Station Bay St. Louis, MS 39522	1
12. Commanding Officer Attn: Dr. William Jobst, Code 7300 Naval Oceanographic Office NSTL Station Bay St. Louis, MS 39522	1
13. Superintendent Attn: Code 68Bf Naval Postgraduate School Monterey, California 93940	2

14. Commanding Officer
Attn: Code 5101
Naval Research Laboratory
Washington D.C. 20375

1

END